Synthesis and Characterization of Decavanadate- and Lindqvist-type Cluster Containing Compounds: Studies on Macro- as well as Nano-crystals

Thesis

Submitted for the degree of

DOCTOR OF PHILOSOPHY

By

YERRA SRIDEVI

School of Chemistry

University of Hyderabad

Hyderabad, 500 046

INDIA

June 2014

CONTENTS

INTRODUCTION

1

In the recent years, remarkable progress has been made in the area of polyoxometalate (POM) chemistry, where several POM anions, for example, decavanadate and mixed addenda Lindqvist anions are given significant importance. In this chapter, a brief introduction on the POM cluster chemistry including the history, synthesis of relevant compounds in macro-/nano-size as well as applications are discussed. The synthesis and characterization of macro-sized as well nano-sized crystals of POM cluster-containing compounds have drawn considerable interest. The key to the rapid growth of this research area is mainly due to the tendency of these materials to meet the vast range of applications in the field of catalysis, medicinal and industrial science. This chapter gives a general overview on the POM associated compounds in terms of introduction and research progress which mainly deal with applications and synthetic procedures.

1.1. Introduction

Over the past few decades, much progress has been made in the development of POM materials. Today, POM chemistry is a key emerging area that promises to allow the development of sophisticated designers molecule-based materials and devices that exploit developments in instrumentation, nano-science and materials fabrication methods.[1] Inorganic metal-oxygen cluster anions (for example, POM anions) form a class of compounds that is unique in its topological and electronic versatility and is important in several disciplines. POMs have found applications in the areas of analytical chemistry, catalysis (including photocatalysis), biochemistry, medicine (antitumor, antiviral, and even anti-HIV activity),[2] and especially in materials science owing to their chemical, structural and electronic versatility. POM like metal-oxygen clusters are also present in geosphere and biosphere.

1.2. Historical background of POM chemistry

Although the first compound of POM was reported more than 150 years ago, new types of POM clusters continue to be discovered for exploring new class of materials with novel functional properties. Berzelius noted the formation of an yellow (heteroployanion) product from the reaction of molybdate with phosphate or arsenate in 1826.[3] The first heteropolytungstates were discovered and characterized by Marignac in 1862. During the next years, POMs were intensively investigated, and hundreds of such compounds were described in the Gmelin volumes, published in the 1930s.[4] In 1893, Alfred Werner proposed his monumental theory[5a] of coordination complexes. Pauling, for an important class of compounds, proposed structures that were based on corner-sharing of MO_6 octahedra,[5b] but it was not until 1933, Keggin reported the structure of the heteroploy acid $[H_3PW_{12}O_{40}]\cdot 6H_2O$ (by analysis of 32 powder X-ray lines),[6a] whereby the importance of more compact edge-shared polyhedral arrangements were revealed. A new polyanion structure was reported by Anderson[6b] in 1937 which was finally confirmed by Evans[6c] in 1948. Later, other POM cluster anions, namely, Lindqvist,[6d] Strandberg,[6e] Dawson types of polyoxoanions were characterized. In 1971, a review published, where 25 X-ray investigations were listed.[7] During the 1987 and 88, almost 66 structures were published due to the development of the X-ray crystallographic hardware and software techniques. Later the development of Raman, ^{17}O NMR[8] and other spectroscopic methods with the

combination of electrochemical measurements and new analytical techniques, such as fast atom bombardment (FAB) mass spectroscopy,[9] established the important link between solid and solution structure. New classes of structures of more than 70 different elements, with "coordination numbers" ranging from 3 to 12, had been confirmed, dozens of stoichiometries and structures were known. This chemistry is well known since 200 years and interest have been increasing worldwide.

1.3. General perspective of POM chemistry

The POMs are a large family of metal-oxygen cluster anions, which are particularly formed by the early transition metals such as Mo, W, V, Nb and Ta ("addenda atoms"). These have been considered as ideal inorganic building blocks for the design and construction of multi-functional materials.[10a] A large number of potential coordination sites (both terminal and bridging oxygen atoms) from the POM cluster-surfaces are the main source for the multifunctional activity. In general, POM clusters are known in anionic forms, and hence appropriate cations are needed for their successful isolation.

The formation of POMs depends on:

(i) the appropriate relationship of coulombic factors of ionic radius and charge (cationic radius should be within the range of 0.65 – 0.80 Å; for addenda atoms V^{5+} (0.68 Å), Mo^{6+} (0.77 Å), W^{6+} (0.74 Å), whereas for Cr^{6+} (0.58 Å).

(ii) on the accessibility of empty d orbital for metal–oxygen bonding; this is why, the formation of POM clusters are limited to only above mentioned inner-transition metals and not from other metals.

There are two generic families of POMs: the isopolyanoins (IPA), that contain only d^0 metal cations and oxide anions, $[M_mO_y]^{p-}$, and the heteropolyanions (HPA), that contain one or more heteroatoms in addition to the other ions, $[X_xM_mO_y]^{q-}$, ($x \leq m$) where M atoms are the addenda atoms and X is hetero element, namely, P, S, Si, As, etc. The heteroatoms in the heteropolyoxometalates can reside in either buried (not solvent accessible) or surface (solvent accessible) positions in the POM structure. Over half of the elements in the periodic table are known to function as heteroatoms in heteropolyoxometalates. As heteropoly compounds are more numerous and their structural and electronic properties are easier to modify synthetically than those of the isopoly compounds, the former members have dominated the medically oriented research on

POMs to date. POM anions can also be classified into three types, based on the presence of number of oxygen atoms, attached to the addenda atom. The "mono-oxo" (C_{4v}) class or type I, which have one terminal oxo group in which lowest unoccupied molecular orbital (LUMO) is approximately non-bonding and metal centered and hence type I class POMs may be reduced reversibly to mixed valence species. Whereas in type II or "cis-dioxo" (C_{2v}) class, there are two terminal oxo groups,[4b] where LUMO for the octahedral is strongly anti-bonding with respect to the M = O bonds. Type III anions (which is observed very rarely) had both kinds of M atom sites. The above entire discussion is offered in the following scheme 1.1.

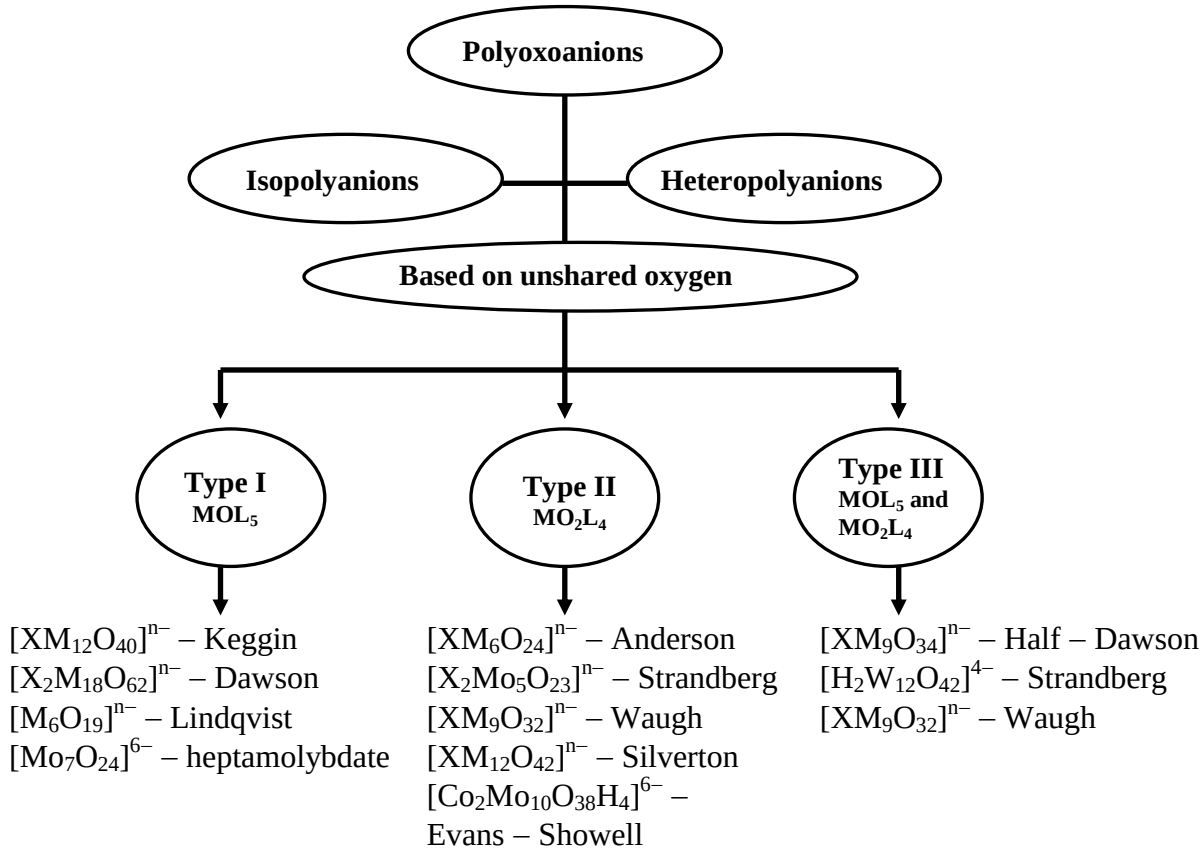

Scheme 1.1. Classification of POM anions, based on composition and unshared oxygens attached to M atom.

The structures of heteropoly and isopolyanions appear to be governed by the electrostatic and radius-ratio principles, observed for extended ionic lattices. Therefore, it is convenient to describe these structures in terms of assemblages of metal-centered MO_n polyhedral, that are linked by shared corners, edges and faces. The metal ion does not lie at the center of its polyhedron of oxide ions but it is displaced strongly towards the exterior of the

polyanion structure. There are two main principles of describing the structures:

Lipscomb: There are no polyanion structures, which contain MO_6 octahedra with more than two unshared oxygen atoms.[1]

Pope: Two kinds of metal atom displacement are observed in polyanions: type I, towards one, always terminal oxygen atom, and type II, towards two cis, usually terminal oxygen atoms.[10a]

1.3.1. Structure

POMs can be regarded as packed arrays of pyramidal MO_5 and octahedral MO_6 units (building blocks) and these entities can be considered as similar as the $–CH_2–$ in organic chemistry. These MO_n units can be packed to form different shapes, but there are some simple rules for them to join one another in order to build the POM frameworks. The molecules as a whole are built by edge- and/or corner sharing MO_n polyhedra, and very rare by face-sharing (Figure 1.1). The most stable linkages are the edge- and corner-sharing models (A and B in Figure 1.1), in which the Mn^+ ions are far enough from each other in order to decrease the columbic repulsion between them (Table 1.1). In the case of the face-sharing contact (C in Figure 1.1), the metallic centers are closer than in A or B. At such distances, the repulsion is not balanced by the stabilization due to the chemical bonding.

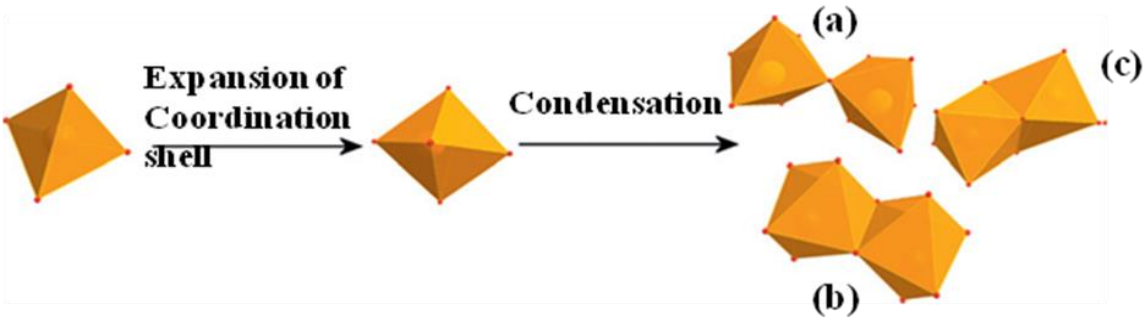

Figure 1.1. Illustration of the self-assembly process, whereby the tetrahedral metal $\{MO_4\}$ expands into octahedra $\{MO_6\}$ and then condenses into larger assemblies sharing oxygen ligands, where M commonly is Mo, W, or V. There are three different sharing modes: (a) corner sharing, (b) edge sharing, and less commonly (c) face sharing. Color scheme: M, gold (polyhedra); O, red.[10b]

Nevertheless, Linking of MO_6 octahedra by face-sharing was first reported by Dexter and Silverton in 1968, observed in the structure of $[CeMo_{12}O_{42}]^{8-}$.[11] This species consists of six pairs of face-shared octahedra (Mo_2O_9 unit) resulting in an icosahedral geometry. The molybdenum atom positions are characterized with Mo···Mo separations of 3.18 and 3.84 Å (face and corner-shared contacts respectively).[10a]

Table 1.1. M···M distances (Å) of corner- and edge- sharing octahedra in POMs

Metal Ion	**corner- sharing**	**edge- sharing**
V(V)	3.50	3.20
W(VI)	3.70	3.41
Mo(VI)	3.70	3.41

1.3.2. Some common structures

1.3.2.1. Isopolymetalates, $[M_mO_y]^{n-}$

1.3.2.1.1. Hexametalate structures

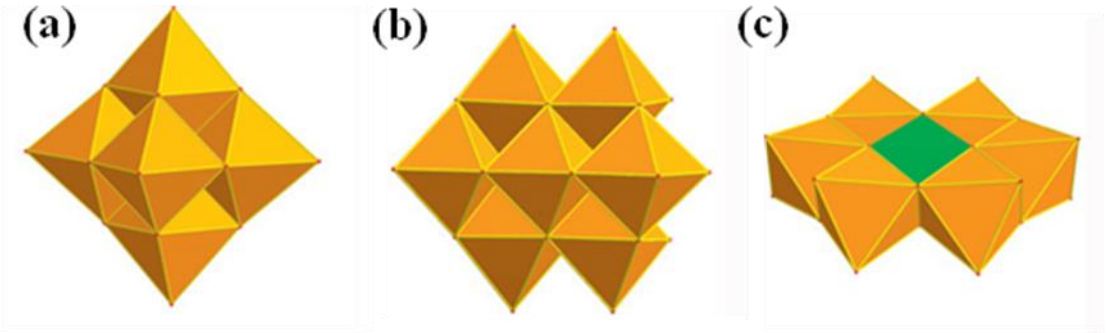

Figure 1.2 Polyhedral representation of (a) Lindqvist anion $[M_6O_{19}]^{2-}$; (b) heptamolybdate anion $[Mo_7O_{24}]^{6-}$ and (c) Anderson anion $[TeMo_6O_{24}]^{6-}$. The gold-colored $\{MO_6\}$ octahedra represent the addenda metal M (Mo, W, V, etc.); the light green $\{MO_6\}$ represents the central heteroatom octahedron); O, red.[10b]

One of the prominent examples of hexametalate structures are Lindqvist structure, such as, observed in the cluster anions $[Nb_6O_{19}]^{8-}$, $[Ta_6O_{19}]^{8-}$, $[Mo_6O_{19}]^{2-}$ and $[W_6O_{19}]^{2-}$. The structure is built by repeating octahedral units with shared edges. In Figure 1.2(a), it can be seen that the metal atom is not in the centre of the octahedral structure, so the structure is called "quasi-octahedral".[10a,12] Two polyanion structures are based on the arrangements

of seven edge-shared octahedral as shown in Figure 1.2(b) and 1.2(c) respectivley. The planar structure was originally proposed by Anderson for the heptamolybdate anion, $[Mo_7O_{24}]^{6-}$, and 6-molybdo-anions, such as $[IMo_6O_{24}]^{5-}$, and these are generally known as the "Anderson structure".[13a] Later, Lindqvist showed that $[Mo_7O_{24}]^{6-}$ has a bent structure (Figure 1.2(b)) (b) and the first authentic Anderson[10a] structure (Figure 1.2(c)) was observed for $[TeMo_6O_{24}]^{6-}$.

1.3.2.1.2. Mixed addenda Lindqvist clusters

Vanadium–tungsten mixed isopolyanions were firstly described by Finkener[13b] and Rosenheim,[13c] then in 1894 by Friedheim[13d-e] and in 1915 by Prandtl[13f]. In 1963, Chauveau and Souchay[13g] confirmed the V/W = 2:4 stoichiometry and determined the pH range for the stability of this species. In 1971, Flynn and Pope[13h] gave efficient methods to prepare the complexes $[V_xW_{6-x}O_{19}]^{-2-x}$ (x = 1, 2). These clusters are shown in Figure. 1.3. IR and Raman spectroscopic studies in solution and in the solid state have shown that these anions have likely the Lindqvist structure[13i-j] with respectively one or two tungsten atoms being replaced by vanadium. The stability in aqueous solution of such species depends strongly on the pH.[13k-l] The high charge and large size of the isopolyanions (Figure 1.3) make them nice building units for self assembly.[13m]

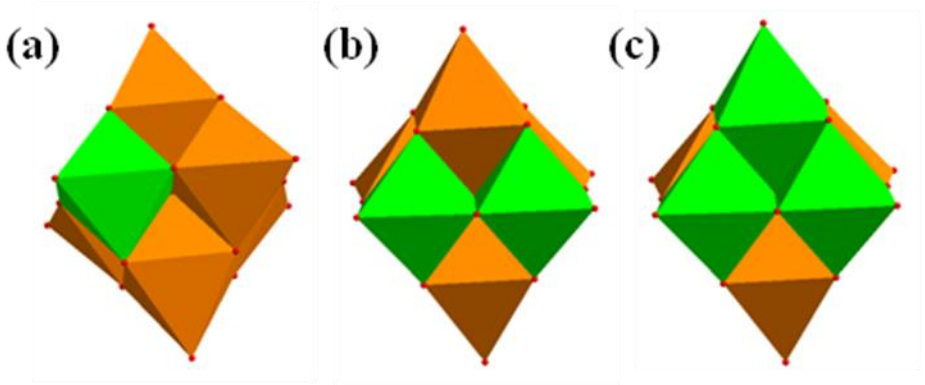

Figure 1.3. Polyhedral representation of (a) $[VW_5O_{19}]^{3-}$, (b) $[V_2W_4O_{19}]^{4-}$ and (c) $[V_3W_3O_{19}]^{5-}$. The gold-colored $\{MO_6\}$ octahedra represent the addenda metal, M (W); the light green $\{MO_6\}$ represents the substituted addenda metal atom, M (V); O, red.[10b]

1.3.2.1.3. Decametalate structures

Examples of these structures are $[H_nV_{10}O_{28}]^{(6-n)-}$, $[W_{10}O_{32}]^{4-}$ and $[Mo_{10}O_{34}]^{8-}$. In these three clusters, decavanadate cluster is the predominant and it was first characterized in 1956.[13n] Decavanadate cluster anion (Figure 1.4) is one of the foremost polyoxovanadate (POV) cluster anion. The structure of decavanadate anion, consisting of six fused VO_6 octahedra having D_{2h} symmetry, is closely related to the representative POM, known as Lindqvist-hexamer, $[M_6O_{19}]^{n-}$ which has approximately O_h symmetry. The decavanadate anion contains three sets of equivalent vanadium atoms.[13o] These include two central VO_6 octahedra and four peripheral tetragonal-pyramidal VO_5 groups. There are seven unique groups of oxygen atoms, two of these bridges to six vanadium centers, four oxygen atoms bridge three vanadium centers and fourteen of these oxygen atoms span edges between pairs of vanadium centers and eight oxygen atoms are peripheral.

Figure 1.4. Polyhedral representation of decavanadate anion $[V_{10}O_{28}]^{6-}$. The gold-colored $\{MO_6\}$ octahedra represent the addenda metal, M (V)); O, red.[10b]

1.3.2.2. Heteropolymetalates, $[X_xM_mO_y]^{q-}$

1.3.2.2.1. The Keggin clusters

Compared to the M_6O_{19} and XM_6 structures described above, Keggin structure is much more complex. As shown in Figure 1.5, a central tetrahedron, surrounded by twelve octahedral, arranged in four groups of three edge-shared octahedral units, M_3O_{13}. These groups are linked by shared corners to each other and to the central tetrahedron. This structure is known as the Keggin structure, called after the scientist who first characterized it.[10a,14]

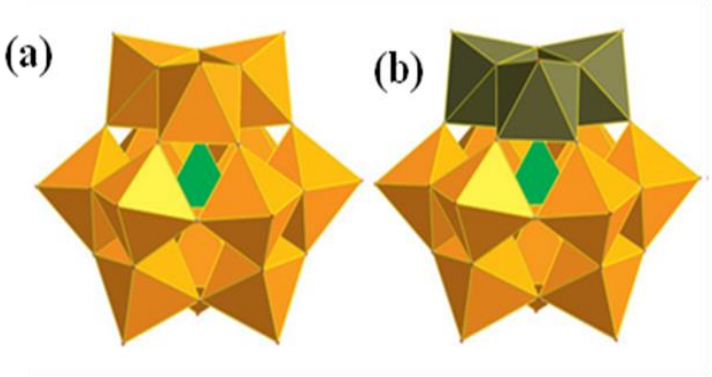

Figure 1.5. Polyhedral representation of the (a) Keggin anion $[XM_{12}O_{40}]^{n-}$ and (b) Trisubstituted Keggin anion. The gold-colored $\{MO_6\}$ octahedra represent the addenda metal, M (Mo, W, V, etc.); the light green $\{MO_6\}$ represents the central heteroatoms; the dark green $\{MO_6\}$ represents the substituted addenda; O, red.[10b]

1.3.2.2.2. Mixed addenda Keggin clusters

The M atoms in the Keggin anion $[XM_{12}O_{40}]^{n-}$ can be partially substituted by a second heterometal atom to form 'substituted' heteropoly Keggin anions, $XM_{12-y}Z_yO_{40}^{p-}$, where Z is a second heterometal (e.g. vanadium). Numerous examples of such 'mixed-addenda' compounds have since been described.[14b] Pope and Flynn[13o,14c] reported syntheses and characterizations of these tungstovanadate heteropolycomplexes. The reported preparative studies reveal that these heteropoly anions can be considered to be derivatives of the unknown (hypothetical) 12-tungstovanadate (V) with partial replacement of tungsten(VI) by vanadium(V), i.e., $[VW_{12-n}V_nO_{40}]^{(3+n)-}$ with n = 2, 3 or 4. Among these 'mixed-addenda' compounds, $[VW_{10}V_2O_{40}]^{5-}$, $[VW_9V_3O_{40}]^{6-}$ and $[VW_8V_4O_{40}]^{7-}$ are of particular interests because vanadium-substituted Keggin anions have been used as catalysts in oxidation of organic compounds.[14d-e]

1.3.2.2.3. The Wells-Dawson clusters

It is a dimeric heteropolyanion of the formula $[X_2M_{18}O_{62}]^{x-}$, where M= W(VI) or Mo(VI). The anion is viewed as a fusion between two A-α-XW_9 units through all six oxygens of the lacuna resulting in a virtual D_{3h} symmetry cluster of the α isomer type (Figure 1.6).

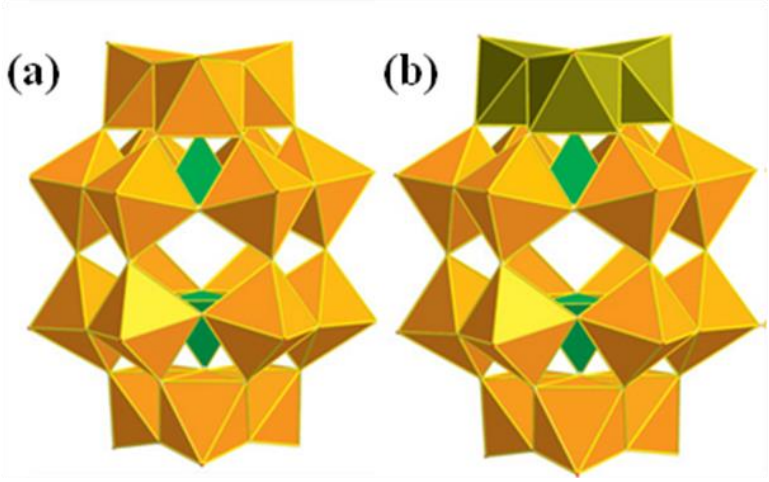

Figure 1.6. Polyhedral representation of the (a) Wells-Dawson anion (b) Trisubstituted Wells-Dowson anion. Color scheme: The gold-colored $\{MO_6\}$ octahedra represent the addenda metal, M (Mo, W, V, etc.); the light green $\{MO_6\}$ represents the central heteroatom tetrahedron; the dark green $\{MO_6\}$ represents the substituted addenda; O, red.[10b]

Two sets of tungsten form this polyanion, six "polar" and twelve "equatorial" positions constituting the two caps and the two belts of the anion respectively. The β isomer forms when one of the caps is rotated by 60°. Similar to the β Keggin, the β Wells-Dawson is more easily reduced.

1.3.3. Current trends in synthesis and properties of POM clusters

In practice, POMs are most frequently prepared by one-pot proton-induced condensation-dehydration reactions in an aqueous medium. The mechanism of the formation of POMs is still not clear and usually described as self assembly. Therefore it is not possible to design a multi-step sequence for the synthesis of novel POM cluster anions. The successful isolation of POM cluster anions depends on many factors during the course of the reaction, such as (i) concentration of the reactants, (ii) pH of the medium, (iii) temperature, (iv) solvent, (v) sequence of adding reagents, and (vi) presence of reducing agents/additional ligands etc.

(a) Synthesis of POMs from aqueous and non-aqueous medium:

The acidification of an aqueous solution contains simple oxoanions such as MoO_4^{2-} or WO_4^{2-} resulting in the formation of isopolyanion (IPA) and heteropolyanion (HPA) with necessary added heteroatom. The formation of isopolyanion and heteropolyanion can be described as

$$7MoO_4^{2-} + 8H^+ \longrightarrow [Mo_7O_{24}]^{6-} + 4H_2O$$

$$6MoO_4^{2-} + [Al(H_2O)_6]^{3+} + 6H^+ \longrightarrow [Al(OH)_6Mo_6O_{18}]^{3-} + 6H_2O$$

The important isopolyanion is decavanadate. The aqueous chemistry of V(V) has been extensively studied and a large variety of molecular species have been described.[14f] Two basic reactions, hydrolysis and condensation, occur when vanadium salt is dissolved in water. Aqueous vanadate (V) compounds undergo various self-condensation reactions.[14g] Depending on pH, major vanadate anions in solution include VO_2^{2+}, VO_4^{3-}, $V_2O_7^{3-}$, $V_3O_9^{3-}$, $V_4O_{12}^{4-}$ and $V_{10}O_{26}^{6-}$. Many of these vanadate ions can be reversibly protonated.[14h]

Decavanadate anion is formed according to this equilibrium:

$$10\ [VO_2(OH_2)_4]^+_{(aq)} \rightleftharpoons H_2V_{10}O_{28}^{4-}{}_{(aq)} + 14\ H^+_{(aq)} + 32\ H_2O$$

Decavanadate is most stable in the region of pH 4–7. Solutions of vanadate turn bright orange at pH 6.5, indicating the presence of decavanadate cluster anion. All other vanadates are colorless. Below pH 2.0, a brown V_2O_5 hydrate gets precipitated.

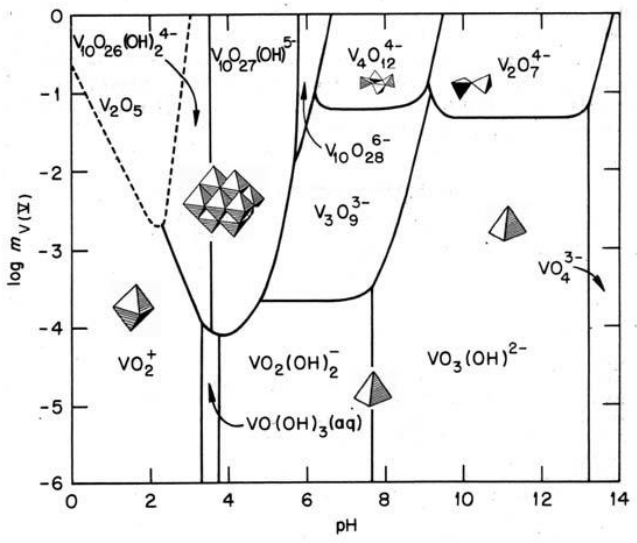

Figure 1.7. V(V) solute species in aqueous solutions as a function of pH and concentration. .[14i]

In non-aqueous solutions, the hexa- and deca-tungstate anions are well characterized. The syntheses of isopolyanions from an organic solution were performed by Jahr and Fuchs.[15] The relevant synthesis was performed by the hydrolysis of the metal esters in the presence

of organic bases. The formation of hexa-tungstate in non-aqueous medium can be described as

$$WO(OEt)_4 + NR_4OH + H_2O \longrightarrow [NR_4]_2[W_6O_{19}]$$

(b) Functionalization of POMs

The functionalization of the POM cluster anions to explore more selective applications is an interesting aspect in recent POM chemistry. The functional POM frameworks have been achieved by using either pure organic linkers or inorganic linkers, e.g., transition / alkali metals. The covalent attachment of organic/inorganic groups to POM via linkages extends their potential uses in various applications.[16] It is interesting that some of the transition/alkali metal linkers can form pure inorganic POM-based polymeric compounds through covalent bonds.[16]

Coordination dimension mainly depends on the number of possible coordination sites available in POMs cluster and transition metal complexes. By taking the advantage of the ability of POMs in forming variety of multidimensional structures, 1D, 2D and 3D structures containing compounds have been synthesized either hydro-thermally or by solution based techniques. A significant contribution was made by Jon Zubieta and co-workers[17a] in this particular field of research work; some of the reported structures are known with open framework containing well defined cavity.[17b] POV clusters have also been used as linker for constructing functional vanadium framework structures, for example, reported vanadium MOF (VMOF).[17c] Ramanan and co-workers have made considerable contribution on fully oxidized vanadium based polyoxoanions in the presence of cage like hexamine as a structure directors.[17d-e]

1.3.4. Applications

1.3.4.1. POMs in catalysis

The use of POM associated compounds as catalysts continues to be one of the most popular application, especially in industry with hundreds of papers and many patents published every year covering this topic. The redox properties of these POMs make them important as catalysts for a number of oxidation and dehydrogenation reactions of organic substrates. The main role of POM[18a] cluster anions in catalysis is to activate peroxides, such as hydrogen peroxide, alkylhydroperoxide etc. As a result of the activation of

peroxides, an inorganic peroxo, hydroperoxo, alkyl peroxo, or acyl peroxo intermediates are formed and those are very reactive species and hence lead to oxygenation of the organic substrate. The superiority of POMs as catalysts, compared to other catalysts, is reflected by their affinity towards strong oxygen donors, such as molecular oxygen and hydrogen peroxide.

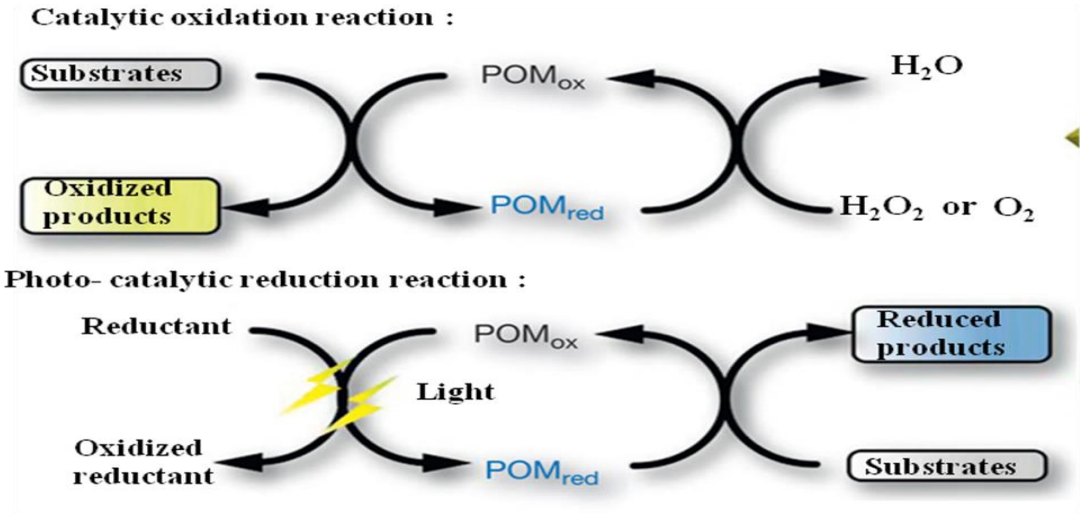

Figure 1.8. POM-catalyzed reaction systems: catalytic oxidation reaction and photo-catalytic reduction.

Mostly transition metal substituted POM clusters or POM supported transition metal complexes show applications in catalysis. The literature shows that about 85% of the patents and applications of POMs are related with catalysis.[18b] A cesium salt of a divanadium-substituted phosphotungstate compound. catalyzes the hydroxylation of alkanes with a complete stereospecificity and regiospecificity.[19] The di-aluminum substituted silicotungstate shows catalytic activity for the intramolecular cyclization of citronellal derivatives, such as citronellal and 3-methylcitronellal without formation of byproducts.[20] POM–MOFs also show interesting catalytic properties. Cationic crown-ether/POM ion pairs exhibit catalytic activities. The cation [Pd(II){(H_3O)[15]crown-5-phen}C_{l2}]·(phen = phenanthroline) and $[PV_2Mo_{10}O_{40}]^{5-}$ anion can catalyze Wacker-type alkene oxidation in essentially quantitative yield using N_2O instead of O_2 as the oxidant.[21] The hybrid complex [Re(I)(15-crown-5-ether)(CO_3)CH_3CN-$MHPW_{12}O_{40}$] (M=Na^+, H_3O^+) catalyzes the reduction of CO_2 to CO in the presence of H_2 under light.[22] The mechanism and kinetics of ether and alkanol cleavage catalyzed by POMs have been examined.[23]

Finally, $H_5PMo_{10}V_2O_{40}$ has been tested as a catalyst and a co-catalyst for methane oxidation in a microfluidic device, to implement genetic algorithms.[24]

1.3.4.2. POMs in magnetism

The unique ability of POMs to act as electron sponges hosting a variable number of electrons in the POM framework can provide an efficient way to tune the strength of the exchange coupling as well as the electron delocalization in the cluster and, consequently, its spin state. Such a control can be achieved either physically, by an electrical gating in a single molecule setup, or chemically, during the synthesis of the POM. Due to chemical control of electron population, POVs represent a remarkable class of high-nuclearity mixed valence clusters.[25a] These compounds are therefore ideal systems for studying the influence of the number of delocalized electrons on the magnetic properties. It is well known that, only two isopolyanions $[V_{10}O_{28}]^{6-}$[(13o)] and $[V_{12}O_{32}]^{4-}$[(25b)] are known in which all the vanadium centers are in +5 oxidation state. Several polyoxovanadates are known in mixed valence (nearly all ratios of V^{4+} to V^{5+} are known) and some of them are known in which all the vanadium centers are in $V^{4+}(d^1)$.[25c] Especially, the mixed valence (V^{5+}/V^{4+}) and reduced (only V^{4+}) vanadium clusters show an interesting magnetic behavior. In such a way, fully reduced vanadium clusters (containing only V^{4+}) can be viewed as fully magnetic cluster in which S = ½ spins for each V^{4+} and V^{4+} centers are anti-ferromagnetically coupled. Consequently, the intermolecular magnetic interactions are expected to be a maximum which opens up a new gateway in molecular magnetism.

1.3.4.3. POMs in electrochemistry

There is a potential for exploitation of their electronic and optical properties. The first attempts of electrical measurements on POM-based systems have been carried out by the groups of Glezos and Tour.[26,27] POMs were examined as components of polymeric materials with potential use in nanolithography, molecular devices and also properties such as charging and electron tunneling through molecules in quantum switching applications. An important requirement in this case is that the guest POM molecule should not interact chemically with the polymer host material. The transport properties of these materials were investigated by varying the inter-electrode spacing and the POM concentration. Another interesting result obtained was resonant tunneling at room

temperature condition for film thickness in the range of 10nm.[26] Quantum tunneling effects depends strongly on three factors, primarily on a) the POM concentration and therefore the intermolecular distance, b) the electrode distance, and less on c) the electrode material.[27] This study concluded that the selective charging of POMs can be exploited in future memory devices.

1.3.4.4. POMs in medicine

Two general types of POM biological activity, anti-viral and antitumoral, have been known for some time. The putative applications of poly-, oligo- and mono-oxometalates in biochemistry, biology, pharmacology and medicine have rapidly been attracting interest. In particular, these compounds may act as potent ion pump inhibitors and have the potential to play a role in the treatment of e.g. ulcers, cancer and ischemic heart disease.[28] The mechanism for the antitumoral activity of POMs is proposed by Yamase.[29] The first antiviral activity of POMs was reported in 1971. The inhibition of viral adsorption / fusion as a function of POM structure in a cell-based assay was first studied by Hill et al.[30] They showed that the POM anions $[SiW_{12}O_{40}]^{4-}$, $[BW_{12}O_{40}]^{5-}$ and $[NaSb_9W_{21}O_{86}]^{18-}$ were able to completely inhibit cell fusion in HIV-infected lymphocytes.

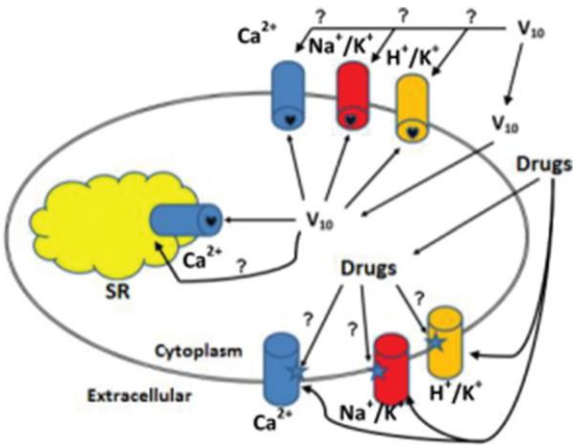

Figure 1.9. E1–E2 ATPases, a family of cation pump enzymes, are known targets whereas decavanadate binds to a pocket formed by protein domains at the cytoplasmic side. Decavanadate and other POMs need to cross the bilayer before targeting the ion pumps, something which probably occurs through transport membrane systems such as channels, or specific transporters and/or pumps. In contrast, established organic drugs do not apparently need to cross the membrane, and probably for V_{10} this mechanism of action cannot be completely excluded. Na^+/K^+, H^+/K^+, and Ca^{2+} stand for Na^+, K^+-ATPase, H^+, K^+-ATPase, and Ca^{2+}-ATPase, respectively. SR denotes sarcoplasmic reticulum.[28]

The mode of action of decavanadate and the other oxometalates implies that the main focus of the interaction is on the cytoplasmic domain of the protein, more specifically at the nucleotide or phosphorylation domains or at a pocket involving several cytoplasmic domains. Although decavanadate interacts most strongly with the E2 conformation of the Ca^{2+}-ATPase, as do some of the other drugs, decavanadate also interacts with other conformations (Figure 1.9). Therefore, decavanadate exhibits a particular feature that may be useful for the understanding the mode of action of ion pump inhibitors in general.[28] Besides, the specific behavior of decavanadate towards ion pumps may guide the development of new drugs that would have these pumps as therapeutic targets.

1.3.4.5. POMs in nuclear waste treatments

Much research work has been focused on safe disposal of the long lived radioactive isotopes, like Np-237, etc. Owing to its highly oxophilic and higher coordination number, the f-block elements are better candidates for forming ideal POM based compounds, which finds applications in nuclear waste treatment process.[31] For example, POM anions like AsW_9[32] and $P_2W_{17}O_{61}$[33] have been used as coordinating ligand in radioactive waste treatment via sequestration of trans-uranium elements. The outstanding similarity in coordination chemistry of POMs may have great significance of the development of new waste treatment technologies.

1.3.4.6. Supramolecular interactions in POMs

POMs are basically oxo-clusters, which contain many number of oxygen atoms on the cluster surface and also crystallized with significant number of lattice water molecules. Due to the presence surface oxygen atoms/ lattice water molecules, the relevant crystal structure is often stabilized by O–H···O hydrogen bonding interactions (in case of hybrid compounds C–H···O, N–H···O, C–H···N are also included). Basically supramolecular chemistry has been varied by changing the cation. Recently various reports have come in the context of supramolecular chemistry of decavanadate- and mixed addenda Lindqvist-based cluster containing compounds.[34]

1.4. Uniqueness of nano-materials

In materials science, a new dimension is now added by 'size', a feature that controls properties in the world of nano-materials. Size, shape and size-distribution in nanoscale regime permit the control of fundamental properties of the materials without changing the materials, chemical composition and lattice structure. The term "*nano"* originates etymologically from the Greek, and it means "dwarf". The term indicates physical dimensions that are in the range of one-billionth (10^9) part of a meter. Nano-materials show unique properties because of their surface as well as the small physical size.[35] Atoms on the surface have less number of neighbors than in the bulk, and the increasing "surface to volume ratio" at small physical sizes leads to unusual effects like change in melting points and phase transition temperatures. In a broad sense, nanoscience can be defined as the study of phenomena and manipulation of materials at atomic, molecular and supramolecular level, where properties differ significantly from those at a macroscopic scale,[36a] and become size-dependent.

Nano-materials had made a strong impact already and will continue to impact upon a range of areas like energy, environment, textiles, cosmetics, food and information technology. The unusual facets of nano-materials ensure that these are unique materials for futuristic path breaking investigations and novel applications.

1.4.1. POMs in nano-size

POMs are ideal models for the construction of organic-inorganic hybrid systems and are regarded as potential candidate to be transformed into nanometer-sized materials. It is believed that the assembly of POMs-based composite on the nanometer scale can provide a path for exhibiting their unique properties in many fields. The synthesis of organic–inorganic hybrid compounds using POM clusters as nano-building blocks is an attractive idea that can utilize the myriad and potentially important functions of POMs in areas as diverse as catalysis, molecular magnetism, photochemistry and medicine. The rational design of POM multi-component materials with well defined supramolecular architectures, represent the next milestone to implement POMs into functional materials and devices. Cronin and co-workers reported silver decavanadate and other polyoxotungstate based nanostructures.[36b]

The POM based clusters can serve as both the reductants and the stabilizers [37] and the process may provide an effective approach for the synergic catalysis of the oxidation and hydrogenation. Thus, developing a simple method to combine POMs and metal nanoparticles (MNPs) in one confined domain in a well dispersed state is of considerable interests in terms of both fundamental and practical importance. Currently, most of the reported examples include the POM reduction in aqueous solutions,[37] films,[38] liquid-liquid interface,[39] and in bulk silica.[40,41]

Metal oxide based nanocapsules of the type $\{(M^{VI})M^{VI}_5\}\{Mo^{V}_2\}_{30}$ ($\equiv\{M^{VI}_{72}Mo^{V}_{60}\}$) and $\{(M^{VI})M^{VI}_5\}_{12}\{M'\}_{30}$ (M = Mo or W; M′ = VO^{2+}, Fe^{3+}, or Cr^{3+}) are popularly called Keplerates. In POM chemistry, the concept of "transferable" building blocks (for example, the pentagonal unit [(Mo) $Mo_5O_{21}(H_2O)_6]^{6-}$) is the key point to understanding the formation of very large cluster entities of diverse architectures, e.g., giant spheres, giant wheels, etc (Figure 1.10).[42]

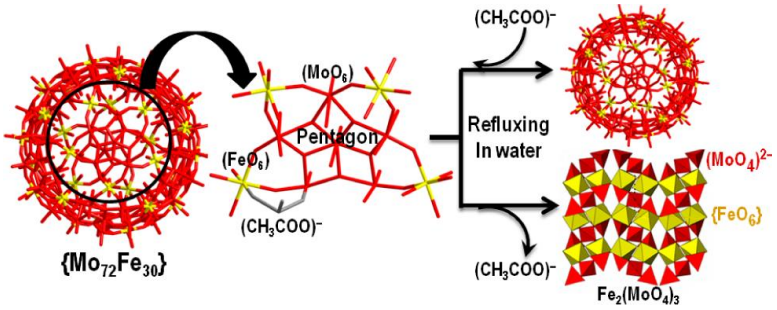

Figure 1.10. Schematic representation demonstrating the thermal stability of a giant nano-object in an aqueous solution.[42] In the absence of acetic acid, this nano-capsule leads to the formation of nano-ferric molybdate at boiling water.[42]

1.4.2. Synthesis of nano-sized POMs

In recent years, systematic methods for POM synthesis and derivatization have been explored, providing an expanding range of robust ‘‘designer’’ components for ‘‘bottom-up’’ method in materials synthesis. Generally, two methods are applied to the incorporation of POMs into the polymer matrix. (i) *Two-step method* (Figure. 1.11A): A polymer film is first deposited on the substrate by spin-coating or electro-polymerization and then soaked in the solution containing POMs to allow its passive diffusion into the polymer matrix. The electrostatic interaction between cationic polymer matrix and POM

anions is stronger than that between the polymers and small counter anions such as sulfate, chloride, and perchlorate in the electrolyte. Hence, POMs are efficiently immobilized in the polymer matrix. (ii) *One step method* (Figure. 1.11B): The incorporation process involves the chemical or electrochemical oxidation of a polymerizable monomer to form a polymer film in the presence of POM solution.[48b] In this way, nano structured films are prepared and the heteropolyanions are trapped within the framework of the polymer matrix (Figure. 1.11C).[43]

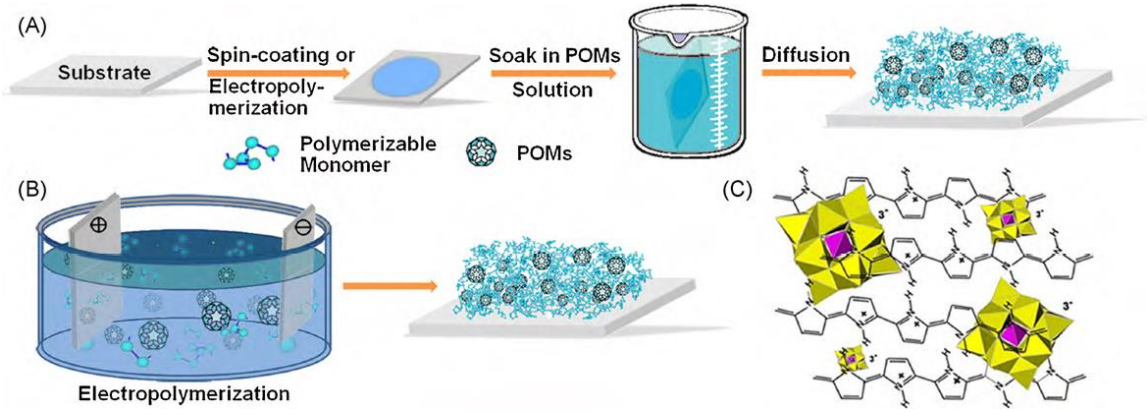

Figure 1.11 Scheme of preparation of POM—polymer matrix via two-step (A) and one-step (B) methods. (C) Schematic diagram of the structure of the hybrid polypyrrole/$PMo_{12}O_{40}^{3-}$.[43]

1.4.2.1. Self-organized nanomaterials based on POMs and cationic surfactants

Self-organization of surfactants and POMs usually results in nano-structured organic—inorganic hybrid materials. These materials are analogous to the known organic polyelectrolyte- surfactant materials. It is a non-covalent synthesis strategy that makes use of the electrostatic interactions between positively charged surfactants and oppositely charged POMs. Owing to the structural incompatibility of the surfactant alkyl tails and POMs via the ionic connection, phase separation is achieved on a molecular scale, leading to the formation of nano structured materials. In 1994, Ichinose et al. used bilayer membranes and isopolyanions, $V_{10}O_{28}^{6-}$, as hosts and guests, respectively, to prepare a composite material with a layered architecture by an ion exchange technique.[44] Afterwards, the layered and hexagonally ordered mesostructured materials were constructed with different types of POMs such as $H_2W_{12}O_{40}$, $PW_{11}O_{39}^{7-}$, $SiW_{12}O_{40}^{4-}$, $[W_{10}O_{32}]^{4-}$ and surfactants, respectively (Figure 1.12).[45]

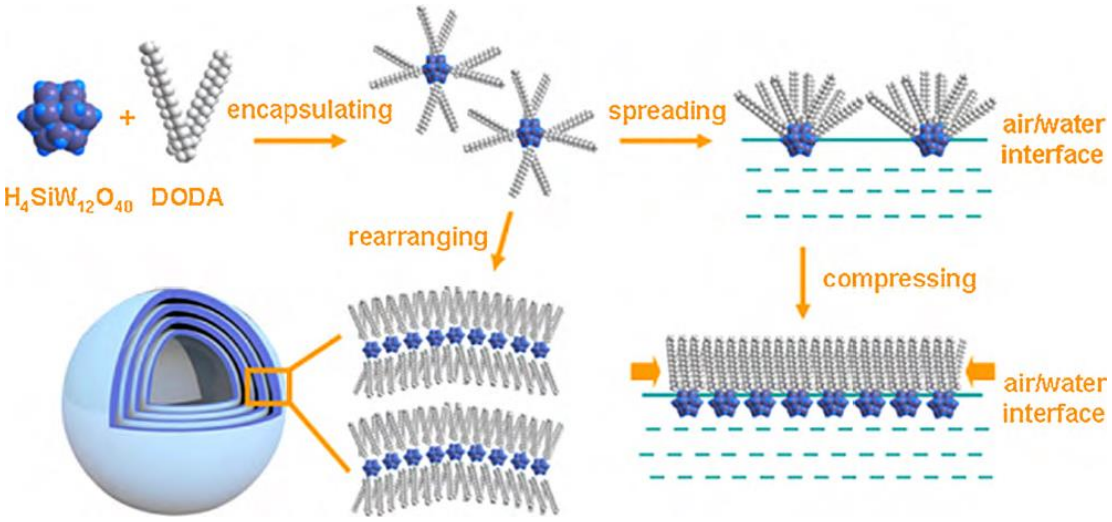

Figure 1.12. Assembly mechanism of $(DODA)_4SiW_{12}O_{40}$ under different conditions, including initial formation by encapsulation, inverted-vesicle assembly in organic solvent, and rearrangement at the air/water interface. Much work on the intercalation of various POMs into the interlayer of layered double hydroxides (LDHs), a kind of inorganic lamellar solids, and have investigated the catalytic properties of these materials.[45]

1.4.2.2. Langmuir—Blodgett technique

So far, several publications have been reported on the incorporation of POMs into the microspaces of LB films.[37] The fabrication of photoluminescent multibilayer composite films, consisting of a rare-earth-containing POM, $Na_9[EuW_{10}O_{36}]$ and dimethyldioctadecylammonium chloride (DODA), can be achieved by the ion-exchange method.[46]

The surfactant encapsulated POM[47] (SEP) is an organic- inorganic supramolecular complex. By co-condensation with the alkylorthosilicate, the SEP complexes were covalently doped into SiO_2 spheres. The hybrid silica spheres display obvious advantages: the complexes are well dispersed in the silica spheres uniformly and well fixed in inner spheres chemically; the POMs are located at the microenvironment formed by the hydrophobic surfactants; the structure and stability of POMs are well retained and the POMs in the hybrid spheres can communicate with outside stimulus, such as photoreduction, which can be employed for the in situ preparation of metal nanoparticles (MNPs). More significantly, the hybrid nanospheres integrated multicomponents, serving as the catalyst carrier, should be potentially useful for the oxidation and hydrolysis of some organic molecules through the synergetic catalysis of POMs and MNPs as well as the hydrophobic microenvironment.[48]

1.4.2.3. Layer-by-layer (LbL) assembly technique

The layer-by-layer (LbL) deposition technique, developed by Decher,[49a] falls into the category of template assisted assembly and involves the adsorption of a single species in each adsorption step. The resulting multilayer film has a defined layer sequence depending on the deposition sequence. The LbL assembly method provides a powerful tool for the formation and development of POM-based functional films and devices. The only requirement is that the inter-layer has sufficiently strong interactions in order to adsorb irreversibly at the interface. This approach has spread from laboratory to industry because it combines several advantages. In 1996, Kuhn and Anson[49b] firstly reported the deposits of multilayers of $Os(bpy)_3^{2+}$—$P_2Mo_{18}O_{62}^{6-}$ on different electrode surfaces by using this method. Later, Moriguchi et al.[49c] prepared the ultrathin films self-assembled from poly (diallyldimethylammonium) (PDDA) chloride and sodium decatungstate, and studied their electrochromic properties. Incorporation of nanoparticles into POM-containing multilayer films allows an interesting combination of the properties from both POMs and nanoparticles.

Wang et al. reported a new route to fabricate POM based nano-/micrometer composite films by the electrophoretic deposition (EPD) method, in which surfactant-encapsulated complexes (SEC) can be deposited on an ITO electrode from colloidal dispersion.[49d]

1.4.3. Applications of nano-sized POMs

Currently, catalysis and materials science are still the two main fields of applications of POMs. A major challenge in POM application is to devise general methods for constructing functional nano-scale architectures from these versatile building blocks. The integration of POMs into functional architectures and devices (Scheme 1.2), however, requires the development of methods to position, orient and integrate these nano-clusters in well-defined architectures, thin films, or meso phases. [49e]

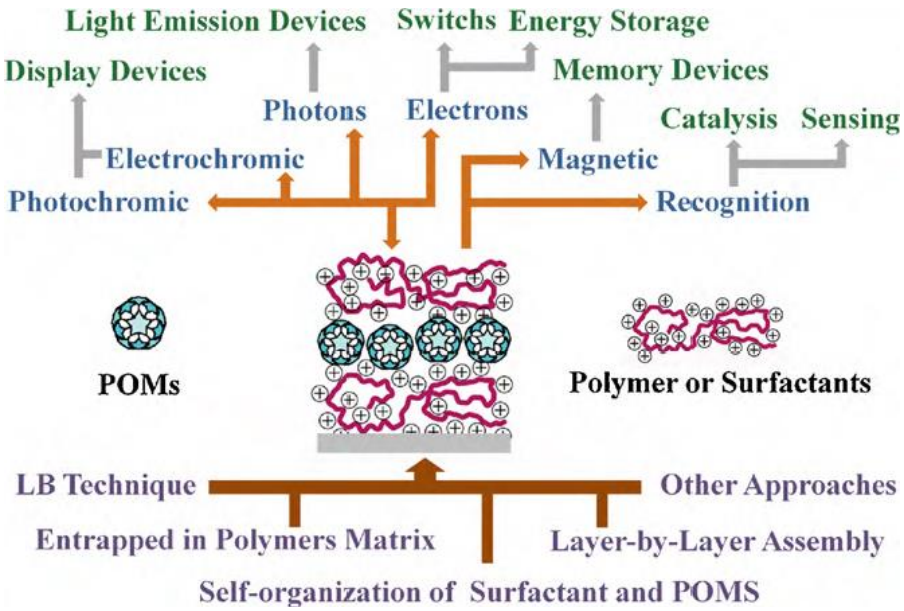

Scheme 1.2. Brief summary of preparation (bottom half) and application (top half) of POM-based nanostructured thin films. [49e]

1.4.3.1. Catalysis

Several groups reported the electrocatalytic application of POM-based composite films by LbL technique,[50] especially the multilayer films consisting of POMs and other types of nanomaterials like nanoparticles and carbon nanotubes.[51] For example, Dong and co-workers[51g] alternately deposited iron oxide nanoparticles and P_5W_{30} on quartz and ITO substrates. Kulesza et al. deposited platinum nanoparticles on electrocatalytic network films with POMs as inorganic templates,[51d-e] which showed remarkable electrocatalytical activity for the hydrogen evolution reaction. Ma and co-workers[50c] demonstrated that a composite film consisting of $K_3PMo_3W_9O_{40}$ and silver nanoparticles exhibited electrocatalytic activity towards the reduction of NO^{2-}, H_2O_2, ClO^{3-}, BrO^{3-} and IO^{3-} through tungsten-centered and molybdenum-centered redox processes of POM. Song and co-workers have prepared a nanotubular catalytic reactor composed of a parallel array of Pt-loaded POMs/polyelectrolyte nanotubes.[51f] The Pt based POM nanotubular reactor with smaller inside diameters showed higher catalytic activities for cyclohexene hydrogenation, indicating promising potential in designing reactors with specific sizes for specific reactions. Also, a hybrid carbon nanotube– POM can electrocatalytically oxidize methanol when the POM modified carbon nanotube electrode is coated by Pt–Ru

nanoparticles.[51h] The electrocatalytic activity of POM-based nanostructured films can be used for chemical (bio) sensing. For instance, Kurth and co-workers explored that some ordered POM-containing multilayer films had potential application for NO sensing.[52] Gu and co-workers demonstrated that the POM/TiO_2 film had great potential for gas sensitivity at lower temperatures.[53]

1.4.3.2. Photocatalyic activity of POM containing nanofilms

Several reports have also been made on photocatalytic application of POM-containing composite films. Cao and co-workers[54] have reported the LbL films incorporating Keggin-type POMs showed high photocatalytic activity to degradation of methyl orange.[49e]

1.4.3.3. Photoluminescent devices

Since an intramolecular energy transfer from the oxygen-to metal charge transfer (O→M CT) to a lanthanide cation can occur in the POM lattice, the photoluminescence (PL) behavior of some POMs-containing lanthanide cations is observed.[55] Xu et al.[56] incorporated several types of polyoxotungstoeuropate anions into ultrathin multilayer films and found that the PL behavior of the multilayer films was essentially identical to that of the POMs solids. Hu and co-workers have reported the photoluminescent properties of $Na_9[EuW_{10}O_{36}]$/PAH, $K_{17}[Eu(P_2W_{17}O_{61})_2]$/PAH and $K_{13}[Eu(SiW_{11}O_{39})_2]$/PAH multilayers.[57] Wu et al. found that polarized emission from the Eu^{3+} centers could be observed in the complexes of various Eu-containing POMs and DODA.[58] Furthermore, Zhang et al.[59] produced a range of inorganic sandwiched heteropolytungstomolybdate $K_{13}[Eu(SiW_9Mo_2O_{39})_2]$ and $[EuP_5W_{30}O_{110}]^{12-}$ with a series of commercial and novel cationic surfactants, and systematically investigated the effects of surfactants on luminescent properties.

1.4.3.4. Photo- and electrochromic devices

Interestingly, most POM-based composite films, especially POM LbL multilayers, exhibit excellent photochromic properties and good photochromic reversibility,[60] although only few pure POM solids have been reported to exhibit good reversible coloration. The Preyssler-type POM/poly (4-vinylpyridine) LbL multilayer could reversibly change color from transparent to blue by photo- and/or electroinduced stimulation.[60a] Zhang et al. investigated the electrochromic behavior of cast film of surfactant-encapsulated

$[EuP_5W_{30}O_{110}]^{12-}$ polyanion.[60b] The complexes of $[EuP_5W_{30}O_{110}]^{12-}$ polyanion with alkyl chain surfactants and viologens exhibited a visible and reversible electrochromism.

1.5. Motivation of the present work

Above mentioned discussion presents general over-view of POMs and their related topics. Since the time first POM based compounds discovered, the application of POMs as a material has been emerging step by step. Currently we are in the position to seek out such categories of materials with some unique properties. Further work on developing reliable and versatile functional materials with useful properties is essential. The studies on solid state properties of POMs-based crystalline materials in new perspectives open up unexplored solid state aspects on their possible applications in the interdisciplinary areas. In general, POMs are in anionic forms which can be isolated as crystalline material with appropriate cations and the properties of the same also can be tuned to a large extent.

This present work describes POM-based materials in terms of their synthesis, crystal structures in macro-size as well as nano-size and their possible studies. The mixed addenda Lindqvist anion containing compounds are known since 1960s and also important in the context of catalysis; these compounds are not well explored, so we have discussed such systems in chapter 2. Some of the mixed addenda Lindqvist clusters with organic ligand HMTA and also with transition metals were described. The decavanadate anion based clusters are well known in literature; there are huge numbers of compounds reported with various organic ligands and transition/alkali metals. The nano-sized decavanadate based clusters were not well explored, and thus motivated us to study the morphological variation of decavanadate based clusters using the sonochemical synthesis in various solvents as discussed in the chapter 3. Functionalized POMs gives rise to vast diversity of materials, used as building blocks for creating highly classy hierarchical systems with various interdependent functionalities. Presently, the functionalization of the POM cluster anions to explore more selective applications is more interesting scenario. The essential step in the assembly of functional POM frameworks has so far been achieved by using either organic linkers or by ligand supported transition metal bridges; both the approaches however are limited by the reduced framework stability intrinsic to metal–organic framework materials. Thus the assembly of purely inorganic POM based networks offers high potential for the formation of new type of materials. The planned synthesis of pure

inorganic based clusters, polyanion-polycation polymeric compounds is a big challenge in modern inorganic chemistry because of their essential applications in the various fields. The functionalization of the decavanadate anion gives different dimensionalities and also influences the properties of the resulting material. This motivated us to synthesize the pure inorganic cations like sodium, and transition metals as linking units in conjunction with larger isopolyoxometalates to construct the 1D to 3D frameworks containing compounds. These results have been discussed in the chapters 4 and 5.

1.6. References

1. Pope, M. T.; Müller, A. *Angew. Chem. Int. Ed.*, **1991**, *30*, 34.
2. Tiago, T.; Martel, P.; -Merino, C. G.; Aureliano, M. *Biochimica et Biophysica Acta*, **2007**, *1774*, 474.
3. Berzelius, J. *Pogg. Ann.*, **1826**, *6*, 369.
4. (a) Gmelin Handbuch der Anorganischen Chemie, Verlag Chemie, Berlin; System – No. 53 (Molybdan) **193**5; System-No. 54 (Wolfram) **1933**.
5. (a) Werner, A. *Z. Anorg. Chem.*, **1893**, *3*, 267; (b) Pauling, L. *J. Am. Chem. Soc.* **1929**, *51*, 2868.
6. (a) Keggin, J. F. *Nature* **1933**, *131*, 908; (b) Anderson, J. S. *Nature* **193**7, *140*, 850; (c) Evans, H. T., Jr., *J. Am. Chem. Soc.* **1948**, *70*, 1291; (d) Lindqvist, I. *Arkiv Kemi*. **1950**, *2*, 325; (e) Strandberg, R. *Acta Chem. Scand*. **1973**, *27*, 1004.
7. Evans, H. T., Jr., *Perspect. Struct. Chem.* **1971**, *4*, 1.
8. (a) Fuchs, J., *Z. Naturforsch.* ***1*973**, *B 28*, 389; (b) Filowitz, M.; Ho, R. K. C.; Klemperer, W. G.; Shum, W. *Inor. Chem.*, **1979**, *18*, 93.
9. (a) Suslick, K. S.; Cook, J. C.; Rapko, B.; Droege, M. W.; (b) Finke, R. G. *Inorg. Chem.*, **1986**, *25*, 241.
10. (a) Pope, M. T. *Heteropoly and Isopoly Oxometalates;* Springer-Verlag: Berlin, **1983**; (b) Hutin, M.; Rosnes, M. H.; Long, D. –L.; Cronin, L. *Polyoxometalates: synthesis and structure – from building blocks to emergent materials*; Glasgow, UK, **2013**.
11. Dexter, D. D.; Silverton, J. V. *J. Am. Chem. Soc.* **1968**, *90*, 3589.
12. Baker, L. C. W. *Advances in the chemistry of the coordination compounds,* Macmillan, New York, **1961**.

13. (a) Evans, H. T. *Acta Cryst.*, **1974**, *B30* ,2095; (b) Finkener, R. *Ber. Dtsch. Chem. Ges.* **1878**, *11*, 1638; (c) Rosenheim, A.; Jahn, H. *Ber. Dtsch. Chem. Ges.* **1893**, *26*, 1191; (d) Friedheim, C.; *Z. Anorg. Chem.* **1894**, *6*, 11; (e) Friedheim, C. *Z. Anorg. Chem.* **1894**, *6*, 27; (f) Prandtl, W. *Z. Anorg. Allg. Chem.* **1915**, *92*, 198; (g) Chauveau, F.; Souchay, P. *Bull. Soc. Chim.* **1963**, *3*, 561; (h) Flynn, C.M.; Pope, M.T. *Inorg. Chem.* **1971**, *10*, 2524; (i) Flynn, C.M.; Pope, M.T. *Inorg. Chem.* **1973**, *12*, 1626; (j) Thouvenot, R.; Doctoral Dissertation, Université Pierre et Marie Curie, Paris, **1978**; (k) Dabbabi, M.; Boyer, M. J. *Inorg. Nucl. Chem.* **1976**, *38*, 1011; (l) Flynn, Jr. C.M.; Pope, M. T. *Inorg. Chem.* **1971**, *10*, 2745; (m) Franca, M.C.K.; Eon, J.G.; Fournier, M.; Payen, E.; Mentre, O. *Solid State Sci.* **2005**, *7*, 1533; (n) Rossotti, F. J.; Rossotti, H. *Acta Chemica Scandinavica* **1956**, *10*, 957; (o) Evans Jr., H. T. *Inorg. Chem.* **1966**, *5*, 967.

14. (a) Pope, M. T.; O'Donnell, S. E.; Prados, R. A. *J. Chem. Soc. Chem.Comm.*, **1975**, 22; (b) Baker, L.C.W.; Baker, V.E.S.; Eriks, K.; Pope, M.T.; Shibata, M.; Rollins, O.W.; Fang, J.H.; Koh, L.L. *J. Am. Chem. Soc.* **1966**, *88*, 2329; (c) Flynn, C. M.; Pope, M.T. *Inorg. Chem.***1972**, *11*, 1950; (d) Neumann, R.; Lissel, M. *J. Org. Chem.* **1989**, *54*, 4607; (e) Shivaiah, V.; Hajeebu, S.; Das, S. K. *Inorg. Chem. Commun.* **2002**, *5*, 996; (f) Baess, C.F.; Mesmer, R.E. *Hydrolysis of cations*; Wiley: New York, NY, USA, **1976**; (g)Tracey, A.S.; Crans, D.C. *Vanadium Compounds*. Washington D.C.: American Chemical Society. **1998**; (h) Rehder, D. *Bioinorganic Vanadium Chemistry*. Wiley & Sons. **2008**, 13; (i) Livage, J. *Materials* **2010**, *3*, 4175.

15. (a) Jahr, K. F.; Fuchs, J. *Chem. Ber.*, **1963**, *96*, 2457; (b) Fuchs, J.; Jahr, K. F. *Chem. Ber.*, **1963**, *96*, 2460; (c) Fuchs, J.; Jahr, K. F. *Chem. Ber.*, **1963**, *96*, 2472.

16. Rhule, J. T.; Hill, C. L.; Judd, D. A.; Schinazi, R. F. *Chem. Rev.* **1998**, *98*, 327.

17. (a) Burkholder, E.; Golub, V.; P'Connor, C. J.; Zubieta, J. *Inorg. Chem. Commun.*, **2004**, *7*, 363; (b) Soghomonian, V.; Chen, Q.; Haushalter, R. C.; Zubieta, J.; O'Connor, C. J. *Science*, **1993**, *259*, 1596; (c) Kanoo, P.; Ghosh, A. C.; Maji, T. K. *Inorg. Chem.*, **2011**, *50*, 5145; (d) Duraisamy, T.; Ramanan A.; Vittal, J. J. *Crystal Engineering*, **2000**, *3*, 237; (e) Duraisamy, T.; Ojha, N.; Ramanan A.; Vittal, J. J. *Chem. Mater.*, **1999**, *11*, 2339.

18. (a) Brégeault, J. –M. *J. Chem. Soc., Dalton Trans.*, **2003**, 3289; (b) Katsoulis, D. E. *Chem. Rev.* **1998**, *98*, 359.

19. Kamata, K.; Yonehara, K.; Nakagawa, Y.; et al. *Nature Chem.* **2010**, *2*, 478.
20. Kikukawa, Y.; Yamaguchi, S.; Nakagawa, Y.; *J. Am. Chem. Soc.* **2008**, *130*, 15872.
21. Ettedgui, J.; Neumann, R. *J. Am. Chem. Soc.* **2009**, *131*, 4.
22. Ettedgui, J.; Diskin-Posner, Y.; Weiner, L.; *J. Am. Chem. Soc.* **2011**, *133*,188.
23. Macht, J.; Janik, M. J.; Neurock, M.; *J. Am. Chem. Soc.* **2008**, *130*, 10369.
24. Kreutz, J. E.; Shukhaev, A.; Du, W.; et al. *J. Am. Chem. Soc.* **2010**, *132*, 3128.
25. (a) Clemente-Juan, J. M.; Coronado, E.; Gaita-Arino, A. *Chem. Soc. Rev.* **2012**, *41*, 7454; (b) Day, V. W.; Klemperer, W. G.; Yaghi, O. M. *J. Am. Chem. Soc.* **1989**, *111*, 5959; (c) Barra, A. L.; Gatteschi, D.; Pardi, L.; Müller, A.; Doring, J. *J. Am. Chem. Soc.* **1992**, *114*, 8509.
26. (a) Glezos, N.; Velessiotis, D.; Chaidogiannos, G.; Argitis, P.; Tsamakis, D.; Zianni, X. *Synth. Met.* **2003**, *138*, 267; (b) Chaidogiannos, G; Velessiotis, D.; Argitis P.; Koutsolelos, P.; Diakoumakos, C. D.; Tsamakis, D.; Glezos, N. *Microelectron. Eng.* **2004**, *73-74*, 746; (c) Glezos, N.; Argitis, P.; Velessiotis, D.; Diakoumakos, C. D. *Appl. Phys. Lett.* **2003**, *83*, 488.
27. Velessiotis, D.; Glezos, N.; Ioannou-Sougleridis, V. *J. Appl. Phys.* **2005**, *98*, 084503.
28. Aureliano, M.; Fraqueza, G.; Ohlin, C. A. *Dalton Trans.*, **2013**, *42*, 11770.
29. Yamase, T. *Mole. Eng*. **1993**, *3*, 241.
30. Hill, C. L.; Hartnup, M.; Faraj, M.; Weeks, M.; Prosser-Mccartha, C. M.; Brown Jr, R. B.; Kadkhodayan, M.; Sommadossi, J, –P,; Schinazi, R. F. In Advances in Chemotherapy of AIDS; Diasio, R. B.; Sommadossi, J. –P. Eds.; Pergamon Press, Inc.: New York, **1990**.
31. Yosov, A. B.; Shilov, V. P. *Radiochemistry*, **1999**, *41*, 3.
32. (a) Wassermann, K.; Pope, M. T.; Salmen, M.; Dann, J. N.; Lunk, H. –J. *J. Solid State Chem.* **2000**, *149*, 378; (b) Pope, M. T.; Wei, X.; Wassermann, K.; Dickman, M. H. C. R. *Acad. Sci., Ser. IIc* **1998**, *I*, 297; (c) Wassermann, K.; Dickman, M. H.; Pope, M. T. *Angew. Chem. Int. Ed.*, **1997**, *36*, 1445.
33. (a) Kremlyakova, N. Y.; Novikov, A. P.; Myasoedov, B. F.; Katargin, N. V. *J. Radioanal. Nucl. Chem.*, **1990**, *145*, 183; (b) Molochnikova, N. P.; Frenkel, V. Y.; Myasoedov, B. F. *Radiokhimiya*, **1989**, *31*, 65.

34. Rao, A. S.; Arumuganathan, T.; Shivaiah, V.; Das, S. K. *J. Chem. Sci.* **2011**, *123*, 229.

35. Zhang, J. Z. *Acc. Chem. Res*. **1997**, *30*, 423.

36. (a) Pitkethly, M. J. *Nanotoday* **2004**, *7*, 20; (b) McGlone, T. ; Streb, C.; -Fite, M. B.; Yan, J.; Gabb, D.; Long, D. –L.; Cronin, L. *Cryst. Growth Des.*, **2011**, *11*, 2471.

37. (a) Troupis, A.; Hiskia, A.; Papaconstantinou, E. *Angew. Chem., Int. Ed*. **2002**, *41*, 1911; (b) Sanyal, A.; Mandal, S.; Sastry, M. *Adv. Funct. Mater.* **2005**, *15*, 273; (c) Zhang, G. J.; Keita, B.; Dolbecq, A.; Mialance, P.; S_echeresse, F.; Miserque, F.; Nadjo, L. *Chem. Mater.* **2007**, *19*, 5821; (d) Mandal, S.; Selvakannan, P. R.; Pasricha, R.; Sastry, M. *J. Am. Chem. Soc.* **2003**, *125*, 8440; (e) Yang, L. B.; Shen, Y. H.; Xie, A. J.; Liang, J. J.; Zhu, J. M.; Chen, L. *Eur. J. Inorg. Chem.* **2007**, 1128.

38. (a) Zhang, L.; Shen, Y. H.; Xie, A. J.; Li, S. K.; Wang, C. *Mater. Chem.* **2008**, *18*, 1196; (b) Kishore, P. S.; Viswanathan, B.; Varadarajan, T. K. *Nanoscale Res.Lett.* **2008**, *3*, 14; (c) M.; Liu, C. L.; Xu, Y.; Li, W.; Wu, L. X. *Colloids Surf. A* **2009**, *333*, 46.

39. Kida, T. *Langmuir* **2008**, *24*, 7648.

40. Qi, W.; Li, H. L.; Wu, L. X. *Phys. Chem. B* **2008**, *112*, 8257.

41. Qi, W.; Li, H. L.; Wu, L. X. *Adv. Mater.* **2007**, *19*, 1983.

42. Mekala, R.; Supriya, S.; Das, S. K. *Inorg. Chem.* **2013**, *52*, 9708; (b) Sadakane, M.; Steckhan, E. *Chem. Rev.* **1998**, *98*, 219.

43. (a) Clemente-León, M.; Coronado, E.; Galán-Mascarós, J.R.; Giménez-Saiz, C.; Gómez-GarcIa, C.J.; Fernández-Otero, T. *J. Mater. Chem.***1998**, *8*, 309; (b) Gómez-Romero, P.; Cuentas-Gallegos, K.; Lira-Cantú, M.; Casa˜n-Pastor, N. *J. Mater. Sci.* **2005**, *40*,1423.

44. (a) Hu, C. W.; He, Q.L.; Zhang, Y. H.; Wang, E.B. *Catal. Today*, **1996**, *30*, 141; (b) Hu, C. W., He, Q. L.; Zhang, Y.H.; Liu, Y.Y.; Zhang, Y. F.; Tang, T.D.; Zhang, J. Y.; Wang, E. B. *Chem. Commun.*, **1996**, 121; (c) Liu, Y.Y.; Hu, C.W.; Wang, Z. P.; Zhang, J. Y.; Wang, E.B. *Sci. China*, Ser. B, **1996**, *39*, 1, 86; (d) Hu, C.W.; Zhang, X. ; Xu, L.; Mu, B. L.; Zu, W. ; Wang, E. B. *Appl. Clay Sci.*, **1998**, *11*, 5– 6, 495; (e) Hu, C.W.; Zhang, X.; Wang, E. B. *Trans. Met. Chem.*, **1997**, *22*, 197; (f) Hu, C.W.; He, Q. L.; Wang, E.B. *Prog. Nat. Sci.*, **1996**, *6*, 5, 524; (g) Guo,

Y. H.; Li, D. F.; Hu, C.W.; Wang, Y. H.; Wang, E. B. *Appl. Catal. B*, **2001**, *30*, 3 – 4, 337.

45. Li, H.; Sun, H.; Qi, W.; Xu, M.; Wu, L. *Angew. Chem. Int. Ed.* **2007**, *46*, 1300.
46. Ichinose, I.; Asai, T.; Yoshimura, S.; Kimizuka, N.; Kunitake, T. *Chem. Lett.*, **1994**, 1837.
47. Zhao, Y.; Qi, W.; Li, W.; Wu, L. *Langmuir*, **2010**, *26*, 4437.
48. (a) Maayan, G.; Neumann, R. *Chem. Commun.* **2005**, 4595; (b) Hetterley, R. D.; Kozhevnikova, E. F.; Kozhevnikov, I. V. *Chem. Commun.* **2006**, 782; (c) De bruyn, M.; Neumann, R. *Adv. Synth. Catal.* **2007**, *349*, 1624; (d) Boujday, S.; Blanchard, J.; Villanneau, R.; Krafft, J.–M.; Geantet, C.; Louis, C.; Breysse, M.; Proust, A. *Chem. Phys. Chem.* **2007**, *8*, 2636; (e) Inumaru, K.; Ishihara, T.; Kamiya, Y.; Okuhara, T.; Yamanaka, S. *Angew. Chem., Int. Ed.* **2007**, *46*, 7625; (f) Jiang, C. J.; Lesbani, A.; Kawamoto, R.; Uchida, S.; Mizuno, N. *J. Am. Chem. Soc.* **2006**, *128*, 14240; (g) Mandal, S.; Das, A.; Srivastava, R.; Sastry, M. *Langmuir* **2005**, *21*, 2408.
49. (a) Decher, G. *Science* **1997**, *277*, 1232; (b) Kuhn, A.; Anson, F.C. *Langmuir* **1996**, *12*, 5481; (c) Moriguchi, I. ; Fendler, J.H. *Chem. Mater*.**1998**, *10*, 2205; (d) Wang, Y.; Xu, L.; Jiang, N.; Xu, B.; Gao, G.; Li, F. *J. Colloid Inter. Sci.* **2009**, *333*, 771; (e) Liua, S.; Tang, Z. *Nano Today* **2010**, *5*, 267.
50. (a) Liu, S.Q. ; Volkmer, D.; Kurth, D.G. *J. Cluster Sci.* **2003**, *14*, 405.; (b) Huang, M.H.; Bi, L.H.; Shen, Y.; Liu, B.F.; Dong, S.J. *J. Phys. Chem. B*, **2004**, *108*, 9780.
51. (a) Gu, Y. ; Ma, H.Y.; O'Halloran, K.P.; Shi, S.L.; Zhang, Z.J.; Wang, X.G. *Electrochim. Acta*, **2009**, *54*, 7194; (b) Li, C.X.; O'Halloran, K.P.; Ma, H.Y.; Shi, S.L. *J. Phys. Chem. B*, **2009**, *113*, 8043.; (c) Qian, L.; Yang, X.R. *Electrochem. Commun.* **2005**, *7*, 547; (d) Kulesza, P.J.; Chojak, M.; Karnicka, K.; Miecznikowski, K.; Palys, B.; Lewera, A. *Chem. Mater.*,**2004**, *16*, 4128; (e) Karnicka, K.; Chojak, M.; Miecznikowski, K.; Kulesza, P.J. *Bioelectrochemistry*, **2005**, *66*, 79; (f) Ma, Z.; Liu, Q. ; Cui, Z.M.; Bian, S.W.; Song, W.G. *J. Phys. Chem. C*, **2008**, *112*, 8875; (g) M.H. Huang, L.H. Bi, Y. Shen, B.F. Liu, S.J. Dong, *J. Phys. Chem. B*, **2004**, *108*, 9780; (h) Pan, D. W.; Chen, J. H.; Tao, W. Y.; *Langmuir* **2006**, *22*, 5872.
52. Liu, S.Q.; Volkmer, D.; Kurth, D.G. *Anal. Chem.* **2004**, *76*, 4579.
53. Li, D. F.; Gu, C.Z.; Guo, C.X.; Hu, C.W. *Chem. Phys. Lett.* **2004**, *385*, 55.

54. Li, T.H.; Gao, S.Y.; Li, F.; Cao, R. *J. Colloid Interface Sci.*, **2009**, *338*, 500.

55. Yamase, T. *Chem. Rev.* **1998**, *98*, 307.

56. (a) Xu, L.; Zhang, H. Y.; Wang, E. B.; Wu, A. G.; Li, Z. *Mater. Chem.Phys.* **2003**, *77*, 484; (b) Xu, L.; Zhang, H. Y.; Wang, E.; Kurth, D.G.; Li, Z. *J. Mater. Chem*.**2002**, 12, 654.

57. Wang, Y.; Wang, X.; Hu, C.; Shi, C. *J. Mater. Chem.* **2002**, *12*, 703.

58. (a) Bu, W.; Li, H.; Li, W.; Wu, L.; Zhai, C.; Wu, Y. *J. Phys. Chem. B*, **2004**, *108*, 12776; (b) Li, W.; Yi, S.; Wu, Y.; Wu, L. *J. Phys. Chem. B* **2006**, *110*, 16961.

59. (a) Zhang, T. R.; Liu, S.Q.; Faul, C. F. J.; Kurth, D. G. *Adv. Funct. Mater.* **2009**, *19*, 642; (b) Zhang, T. R.; Spitz, C.; Antonietti, M.; Faul, C. F. J. *Chem. Eur. J.* **2005**, *11*, 1001.

60. (a) Zhang, G. J. ; Chen, Z. H.; He, T. ; Ke, H. H.; Ma, Y.; Shao, K. *J. Phys. Chem. B* **2004**, *108*, 6944; (b) Liu, S.Q.; Möhwald, H.; Volkmer, D.; Kurth, D. G.; *Langmuir*, **2006**, *22*, 1949.

Synthesis and structural characterization of Lindqvist type mixed-metal cluster anion $[V_2W_4O_{19}]^{4-}$ in discrete and coordination polymer compounds

2

Chapter 2 describes four vanadium substituted Lindqvist type tungsten heteropolyanion containing compounds with molecular formulae $[HMTAH]_2[H_2V_2W_4O_{19}]\cdot 4H_2O$ (1), $[Na_2(H_2O)_4]_n[H_2V_2W_4O_{19}]_n\cdot 2nHMTA\cdot 2nH_2O$ (2), $[HMTAH]_{2n}[Na_2(H_2O)_8(V_2W_4O_{19})]_n\cdot 4nH_2O$ (3), $[HMTAH]_2[Cu(H_2O)_6][V_2W_4O_{19}]\cdot 4H_2O$ (4), where HMTA is hexamethylene-tetramine. Compounds 1 and 4 are discrete, whereas, compounds 2 and 3 are coordination polymers. Compounds 1-4 are characterized by routine elemental analyses, FT-IR spectroscopy and single crystal X-ray crystallography. The presence of vanadium in the cluster anion is confirmed by ^{51}V NMR spectroscopy, EDS and ICP analyses. The crystal structures of compounds are refined in orthorhombic space group Immm (compound 1), monoclinic space group C2/c (compound 2) and triclinic space group P-1(compounds 3-4). In the crystal structure of compound 1, the supramolecular architecture is characterized by C–H···O and O···O weak interactions. Compound 2 has a 3-dimensional framework, based on the coordination of sodium aqua-complex with the $[V_2W_4O_{19}]^{4-}$ cluster anion and hexamethylenetetramine, whereas compound 3 is a 1-dimensional coordination polymer, based on the coordination of di-sodium aqua-complex cation with the cluster anion. Compound 4 is a discrete compound with the $[V_2W_4O_{19}]^{4-}$ cluster anion, protonated hexamethylenetetramine and hexa-hydrated copper complex cations.

2.1. Introduction

A variety of shapes, sizes, charges and constituting metals of POMs make them promising materials in diverse research areas, such as, catalysis, materials-, medicinal- and analytical chemistry, nano-science and magneto-chemistry.[1-6] Among the POMs, some polyoxovanadates,[6-7] polyoxotungsates[8-9] and vanadium substituted polyoxotungstates[10] are biologically important compounds. POM clusters offer diverse architectures with different charge, shapes and sizes, which are interesting in supramolecular relevance.[11-12] In several cases, it is possible to change the anionic charge of the POM cluster anions, keeping unchanged their structures.[13-14] The variation of charges and large size of the isopolyanion (IPA) type POM anion with amine ligands make them promising building units for the self assembly resulting in two-dimensional and three-dimensional networks containing compounds. Among this series of IPAs, a great number of studies were particularly focused on Lindqvist type anions of general formula $M'_xM_{(6-x)}O_{19}^{n-}$ (M' = V, Nb, Ta, Mo; M = W, Mo). Furthermore, the substitution of addenda atoms, e.g., W^{6+} by V^{5+} or Nb^{5+}, modifies the anionic charge of the cluster, leading to a complex chemistry, when the stability of the species $M'_xM_{(6-x)}O_{19}^{n-}$ is strongly dependent on pH and the nature of M and M' ions. The early literature had described a variety of vanadium–tungsten heteropoly complexes including the species with V:W mole ratio of 1:2. The existence of $[V_2W_4O_{19}]^{4-}$ species in solution was confirmed by Chauveau[15]; later Flynn and Pope[16-19] proposed this cluster in solution at the pH 4-7. In recent time, there are several reports, based on $[V_2W_4O_{19}]^{4-}$ cluster anion, that are characterized by single crystal X-ray diffraction studies; however, all these di-substituted cluster anions are crystallographically disordered, [20-25] where definite positions of vanadium cannot be located. Extended structures (for example, coordination polymers), based on mixed addenda POMs, are not much explored. In the relevant reported crystal structure of compound $(NH_4)_2Na_3(V_3W_3O_{19})(H_2O)_{12}$, the mixed addenda Lindqvist clusters align in one-dimensional chains, whereas, the compound $Na(TMA)_2(VW_5O_{19})(H_2O)$ shows three-dimensional network in its crystal structure.[26-28]

The compounds described in this chapter are

$[HMTAH]_2[H_2V_2W_4O_{19}]\cdot 4H_2O$ (**1**)

$[Na_2(H_2O)_4]_n[H_2V_2W_4O_{19}]_n\cdot 2n HMTA\cdot 2nH_2O$ (**2**)

$[HMTAH]_{2n}[Na_2(H_2O)_8(V_2W_4O_{19})]_n\cdot 4nH_2O$ (**3**)

$[HMTAH]_2[Cu(H_2O)_6][V_2W_4O_{19}]\cdot 4H_2O$ (**4**)

The four compounds are based on mixed-addenda Lindqvist type cluster anion $[V_2W_4O_{19}]^{4-}$, which is nothing but di-vanadium substituted hexatungstate anion. Compounds **1**, **4** are discrete compounds and compounds **2** and **3** are coordination polymers.

2.2. Experimental Section

2.2.1. Materials and Methods

All the reactions were performed in an ambient condition. The starting materials, sodium metavanadate, sodium tungstate dihydrate, oxalic acid, nickel chloride hexahydrate, HMTA were obtained from SISCO, Loba Chem. and distilled water was used throughout the experiment. Micro analytical (C, H, N) data were obtained with a FLASH EA 1112 Series CHNS Analyzer. Infrared (IR) spectra were recorded on KBr pellets with a JASCO FT/IR-5300 spectrometer in the region of 400–4000 cm^{-1}. Field emission scanning electron microscope (FESEM) imaging with energy dispersive X-ray spectroscopy (EDS) was carried out on a Carl Zeiss model Ultra 55 microscope. ^{51}V NMR spectra were recorded on Bruker DRX–400 spectrometer using $VOCl_3$ as an internal standard. The relevant sample was prepared by dissolving in DMSO–d_6. The metal contents of the sample were analyzed using a Varian 720-ES Inductively Coupled Plasma-Optical Emission Spectrometer (ICP-OES) for the composition. Sample for the concerned analysis was prepared by dissolving a known weight of the crystals in 100 mL DMSO.

2.2.2. Synthesis

2.2.2.1. Synthesis of compound $[HMTAH]_2[H_2V_2W_4O_{19}]\cdot 4H_2O$ (**1**)

A mixture of sodium tungstate dihydrate (7.0 g, 21.2 mmol), sodium metavanadate (2.0 g, 16.4 mmol) in 100 mL water was kept at 70 °C for one day; to this pale yellow solution, conc. hydrochloric acid was added to maintain the pH 5.0 followed by the addition of

10 mL aqueous solution of hexamine (2.0 g, 14.2 mmol). It was then concentrated to 50 mL and then it was kept at an open condition for crystallization. Orange colored crystals were noticed in the solution after 24 h, and washed with water followed by acetone and dried in air. Yield: (1.0 g). CHN analysis: Anal. calcd. (%) for $C_{12}H_{36}N_8O_{23}V_2W_4$: C, 9.62; H, 2.42; N, 7.48; V, 6.80; W, 49.10. Found C, 9.55; H, 2.45; N, 7.46; V, 6.59 (ICP); W, 49.12 (ICP). IR (KBr pellet) (υ/cm^{-1}) for **1**: 3368 (br), 1653 (m), 1467 (m), 1388 (w), 1317(w), 1263(s), 1147(sh), 1097(sh), 1043(sh), 1020(sh), 993(sh), 958(s), 796(s), 661(w), 592(m), 505(w), 445(m) (w, weak; br, broad; m, medium; s, strong; sh, shoulder).

2.2.2.2. Synthesis of compound $[Na_2(H_2O)_4]_n[H_2V_2W_4O_{19}]_n \cdot 2n\text{HMTA} \cdot 2nH_2O$ (**2**)

The same synthetic procedure was used to synthesize **2** as that for **1** except oxalic acid (1.0 g, 7.9 mmol) was added and pH was maintained at 5.0 using acetic acid. Orange colored-crystals were formed after one week that were filtered and washed with water followed by acetone and dried in air. Yield: (1.5 g) CHN analysis: Anal. calcd. (%) for $C_{12}H_{38}N_8O_{25}Na_2V_2W_4$: C, 9.14; H, 2.42; N, 7.10; Na, 2.91; V, 6.46 ; W, 46.61. Found C, 9.16; H, 2.44; N, 7.17, Na, 3.01 (ICP); V, 6.11 (ICP); W, 45.33(ICP). IR (KBr pellet)(υ/cm^{-1}) for **2**: 3410(br), 3184(br), 1653(m), 1419(s), 1390(sh), 1249(s), 1147(m), 1039(sh), 1014(sh), 991(sh), 956(s), 856(m), 827(br), 746(m), 655(w), 592(m), 503(w), 468(w)(w, weak; br, broad; m, medium; s, strong; sh, shoulder).

2.2.2.3. Synthesis of compound $[HMTAH]_{2n}[Na_2(H_2O)_8(V_2W_4O_{19})]_n \cdot 4nH_2O$ (**3**)

The same synthetic procedure was used to synthesize **3** as that for **1** except nickel chloride hexahydrate (1.0 g, 4.2 mmol) was added and pH is maintained at 5.0 using acetic acid. Yellow color crystals were formed after one week, filtered and washed with water followed by acetone and dried in air. Yield: (1.3 g) CHN analysis: Anal. calcd. (%) for $C_{12}H_{50}N_8O_{31}Na_2V_2W_4$: C, 8.54; H, 2.98; N, 6.64; Na, 2.73; V, 6.04; W, 43.62. Found C, 8.74; H, 2.99; N, 6.17; Na, 2.85; V, 6.21 (ICP); W, 43.52 (ICP).. IR (KBr pellet)(υ/cm^{-1}) for **3**: 3369(br), 2988(w), 1651(m), 1467(m), 1390(m), 1356(w), 1249(s), 1147(m), 993(sh), 958(br), 827(sh), 792(br), 644(m), 596(w), 507(w), 439(m).

2.2.2.4. Synthesis of compound $[HMTAH]_2[Cu(H_2O)_6][V_2W_4O_{19}] \cdot 4H_2O$ (**4**)

The same synthetic procedure was used to synthesize **4** as that for **1** except cupric chloride dihydrate (1.0 g, 5.8 mmol) was added and pH is maintained at 5.0 using acetic acid.

Yellow color crystals were formed after one week, filtered and washed with water followed by acetone and dried in air. Yield: (1.6 g) CHN analysis: Anal. calcd. (%) for $C_{12}H_{46}N_8O_{29}CuV_2W_4$: C, 8.64; H, 2.78; N, 6.72; V, 6.11; Cu, 3.81; W, 44.10. Found C, 8.62; H, 2.99; N, 6.77; V, 6.17 (ICP); Cu, 3.86 (ICP); W, 44.18 (ICP). IR (KBr pellet)(υ/cm^{-1}) for **4**: 3369(br), 2988(w), 1651(m), 1467(m), 1390(m), 1356(w), 1249(s), 1147(m), 993(sh), 958(br), 827(sh), 792(br), 644(m), 596(w), 507(w), 439(m).

2.2.3. Single crystal X-ray structure determination of the compounds 1-4

The data were collected at 298(2) K on a Bruker SMART APEX CCD area detector system [λ(Mo-K_α) = 0.71073 Å], graphite monochromator, 2400 frames were recorded with an ω scan width of 0.3^o, each for 10 s, crystal-detector distance 60 mm, collimator 0.5 mm. The data were reduced by using SAINTPLUS[29] and a multi-scan absorption correction using SADABS[29] was performed. Structure solution and refinement were done using programs of SHELX-97.[30] All non hydrogen atoms were refined anisotropically. Hydrogen atoms on the C atoms of the hexamine were introduced on calculated positions and were included in the refinement riding on their respective parent atoms. Hydrogen atoms of the crystal water could not be found in the crystal structures of compounds **1** and **2**. The crystallographic information of compounds **1**, **2** and **3** has been listed in Table 2.3, whereas for the compound **4** has been listed in Table 2.10.

2.3. Results and discussion

2.3.1. Synthesis

Compounds **1-4** have been synthesized by a direct one pot reaction of sodium metavanadate, sodium tungstate dihydrate with hexamine at temperature 70 $^\circ$C in an acidic aqueous medium. It was reported in the literature that the best pH range for the preparation of $[V_2W_4O_{19}]^{4-}$ cluster compounds was around 5.0, that has been maintained in our present synthesis. Compounds **1** and **2** have been synthesized from an aqueous medium of pH 5, varying different acids and other ingredients of the reaction medium. The strong acid favors the formation of discrete compound **1**, where as the weaker acid supports the formation of extended structure (coordination polymer) in compound **2**. Even though oxalic acid has been used in the synthesis of compound **2**, it does not exist in the relevant crystal structure. Also nickel chloride hexahydrate is used in the synthesis of compound **3**,

though it does not exist in crystal structure of compound **3.** However, without using the oxalic acid and nickel chloride hexahydrate during the syntheses of respective compounds, compounds **2** and **3** cannot be isolated.

2.3.2. Infrared spectroscopy

The IR spectra of compounds **1, 2, 3** and **4** are very similar due to the presence of a common di-vanadium substituted Lindqvist anion $[V_2W_4O_{19}]^{4-}$ and hexamethylenetetramine in all the four compounds, that show characteristic vibrational bands for classic Lindqvist type POM structure. The spectra of the compounds **1**, **2**, **3** and **4** are similar to those for compounds $K_4V_2W_4O_{19}\cdot 8H_2O$[16], $Co(H_2O)_6K_2V_2W_4O_{19}$[22] and $[Co(H_2O)_6]_2V_2W_4O_{19}$[22] reported earlier and the relevant important IR bands have been tabulated in Table 2.1.

Table 2.1. Selected IR data (in cm^{-1}) for compounds $K_4V_2W_4O_{19}\cdot 8H_2O$, $Co(H_2O)_6K_2V_2W_4O_{19}$, $[Co(H_2O)_6]_2V_2W_4O_{19}$, compounds **1**, **2**, **3** and **4**.

	ν M–O_t		ν_{as}M–O_b	ν_s M–O_b	
$K_4V_2W_4O_{19}\cdot 8H_2O$	1005(m)	970 (s)	790 (vs)	590 (m)	440 (s)
$Co(H_2O)_6K_2V_2W_4O_{19}$	990 (m)	957 (s)	787 (vs)	590 (m)	442 (s)
$[Co(H_2O)_6]_2V_2W_4$	962 (m)	962 (s)	787 (vs)	591 (m)	440 (s)
Compound 1	993 (sh)	958 (s)	796 (s)	592 (m)	445 (m)
Compound 2	991 (sh)	956 (s)	746 (m)	592 (m)	468 (w)
Compound 3	993 (sh)	958 (br)	792 (br)	596 (w)	439 (m)
Compound 4	1005 (m)	945 (m)	765 (s)	603 (m)	420 (m)

The broad bands around 3368 cm^{-1} (compound **1**), 3410 cm^{-1} (compound **2),** 3369 cm^{-1} (compound **3**) and 3063 cm^{-1} (compound **4**) can be ascribed to the absorptions of lattice water molecules and coordinated water molecules. The two C−N stretching modes 1263

cm^{-1}, 1020 cm^{-1} (compound **1**), 1249 cm^{-1}, 1014 cm^{-1} (compound **2**), 1249 cm^{-1}, 1043 cm^{-1} (compound **3**), 1211 cm^{-1}, 1037 cm^{-1} (compound **4**) as well as $-CH_2$ wagging and $-CH_2$ deformation modes 1388 cm^{-1}, 1467 cm^{-1} (compound **1**), 1390 cm^{-1}, 1419 cm^{-1} (compound **2**), 1390 cm^{-1}, 1467 cm^{-1} (compound **3**) and 1440 cm^{-1}, 1485 cm^{-1} (compound **4**) are assigned to hexamethylenetetramine, which is present in all the compounds. The stretching modes for terminal oxygen atoms (W/V=O_t bonds) of the cluster anion appear at 993 cm^{-1}, 958 cm^{-1} (compound **1**), 991 cm^{-1}, 956 cm^{-1} (compound **2**), 993 cm^{-1}, 958 cm^{-1} (compound **3**) and 1005 cm^{-1}, 945 cm^{-1} (compound **4**). Among the bridging oxygen atoms, the asymmetric modes of W/V–O_b bonds appear at 796 cm^{-1} (compound **1**), 746 cm^{-1} (compound **2**), 792 cm^{-1} (compound **3**) and 765 cm^{-1} (compound **4**); the relevant symmetric modes appear at 592 cm^{-1}, 445 cm^{-1} (compound **1**), 592 cm^{-1}, 468 cm^{-1} (compound **2**), 596 cm^{-1}, 439 cm^{-1} (compound **3**) and 603 cm^{-1}, 420 cm^{-1} (compound **4**). The cation–anion supramolecular interactions in the four compounds are reflected by some shift of these IR bands to relatively lower wave numbers.[24,27]

The stoichiometric compositions of the oxoanions in compounds **1**, **2**, **3** and **4** are consistent with those in previously reported similar di-vanadium hexatungstate cluster anions. The positional disorder with respect to the vanadium atoms, which is present in the crystal structures, is quite common for the substituted hetero-polyanions. The single crystal X-ray data can be explained assuming the random orientation of vanadium atoms in the tungsten frame work. The stoichiometry of the substituted heteropolyanions in the single crystal X-ray crystal structures can only be inferred from the relative site occupancies, but this kind of analysis is intrinsically associated with large errors. Thus, the presence / existence of vanadium atoms in such di-vanadium substituted hexatungstate cluster containing compounds can be confirmed by the ^{51}V NMR, EDS and ICP analyses, which have been discussed in the following sections.

2.3.3. Powder XRD analysis

The powder XRD analyses were done for the confirmation of phase purity for compounds **1**, **2**, **3** and **4** (Figure 2.1)**.** As experimental / observed PXRD patterns for compounds **1**, **2**, **3** and **4** are in good agreement with the PXRD patterns, simulated from their corresponding single crystal X-ray data, it indicates the phase purity of the bulk compounds.

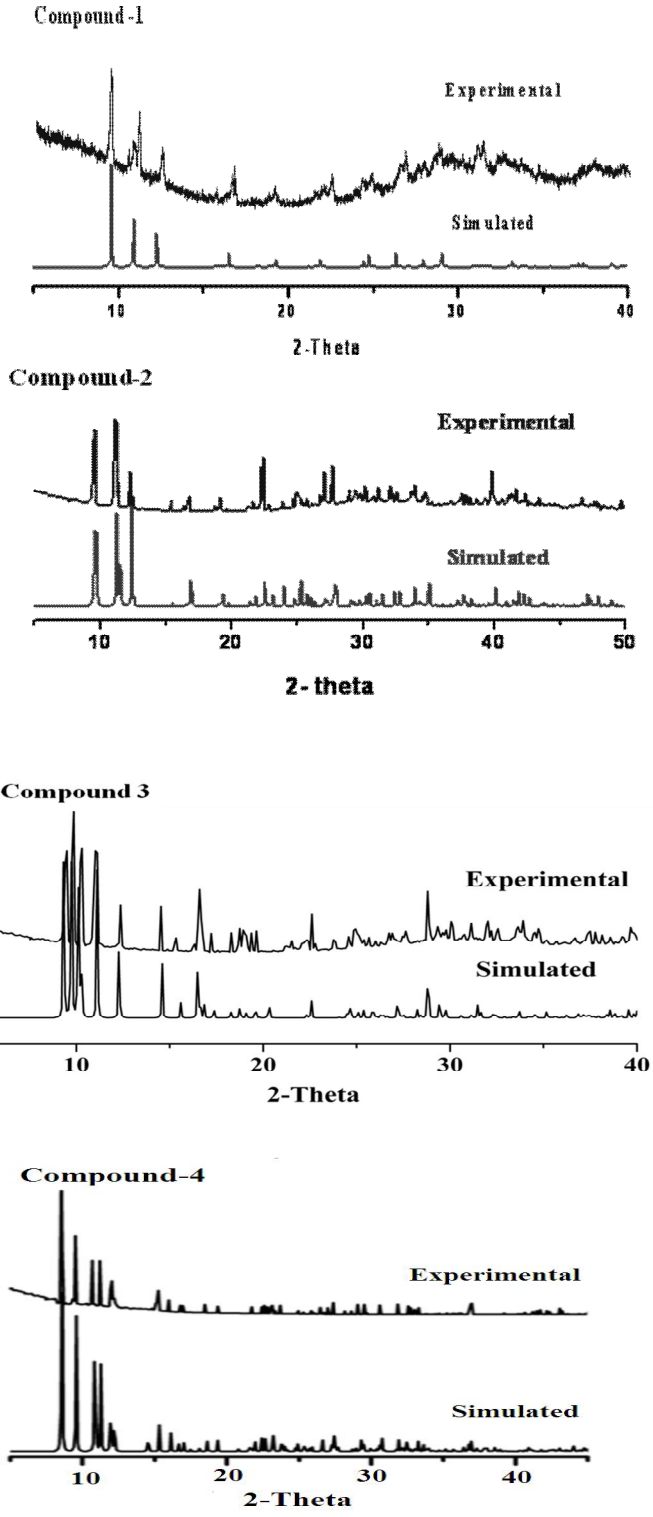

Figure 2.1. Powder X-ray patterns of compounds **1**, **2**, **3** and **4.**

2.3.4. ^{51}V NMR

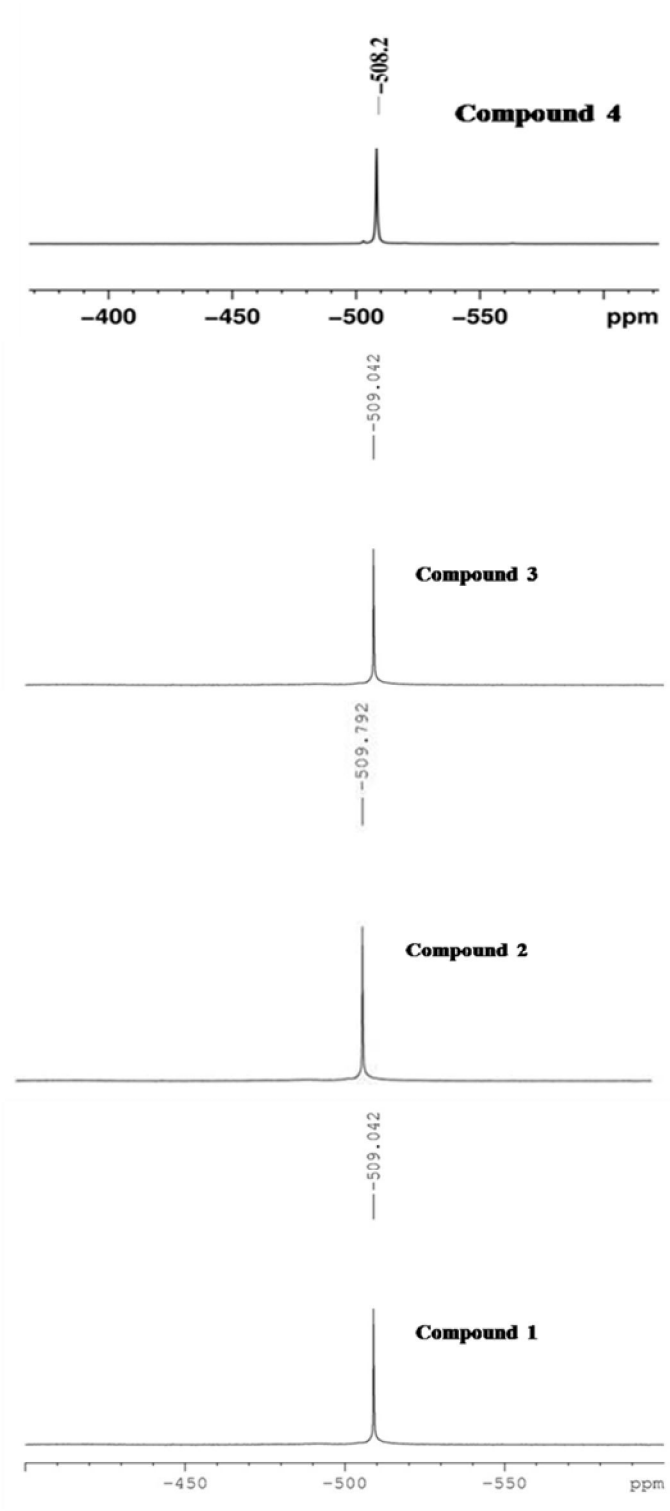

Figure 2.2. ^{51}V NMR spectra of compounds **1**, **2**, **3** and **4**.

The ^{51}V NMR spectra of the compounds **1**, **2**, **3** and **4** are shown in Figure. 2.2. All four compounds show a narrow resonance at around -508 to -510 ppm. For the reported $[V_2W_4O_{19}]^{4-}$ cluster containing compounds, the ^{51}V NMR spectra always exhibit the resonance peak in the range of -500 to -515 ppm.[1,20] Thus the presence of two vanadium atoms in the cluster in compounds **1**, **2**, **3** and **4** is supported by ^{51}V NMR spectroscopy.

2.3.5. EDS and ICP

The composition of compounds **1**, **2**, **3** and **4** are determined by energy dispersive X-ray spectroscopy (EDS). This confirms the presence of two vanadium atoms along with four tungsten atoms in the common cluster anion in compounds **1**, **2**, **3** and **4**. The wt % of compounds **1**, **2**, **3** and **4** confirms that the total cluster can be formulated as $[V_2W_4O_{19}]^{4-}$. ICP analyses confirm the formulation $[HMTAH]_2[H_2V_2W_4O_{19}]\cdot 4H_2O$ (**1**) $[Na_2(H_2O)_4]_n[H_2V_2W_4O_{19}]_n\cdot 2n HMTA\cdot 2nH_2O$ (**2**), $[HMTAH]_{2n}[Na_2(H_2O)_8(V_2W_4O_{19})]_n\cdot 4nH_2O$ and $[HMTAH]_2[Cu(H_2O)_6][V_2W_4O_{19}]\cdot 4H_2O$ (**4**) in terms of 1:2 ratio of V:W.

2.3.6. Description of crystal structures

Compounds **1**-**4** crystallize in orthorhombic *Immm* (compound **1**), monoclinic space group *C2/c* (compound **2**) and triclinic space group *P-1*(compounds **3**-**4**), respectively. The common cluster anion in these compounds is $[V_2W_4O_{19}]^{4-}$, which is iso-structural with the parent cluster anion $[W_6O_{19}]^{2-}$, the so-called Lindqvist type isopolyanion. This versatile cluster anion is build with six edge sharing octahedra with overall octahedral symmetry. There are three types are M–O bonds, present in the cluster anion: six terminal ($M–O_t$) bonds, twelve bridging ($M–O_b$) bonds and one central ($M–O_c$) bond.

The comparison of M–O bond distances in the crystal structures of mixed metal Lindqvist anion $[V_2W_4O_{19}]^{4-}$ in compounds **1**, **2**, **3** and **4** with those of $[W_6O_{19}]^{2-}$ and some reported $[V_2W_4O_{19}]^{4-}$ structures has been tabulated in Table 2.2, that shows the values M–O bond distances of in the crystal structures of all four compounds are close / comparable to those of previously reported $[V_2W_4O_{19}]^{4-}$.[21,31] The cluster anion in the present study is slightly distorted octahedron as shown in the Table 2.2.

Table 2.2. Comparison of M–O average bond distances of the cluster anion in compounds **1**, **2**, **3** and **4** with those in reported cluster anions.

ANION	$M–O_c$ ( )	$M–O_b$ ( )	$M–O_t$ ( )
$[W_6O_{19}]^{2-}$ (15)	2.33	1.92	1.69
$[V_2W_4O_{19}]^{4-}$ (25)	2.305	1.922	1.695
Compound **1**	2.271	1.892	1.697
Compound **2**	2.280	1.898	1.692
Compound **3**	2.283	1.912	1.683
Compound **4**	2.286	1.903	1.677

2.3.6.1. Structural description of $[HMTAH]_2[H_2V_2W_4O_{19}]\cdot 4H_2O$ (1)

The molecular structure of $[HMTAH]_2[H_2V_2W_4O_{19}]\cdot 4H_2O$ (**1**) reveals that it is a discrete cluster in which the vanadium substituted Lindqvist anion and protonated hexamethylenetetramine crystallize with four lattice water molecules. ORTEP diagram of compound **1** is shown in the Figure 2.3.

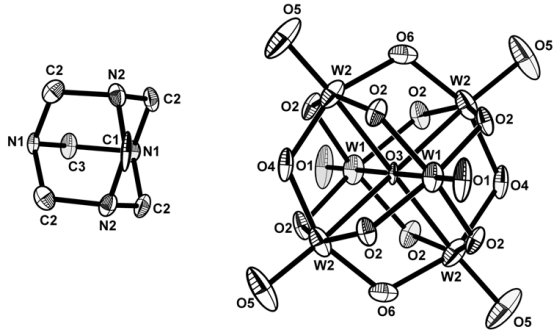

Figure 2.3. Thermal ellipsoidal plot of the crystal structure of compound **1** with 30 % probability (hydrogen atoms and solvent molecules are omitted for clarity).

Selected bond lengths and bond angles in the crystal structure of compound **1** are described in Table 2.6. In the crystal structure of compound **1**, an extensive hydrogen bonding interactions are observed. Two lattice water molecules (O7 and O8: one of them O8 is crystallographically related) generate a non-linear water trimer (O8···O7···O8; taking O···O interaction as hydrogen bond, because relevant hydrogen atoms could not be located in the crystal structure)[32]. These water trimers (Figure 2.7) and $[V_2W_4O_{19}]^{4-}$ cluster anions are extensively involved hydrogen bonding interactions to form a three-dimensional supramolecular network as shown in Figure 2.4.

Table 2.3. Crystallographic data for $[HMTAH]_2[H_2V_2W_4O_{19}]\cdot 4H_2O$ (**1**), $[Na_2(H_2O)_4]_n[H_2V_2W_4O_{19}]_n\cdot 2nHMTA\cdot 2nH_2O$ (**2**) and $[HMTAH]_2\{Na_2(H_2O)_8(V_2W_4O_{19})\}\cdot 4H_2O$ (**3**)

	1	**2**	**3**
Formula	$C_{12}H_{36}N_8O_{23}V_2W_4$	$C_{12}H_{38}N_8O_{25}Na_2V_2W_4$	$C_{12}H_{50}N_8O_{31}Na_2V_2W_4$
FW	1497	1577	1685
Crystal system	Orthorhombic	Monoclinic	Triclinic
Space group	*I*mmm	*C*2/c	*P-1*
a/Å	9.4000(19)	17.950(4)	9.831(4)
b/Å	11.200(2)	11.440(2)	10.432(4)
c/Å	16.200(3)	17.850(4)	10.749(4)
α [°]	90.00	90.00	63.387(6)
β [°]	90.00	118.35(3)	89.126(6)
γ [°]	90.00	90.00	69.573(6)
Z	2	4	1
ρ_{cal}/ Mg m^{-3}	3.473	3.010	2.889
Goodness-of-fit on F^2	1.222	1.163	1.145
$R_1(F^2_0)$ [$I > 2\ \sigma(I)$]	0.0735	0.0391	0.0464
wR_2 (F^2_0) [$I > 2\ \sigma(I)$]	0.1925	0.0861	0.1184
$R_1(F^2_0)$ (all data)	0.0787	0.0417	0.0531
wR_2 (F^2_0) (all data)	0.1961	0.0874	0.1451
Largest diff. peak and hole [e.$Å^{-3}$]	3.198 and -2.209	1.420 and -1.199	1.725 and -1.638

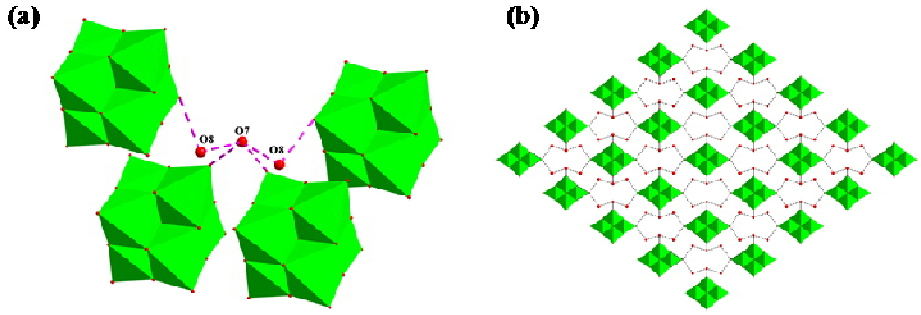

Figure 2.4. (a) A view showing a water trimer connecting four $[V_2W_4O_{19}]^{4-}$ cluster anions by hydrogen bonds. (b) Three-dimensional supramolecular network, generated due to hydrogen bonding interactions between water trimers and $[V_2W_4O_{19}]^{4-}$ cluster anions in compound **1**.

Table 2.4. Selected bond lengths [Å] and angles [°] for compound **1**

W(1)-O(1)	1.68(3)	W(1)-O(2)	1.889(13)	W(1)-O(3)	2.2604(18)
W(2)-O(2)	1.905(12)	W(2)-O(3)	2.2832(13)	W(2)-O(4)	1.893(12)
W(2)-O(5)	1.71(2)	W(2)-O(6)	1.884(15)	C(1)-N(2)	1.44(3)
C(2)-N(1)	1.45(2)	C(2)-N(2)	1.44(2)	C(3)-N(1)	1.42(3)
O(1)-W(1)-O(2)	102.4(4)	O(1)-W(1)-O(3)	180.0(2)	O(2)-W(1)-O(3)	77.6(4)
O(2)-W(2)-O(3)	76.7(4)	O(4)-W(2)-O(2)	86.5(5)	O(4)-W(2)-O(3)	75.3(6)
O(5)-W(2)-O(2)	103.3(4)	O(5)-W(2)-O(3)	176.0(15)	O(5)-W(2)-O(4)	100.7(16)
O(5)-W(2)-O(6)	106.7(17)	O(6)-W(2)-O(2)	87.2(5)	O(6)-W(2)-O(3)	77.2(7)
O(6)-W(2)-O(4)	152.5(10)	C(3)-N(1)-C(2)	108.9(12)	C(1)-N(2)-C(2)	107.0(16)

Cation-anion ionic interactions play a vital role to stabilize inorganic compounds. The crystal structure of compound **1** also shows an extensive hydrogen bonding interactions between cation (protonated hexamethylenetetramine) and $[V_2W_4O_{19}]^{4-}$ cluster anion, that give an extra stabilization. As shown in the Figures. 2.5(a) and 2.5(b), the three-dimensional supramolecular network, viewed along crystallographic *a* axis and *b* axis, are due to C–H···O hydrogen bonding interactions between hexamethylenetetramine and the cluster anion, where the maximum O···H distance has been considered as 2.594 ´.

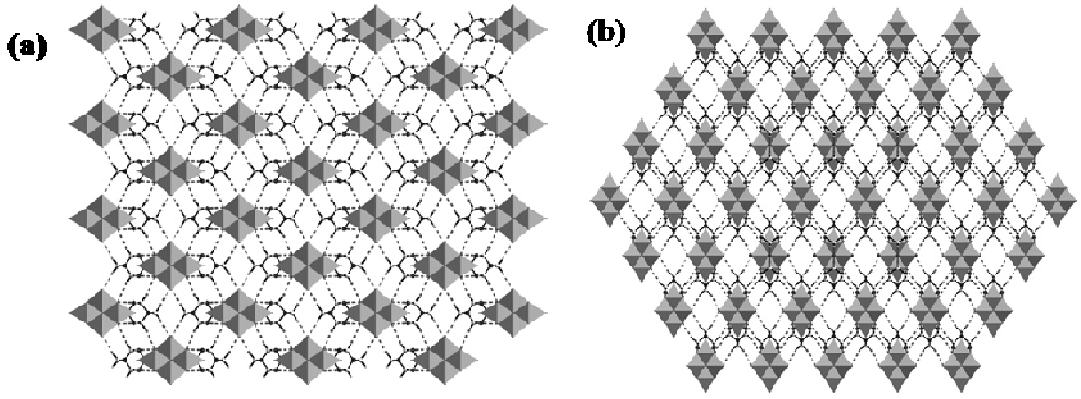

Figure 2.5. Three-dimensional supramolecular network, formed due to C–H···O hydrogen bonding interactions: (a) along crystallographic *a* axis; (b) along crystallographic *b* axis.

Hydrogen bonding environment around the cation, due to C–H···O interactions, is shown in Figure 2.5, where four $[V_2W_4O_{19}]^{4-}$ cluster anions are found to be H-bonded to the cation (taking O···H distances in the range of 2.594 – 2.578 ´).[33] Full list of hydrogen bonding distances and angles are listed in Table 2.5.

Table 2.5. Hydrogen bonding parameters in the crystal structure of compound **1**[Å and °]

D-H···A	d(D-H)	d(H···A)	d(D···A)	<(DHA)
C(1)-H(1A)...O(4)#1	0.97	2.59	3.56(3)	173.7
C(1)-H(1B)...O(4)	0.97	2.59	3.56(3)	173.7
C(2)-H(2A)...O(2)	0.97	2.58	3.53(2)	168.9
C(2)-H(2B)...O(2)#2	0.97	2.63	3.55(2)	157.1
C(3)-H(3A)...O(6)#3	0.97	2.72	3.62(3)	154.5
C(3)-H(3B)...O(6)#4	0.97	2.72	3.62(3)	154.5

Symmetry transformations used to generate equivalent atoms:

#1 -x,-y,-z #2 -x+1/2,-y+1/2,-z+1/2 #3 -x+1/2,-y+1/2,z+1/2 #4 x-1/2,y-1/2,z+1/2

2.3.6.2. Structural description of $[Na_2(H_2O)_4]_n[H_2V_2W_4O_{19}]_n \cdot 2n$HMTA $\cdot 2nH_2O$ (2)

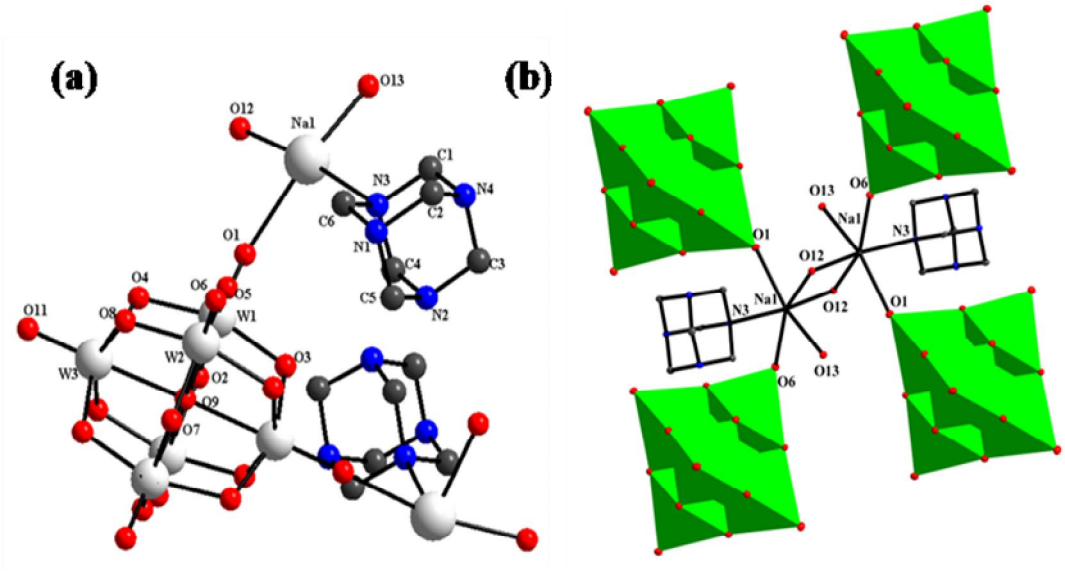

Figure 2.6. (a) Ball- and stick-representation of the total molecule of compound **2** (solvent molecules and hydrogen atoms are omitted for clarity) **(b)** The coordination environment of di-sodium aqua-complex with neighboring cluster anions and hexamine in compound **2**.

The full molecular structure of compound $[Na_2(H_2O)_4]_n[H_2V_2W_4O_{19}]_n \cdot 2n$HMTA$\cdot$ $2nH_2O$ (**2**) is shown in Figure 2.6. Compound **2** is a coordination polymer, in which each sodium ion is coordinated by two $[V_2W_4O_{19}]^{4-}$ cluster anions and one hexamethylenetetramine molecule. Rest three coordination sites are occupied by three water molecules. Two such sodium coordination complexes (sodium atoms are crystallographically related) form a di-

sodium aqua-complex (by sharing two common crystallographically related (O12) water molecules, as μ_2-type bridging ligands), that acts as the cation in compound **2** (Figure 2.6.).

Thus the coordination geometry of each sodium ion can be described by a distorted octahedral arrangement, in which each sodium ion is coordinated to five oxygen atoms (three water molecules and two terminal oxygen atoms from two different cluster anions) and one nitrogen atom from hexamethylenetetramine molecule as shown in Figure 2.6. The repetitions of this coordination between hexamethylenetetramine associated sodium dimmer and the $[V_2W_4O_{19}]^{4-}$ cluster anion, finally, lead to a three-dimensional coordination polymer as shown in Figure 2.7.

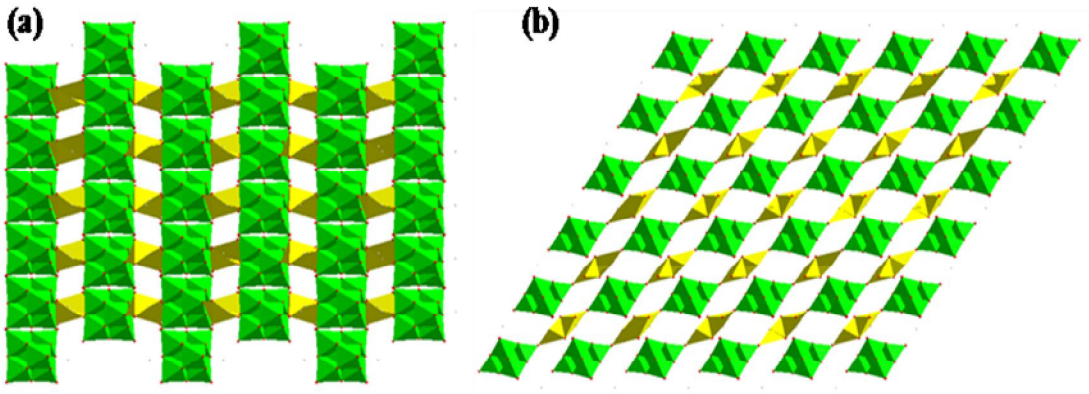

Figure 2.7. Three-dimensional coordination polymer, formed by linking of sodium-aqua-hexamine coordination complex cation and $[V_2W_4O_{19}]^{4-}$ cluster anion, in the crystal structure of compound **2** (a) along *a* axis; (b) along *b* axis.

The cluster anion is assumed to be protonated for charge compensation. The picture of hydrogen bonding environment around HMTA in the crystal structure of compound **2** is shown in Figure 2.8. The list of hydrogen bonding distances and angles are presented in Table 2.6. Selected bond lengths and bond angles in the crystal structure of compound **2** are described in Table 2.7.

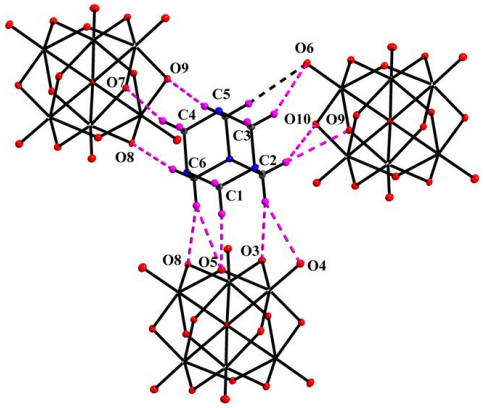

Figure 2.8. Hydrogen bonding environment around the hexamethylenetetramine cation due to C–H···O interaction, observed in the crystal structure of compound **2**.

Table 2.6. Hydrogen bonding parameters in the crystal structure of compound **2** [Å and°]

D-H···A	**d(D-H)**	**d(H···A)**	**d(D···A)**	**<(DHA)**
C(1)-H(1B)...O(8)#1	0.97	2.24	3.168(11)	160.6
C(2)-H(2A)...O(11)#1	0.97	2.70	3.514(12)	141.4
C(2)-H(2A)...O(4)#1	0.97	2.54	3.428(11)	152.8
C(2)-H(2B)...O(2)#2	0.97	2.53	3.438(11)	156.1
C(2)-H(2B)...O(7)#3	0.97	2.60	3.407(12)	140.8
C(3)-H(3B)...O(10)#4	0.97	2.77	3.664(11)	153.5
C(3)-H(3A)...O(6)#3	0.97	2.71	3.557(12)	146.7
C(3)-H(3B)...O(7)#4	0.97	2.77	3.628(11)	147.1
C(4)-H(4B)...O(3)	0.97	2.30	3.244(12)	163.5
C(4)-H(4A)...O(10)#4	0.97	2.85	3.728(12)	150.6
C(5)-H(5B)...O(2)#5	0.97	2.45	3.388(11)	162.2
C(5)-H(5B)...O(3)	0.97	2.88	3.674(10)	139.3
C(5)-H(5A)...O(6)#3	0.97	2.54	3.430(12)	152.8
C(5)-H(5A)...O(7)#3	0.97	2.84	3.594(11)	135.1
C(6)-H(6A)...O(5)	0.97	2.31	3.261(11)	168.0
C(6)-H(6B)...O(5)#1	0.97	2.42	3.331(11)	155.4
C(6)-H(6B)...O(8)#1	0.97	2.68	3.497(11)	142.3

Symmetry transformations used to generate equivalent atoms:

#1 -x+2,-y+1,-z+1 #2 x-1/2,y-1/2,z #3 -x+3/2,y-1/2,-z+1/2 #4 x,y-1,z #5 -x+2,y,-z+1/2.

Table 2.7. Selected bond lengths [Å] and angles [°] for compound **2**

W(1)-O(1)	1.724(6)	W(1)-O(2)	1.894(6)	W(1)-O(3)	1.925(5)
W(1)-O(4)	1.888(6)	W(1)-O(5)	1.933(6)	W(1)-O(9)	2.275(6)
W(2)-O(5)	1.886(6)	W(2)-O(6)	1.684(6)	W(2)-O(7)	1.912(6)
W(2)-O(8)	1.875(7)	W(2)-O(9)	2.2798(7)	W(3)-O(4)	1.931(6)
W(3)-O(8)	1.929(6)	W(3)-O(9)	2.287(6)	W(3)-O(10)	1.890(5)
W(3)-O(11)	1.670(7)	Na(1) - O(12)	2.364(7)	Na(1) - O(13)	2.303(7)
C(1)-N(3)	1.475(11)	C(1)-N(4)	1.470(12)	C(2)-N(1)	1.540(11)
C(2)-N(4)	1.433(12)	C(3)-N(2)	1.470(12)	C(3)-N(4)	1.467(11)
C(4)-N(2)	1.472(12)	C(4)-N(3)	1.466(11)	C(5)-N(1)	1.522(11)
C(5)-N(2)	1.450(12)	C(6)-N(1)	1.503(12)	C(6)-N(3)	1.440(11)
O(1)-W(1)-O(2)	105.0(3)	O(1)-W(1)-O(3)	101.9(3)	O(1)-W(1)-O(4)	104.1(3)
O(1)-W(1)-O(5)	100.2(3)	O(1)-W(1)-O(9)	176.3(2)	O(2)-W(1)-O(3)	87.09(19)
O(2)-W(1)-O(5)	154.7(3)	O(2)-W(1)-O(9)	78.06(19)	O(3)-W(1)-O(5)	85.35(19)
O(3)-W(1)-O(9)	76.0(3)	O(4)-W(1)-O(2)	89.3(3)	O(4)-W(1)-O(3)	153.8(3)
O(4)-W(1)-O(5)	86.9(3)	O(4)-W(1)-O(9)	77.8(2)	O(5)-W(1)-O(9)	76.66(18)
O(5)-W(2)-O(7)	154.6(3)	O(5)-W(2)-O(9)	77.4(2)	O(6)-W(2)-O(5)	100.3(3)
O(6)-W(2)-O(7)	104.9(3)	O(6)-W(2)-O(8)	103.4(3)	O(6)-W(2)-O(9)	177.3(3)
O(7)-W(2)-O(9)	77.3(2)	O(8)-W(2)-O(7)	87.5(3)	O(8)-W(2)-O(5)	89.4(3)
O(8)-W(2)-O(9)	78.2(2)	O(8)-W(3)-O(4)	85.5(3)	O(4)-W(3)-O(9)	76.7(2)
O(8)-W(3)-O(9)	76.98(19)	O(10)-W(3)-O(4)	155.4(3)	(10)-W(3)-O(8)	87.3(2)
O(10)-W(3)-O(9)	78.7(3)	O(11)-W(3)-O(4)	102.1(3)	O(11)-W(3)-O(8)	102.4(3)
O(11)-W(3)-O(9)	178.7(3)	O(11)-W(3)-O(10)	102.4(3)	O(13)-Na(1)-O(12)	87.2(3)
C(2)-N(4)-C(1)	109.6(8)	C(3)-N(4)-C(1)	109.7(7)	C(2)-N(4)-C(3)	109.3(8)
C(3)-N(2)-C(4)	108.9(7)	C(4)-N(3)-C(1)	108.2(7)	C(5)-N(1)-C(2)	108.4(7)
C(5)-N(2)-C(3)	109.0(7)	C(5)-N(2)-C(4)	109.8(7)	C(6)-N(1)-C(5)	108.5(7)
C(6)-N(1)-C(2)	107.3(7)	C(6)-N(3)-C(1)	108.6(7)	C(6)-N(3)-C(4)	109.9(7)

2.3.6.3. Structural description of $[HMTAH]_{2n}[Na_2(H_2O)_8(V_2W_4O_{19})]_n \cdot 4nH_2O$ (3)

The molecular structure of compound **3**, as shown in the Figure 2.9, is also a coordination polymer. Similar to compound **2**, the coordination polymer formed by di-sodium aqua-complex cation supported by substituted Lindquist cluster anion $[V_2W_4O_{19}]^{4-}$. Two hexamine cations and four lattice water molecules are also present in the relevant crystal lattice. The coordination environment around the di-sodium aqua-complex in the crystal structure of compound **3** is different from that in compound **2**; In the case of compound **3**, each sodium has an octahedral geometry (Figure 2.11(a)) with four coordinated water molecules and two coordinated terminal oxygen atoms from the cluster anion.

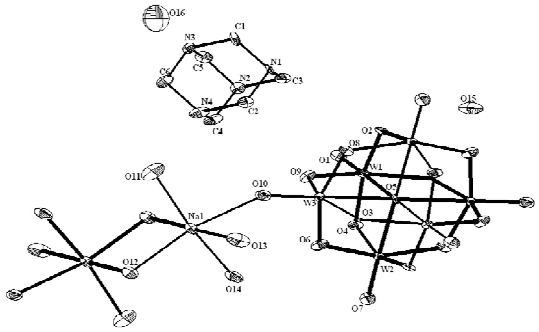

Figure 2.9. Thermal view of the compound **3** with 30 % probability (hydrogen atoms are omitted for clarity).

The coordination of di-sodium aqua-complex cation to $[V_2W_4O_{19}]^{4-}$ anion and its repetition result in the formation of an one-dimensional chain as shown in Figure 2.10.

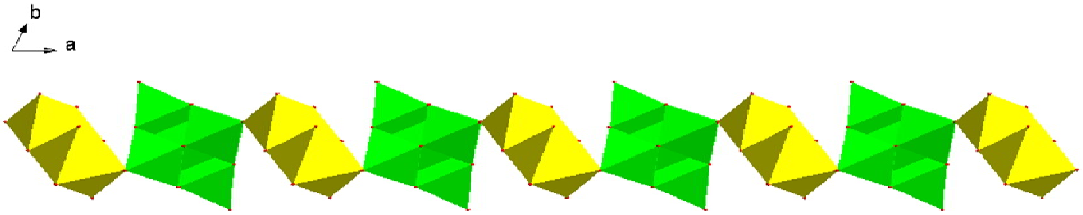

Figure 2.10. Polyhedral representation of 1-dimmensional chain viewed along *c* axis, generated due to coordination of di-sodium aqua-complex cation with cluster anion $[V_2W_4O_{19}]^{4-}$ in compound **3**.

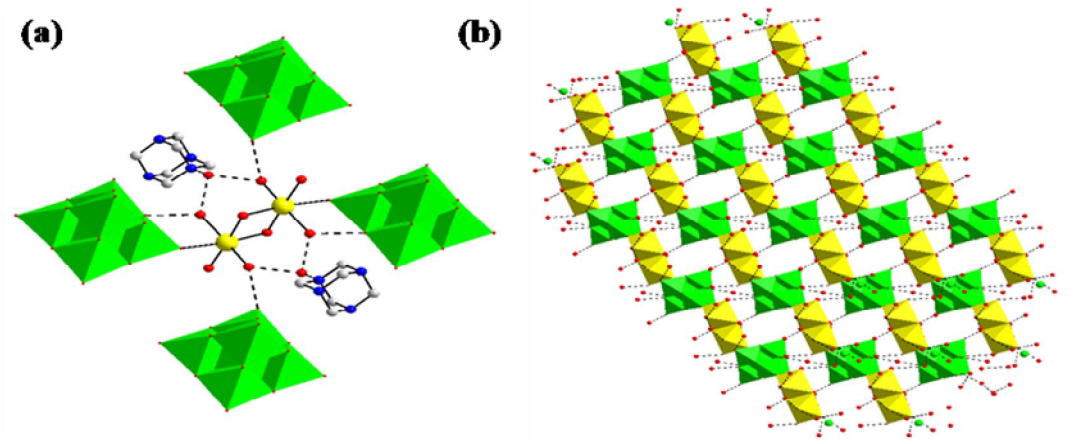

Figure 2.11. (a) The coordination environment of di-sodium aqua-complex with neighboring cluster anions and hexamine in compound **3**; (b) 3-dimensional frame work established due to O···O interactions in compound **3**.

In the crystal structure of compound **3**, an extensive hydrogen bonding interactions exist due to the presence of four lattice water molecules, sodium coordinated water molecules, hydrogen atoms of hexamine cation and weak O···O interactions. As a result, 3-dimmensional framework is established in compound **3** (Figure 2.11(b)). Full list of relevant hydrogen bonding parameters are described in Table 2.8. Selected bond lengths and angles in the crystal structure of compound **3** are listed in the Table 2.9.

Table 2.8. Hydrogen bonding parameters in the crystal structure of compound **3** [Å and°]

D-H···A	**d(D-H)**	**d(H···A)**	**d(D···A)**	**<(DHA)**
C(1)-H(1B)...O(3)#7	0.97	2.52	3.403(16)	151.8
C(1)-H(1A)...O(7)#5	0.97	2.39	3.291(16)	155.1
C(2)-H(2B)...O(8)	0.97	2.49	3.363(17)	149.7
C(2)-H(2A)...O(8)#7	0.97	2.78	3.655(16)	149.8
C(2)-H(2B)...O(10)	0.97	2.73	3.487(17)	135.8
C(3)-H(3B)...O(7)#5	0.97	2.60	3.446(17)	145.7
C(3)-H(3A)...O(8)	0.97	2.56	3.420(16)	147.2
C(4)-H(4A)...O(9)	0.97	2.48	3.385(17)	156.0
C(4)-H(4B)...O(9)#6	0.97	2.40	3.348(18)	165.2
C(4)-H(4A)...O(10)	0.97	2.71	3.476(17)	136.4
C(5)-H(5A)...O(6)#3	0.97	2.67	3.596(18)	160.8
C(5)-H(5B)...O(16)#4	0.97	2.59	3.47(3)	150.9
C(6)-H(6B)...O(1)#3	0.97	2.75	3.489(18)	133.0
C(6)-H(6A)...O(1)#7	0.97	2.59	3.433(16)	145.7
C(6)-H(6B)...O(4)#3	0.97	2.37	3.291(17)	159.2

Symmetry transformations used to generate equivalent atoms:

#1 -x+1,-y,-z #2 -x+2,-y,-z+1 #3 x,y,z+1 #4 -x,-y+1,-z+1 #5 -x,-y+1,-z

#6 -x+1,-y,-z+1 #7 -x+1,-y+1,-z

Table 2.9. Selected bond lengths [Å] and angles [°] for compound **3**

W(1)-O(1)	1.680(9)	W(1)-O(2)	1.920(8)	W(1)-O(3)	1.917(8)
W(1)-O(4)	1.920(9)	W(1)-O(5)	2.2706(10)	W(2)-O(4)	1.891(9)
W(2)-O(5)	2.2974(9)	W(2)-O(6)	1.921(9)	W(2)-O(7)	1.688(10)
W(2)-O(8)	1.912(9)	W(3)-O(3)	1.913(9)	W(3)-O(5)	2.2813(9)
W(3)-O(8)	1.893(8)	W(3)-O(10)	1.681(10)	W(3)-O(9)	1.913(9)
Na(1)-O(10)	2.378(11)	Na(1)-O(11)	2.414(13)	Na(1)-O(12)	2.382(11)
Na(1)-O(13)	2.360(11)	Na(1)-O(14)	2.397(12)	N(1)-C(1)	1.472(18)
N(1)-C(3)	1.479(17)	N(1)-C(2)	1.489(17)	N(2)-C(3)	1.491(18)
N(2)-C(4)	1.487(18)	N(2)-C(5)	1.459(18)	N(3)-C(1)	1.503(17)
N(3)-C(5)	1.487(16)	N(3)-C(6)	1.494(18)	N(4)-C(2)	1.516(19)
N(4)-C(4)	1.500(17)	N(4)-C(6)	1.494(17)		
O(1)-W(1)-O(2)	106(4)	O(1)-W(1)-O(3)	103.1(4)	O(1)-W(1)-O(4)	100.8(4)
O(1)-W(1)-O(5)	178.4(3)	O(3)-W(1)-O(2)	87.2(4)	O(3)-W(1)-O(5)	77.4(3)
O(3)-W(1)-O(4)	88.1(4)	O(2)-W(1)-O(5)	77.9(3)	O(4)-W(1)-O(5)	77.6(3)
O(4)-W(1)-O(2)	155.6(4)	O(4)-W(2)-O(5)	77.5(3)	O(4)-W(2)-O(6)	87.5(4)
O(4)-W(2)-O(8)	88.1(4)	O(7)-W(2)-O(4)	103.2(4)	O(7)-W(2)-O(6)	103.3(5)
O(7)-W(2)-O(5)	179.0(3)	O(7)-W(2)-O(8)	102.1(4)	O(6)-W(2)-O(5)	77.4(3)
O(8)-W(2)-O(5)	77.2(3)	O(8)-W(2)-O(6)	154.5(4)	O(3)-W(3)-O(5)	77.2(2)
O(3)-W(3)-O(9)	154.3(4)	O(8)-W(3)-O(3)	88.3(3)	O(8)-W(3)-O(5)	77.9(3)
O(8)-W(3)-O(9)	87.7(4)	O(10)-W(3)-O(3)	103.7(4)	O(10)-W(3)-O(5)	179.0(3)
O(10)-W(3)-O(8)	102.5(4)	O(10)-W(3)-O(9)	102.0(4)	O(10)-Na(1)-O(11)	89.7(4)
O(10)-Na(1)-O(12)	167.9(4)	O(10)-Na(1)-O(14)	81.3(4)	O(12)-Na(1)-O(11)	102.3(5)
O(12)-Na(1)-O(14)	87.3(4)	O(13)-Na(1)-O(10)	81.5(4)	O(13)-Na(1)-O(11)	98.6(5)
O(13)-Na(1)-O(12)	94.6(4)	O(13)-Na(1)-O(14)	90.2(5)	O(14)-Na(1)-O(11)	166.3(4)
C(1)-N(1)-C(2)	108.5(10)	C(1)-N(1)-C(3)	108.4(10)	C(3)-N(1)-C(2)	109.4(10)
C(4)-N(2)-C(3)	109.9(10)	C(5)-N(3)-C(1)	107.1(10)	C(5)-N(3)-C(6)	109.0(10)
C(6)-N(4)-C(2)	108.9(11)	C(6)-N(4)-C(4)	107.2(10)		

2.3.6.4. Structural description of $[HMTAH]_2[Cu(H_2O)_6][V_2W_4O_{19}]\cdot 4H_2O$ (4)

The asymmetric unit in the crystal structure of compound **4** consists of the half of substituted Lindquist cluster anion $[V_2W_4O_{19}]^{4-}$, half of hexa-hydrated copper cation (copper is in the special position), one protonated HMTA cation and two lattice water molecules. Thus the formulation of compound **4** is given as $[HMTAH]_2[Cu(H_2O)_6][V_2W_4O_{19}]\cdot 4H_2O$ and the relevant molecular structure is shown in Figure 2.12. The crystal structure does not reveal any coordination between the POM cluster anion and the copper hexahydrated complex cation resulting in the compound **4** discrete. The Cu-O bond distances are in the expected range of 1.946 ´ to 2.222 ´.

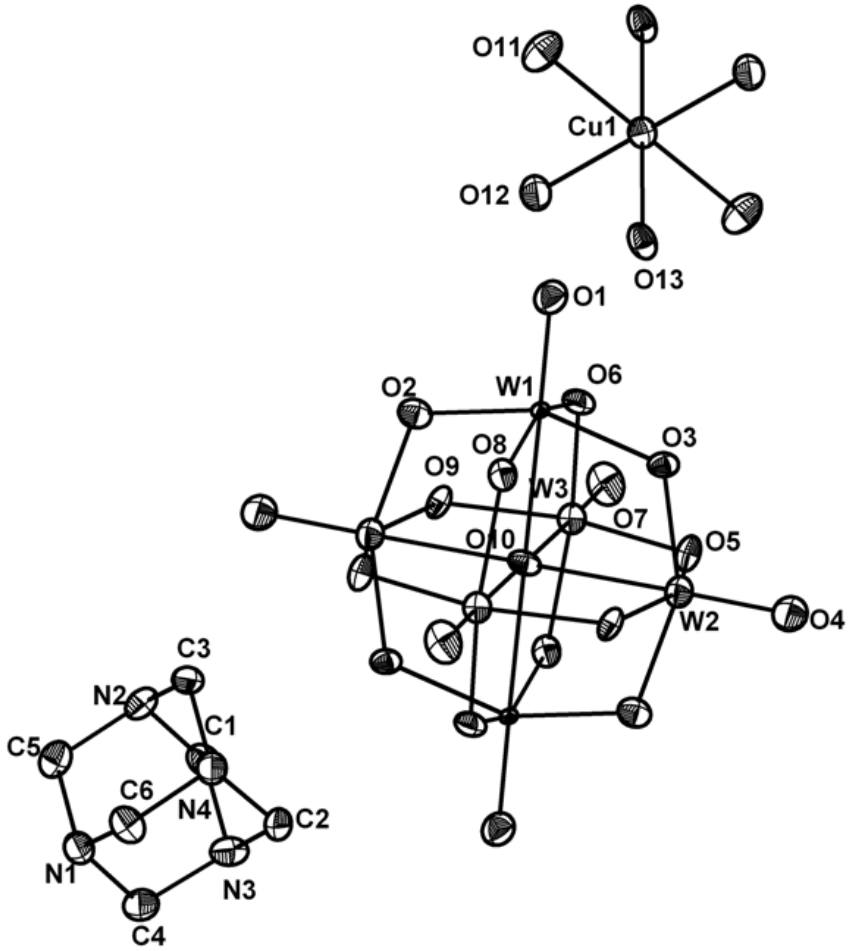

Figure 2.12. Thermal ellipsoidal plot of molecular structure of compound **4** (hydrogen atoms are omitted for clarity).

Table 2.10. Crystallographic data for $[Cu(H_2O)_6][HMTAH]_2[V_2W_4O_{19}]\cdot 4H_2O$ (**4**)

	4
Formula	$C_{12}H_{46}CuN_8O_{29}V_2W_4$
FW	1667
Crystal system	Triclinic
Space group	*P-1*
a/Å	9.1742(9)
b/Å	10.5954(12)
c/Å	11.4898(12)
α [°]	67.207(10)
β [°]	69.447(10)
γ [°]	65.600(10)
Z	1
ρ_{cal}/ Mg m^{-3}	2.847
Goodness-of-fit on F^2	1.094
$R_1(F^2_0)$ [I > 2 σ(I)]	0.0871
wR_2 (F^2_0) [I > 2 σ(I)]	0.2383
$R_1(F^2_0)$ (all data)	0.0931
wR_2 (F^2_0) (all data)	0.2433
Largest diff. peak and hole [e.$Å^{-3}$]	2.335 and -2.294

2.4. Conclusion

In conclusion, we have described a coordination polymer of di-sodium substituted Lindquist- type cluster, which has been structurally characterized by single crystal X-ray crystallography. The composition of $[V_2W_4O_{19}]^{4-}$ cluster anion, common in compounds **1-4**, is confirmed by ^{51}V NMR, EDS and ICP spectroscopy, in addition to crystal structure determination of the concerned compounds. Compound **1** is a discrete cluster containing compound and in its crystal structure, the supramolecular architecture is characterized by C–H···O and O···O weak interactions. Compound **2** is a 3-dimensional framework based on the coordination of sodium aqua-complex with the $[V_2W_4O_{19}]^{4-}$ cluster anion and hexamethylenetetramine. Catalytic applications of these materials are under the progress in our laboratory. Compound **3** is an one-dimensional coordination polymer based on the

coordination of di-sodium aqua-complex cation with the cluster anion; in the relevant crystal structure, a 3-dimmensional supramolelcular network is formed due an extensive hydrogen bonding interactions along with weak O···O interactions.

2.5. References

1. Pope, M. T.; Müller, A. *Angew. Chem. Int. Ed. Eng.* **1991**, *30*, 34.
2. Pope, M. T. Heteropoly and Isopoly Oxometalates, Springer-Verlag, New York, **1983**.
3. Evans H. T. Jr., *Perspect. Struct. Chem.* **1971**, *4*, 1.
4. Pope, M. T.; Müller, A., *Polyoxometalates: From Platonic Solids to Anti-Retroviral Activity*, Kluwer Academic, The Netherlands, **1994**.
5. Ouahab, L.; Golhen, S.; Triki, S.; Pope, M. T.; Müller, A., *Polyoxometalates Chemistry: From Topology via Self-Assembly to Applications*, Kluwer Academic, Elsevier (**2000**) 205.
6. -Qatati, A. A.; Fontes, F. L.; Barisas, B. G.; Zhang, D.; Roessa, D. A.; Crans, D. C. *Dalton Trans.* **2013**, *42*, 11912.
7. Aureliano, M.; Fraquezab, G.; Ohlin, C. A. *Dalton Trans.* **2013**, *42*, 11770.
8. Fukuma, M.; Seto, Y.; Yamase, T. *Antiviral Res.* **1991**, *16*, 327.
9. Ikeda, S.; Nishiya, S.; Yamamoto, A.; Yamase, T.; Nishimura, C.; De Clercq, E. *J. Med. Virol.* **1993**, *41*, 191.
10. Nomiya, K.; Torii, H.; Hasegawa, T.; Namoto, Y.; Nomura, K.; Hashino, K.; Uchida, M.; Kato, Y.; Shimizu, K.; Oda, M. *J. Inorgan. Biochem.* **2001**, *86*, 657.
11. Hwang, W.; Todaro, L.; Franceeon L. C.; Polenova, T. *J. Am. Chem. Soc.* **2003**, *125*, 5928.
12. Son, J. H.; Kwon, Y. U. *Inorg. Chem.* **2004**, *43*, 1929.
13. -León, M. C.; Coronado, E.; -García, C. J. G.; -Ferrero, E. M. *J. Cluster Sci.* **2002**, *13*, 381.
14. Shivaiah, V.; Das, S. K. *J. Chem. Sci.* **2002**, *114*, 107.
15. Chauveau, F. *Bull. Soc. Chim. Fr.* **1960**, 834.
16. Flynn, C. M.; Pope, M. T. *Inorg. Chem.* **1971**, *10*, 2524.
17. Flynn Jr., C. M.; Pope, M. T. *Inorg. Chem.* **1971**, *10*, 2745.
18. Flynn, C .M. Jr.; Pope, M. T. *Inorg. Chem.* **1973**, *12*, 1626.
19. Flynn, C. M. Jr.; Pope, M. T. *Inorg. Chem.* **1987**, *26*, 2112.

20. Wang, C.; Weng, L.; Ren, Y.; Du, C.; Yue, B.**;** Gu, M.; He, H. *Z. Anorg. Allg. Chem.* **2011**, *637*, 472.
21. Bannani, F.; Driss, H.; Thouvenot, R.; Debbabi, M. *J. Chem. Cryst.* **2007**, *37*, 37.
22. Driss, H.; Thouvenot, R.; Debbabi, M. *Polyhedron* **2008**, *27*, 2059.
23. Wang, X.; Zhou, B.; Zhong, C.; Ji, M. *Cryst. Res. Technol.* **2006**, *41*, 874.
24. Nishikawa, K.; Kobayashi, A.; Sasaki, Y .Y. *Bull. Chem. Soc. Jpn.* **1975**, *48*, 889.
25. Dmaille, P. J. *J. Am. Chem. Soc.* **1984**, *106*, 7677.
26. Xu, Y.; Xu, J. Q.; Yang, G. Y.; Wang, T. G.; Xing, Y.; Lin, Y.; Jia, H. Q. *Acta Cryst.* **1983**, *C 54*, 563.
27. Botar, A.; Fuchs, J. Z. *Naturforsch.* **1986**, *B 37*, 806.
28. França, M. C. K.; Eon, J. G.; Fournier, M.; Payen, E.; Mentré, O. *Solid State Sci.* **2005**, *7*, 1533.
29. Bruker. SADABS, SMART, SAINT and SHELXTL, Bruker AXS Inc., Madison, Wisconsin, USA, **2000**.
30. G. M. Sheldrick, SHELX-97, Program for Crystal Structure Solution and Analysis, University of Gottingen, Gottingen, Germany, **1997**.
31. Ma, P.; Yu, C.; Zhao, J.; Feng, Y.; Wang, J.; Niu, J. *J. Coord. Chem.* **2009**, *62*, 3117.
32. Lu, Y.; Feng, Y. *Chin. J. Chem.* **2010**, *28*, 2404.
33. Xiong, J.; Niu, Y.; Xu, H.; Cao, G.; Liu, B.; Hu, B; Xue, G. *New J. Chem.* **2012**, *36*, 1224.

Reversible morphological transition between nano-rods to micro-flowers through micro-hexagonal crystals in a sonochemical synthesis based on a polyoxovanadate compound

3

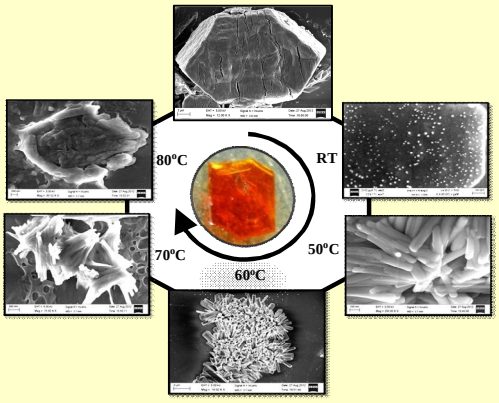

Chapter 3 describes the ultra-sonication assisted morphological evolution in hexagonal macro-crystals of {$V_{10}O_{28}$} type polyoxometalate system $[C_5H_{11}N]_6[V_{10}O_{28}]\cdot 4CH_3COOH\cdot 2H_2O$ (1) as a function of sonication temperatures. Field emission scanning electron microscopy (FESEM) as well as transmission electron microscopy (TEM) studies reveals that at room temperature, sonication of macro-crystals results in formation of spherical nanoparticles that are transformed to nano-rods at the sonication temperature of 50 °C. The morphology is transformed from nano-rods to micro-flowers through hexagonal shaped microcrystals as the sonication temperature rose from 50 to 80 ºC. It is observed that the hexagonal morphology of the original crystal is retained after a complete cycle (from 80 ºC to complete evaporation of solvent) of morphological transitions. Compound 1 is unambiguously characterized by single crystal X-ray structure determination.

3.1. Introduction

POV clusters are belonged to an important class of POMs, studied extensively in recent years because of their potential applications in the fields of medicine, materials science and industrial chemistry.[1-6] Synthesis and characterization of POV-based compounds have been explored in terms of their structural aesthetics, magnetic properties and catalysis.[7-11] Nano-scale preparation of POV compounds is important as far as catalysis work is concerned.[12-14] There are only few reports on nano-scale synthesis of POM based compounds.[15-17] Studies on nano-scale preparation of POV based compounds are scarcely known.[18-19] Generally, nano-structured materials, synthesized by various physical and chemical methods exhibit interesting morphology, such as, spherical particles, nano-rods and nano-tube. Many of the physical and chemical properties of these nano-materials depend on their size, shape and structure. Thus morphology is a crucial parameter that controls the properties and functionality of the pertinent material. Therefore, the phenomenon of morphological changes is an important aspect of a nano-material. Here, we describe ultrasonication-assisted synthesis of nano-scale particles of POV compound $[C_5H_{11}N]_6[V_{10}O_{28}]\cdot 4CH_3COOH\cdot 2H_2O$ (**1**), which undergoes morphological transitions from nano-rod to micro-flowers through hexagonal micro-sized crystals in a reversible cycle as a function of sonication temperature.

3.2. Experimental section

3.2.1. Materials and instrumental methods

The materials sodium metavanadate (extrapure) was purchased from Sisco chem. Pvt Ltd. Piperidine, acetonitrile (HPLC grade), DCM (HPLC grade) were purchased from Fischer chemicals. Millipore water was used throughout the experiments. All chemicals have been used as received without any further purification.

Single crystal X-Ray diffraction data was collected at 298(2) K on a Bruker SMART APEX CCD area detector system [$\lambda_{(Mo\text{-}K_\alpha)}$= 0.71073 Å] with graphite monochromator. Field emission scanning electron microscope (FESEM) imaging with energy dispersive X-ray spectroscopy (EDS) was carried out on a Carl Zeiss model Ultra 55 microscope. Transmission electron microscope images were recorded in a FEI Tecnai G^2 S-Twin, FEI electron microscope operated at 200 kV using Gatan CCD camera. The materials were

prepared as KBr pellets and FTIR spectra were collected in transmission mode using a JASCO FTIR-5300 spectrometer, wavenumbers (ν) are given in cm^{-1}. Micro analytical (C, H, N) data were obtained with a FLASH EA 1112 Series CHNS Analyzer. Powder X-ray diffraction patterns were recorded on a Bruker D8-Advance diffractometer using a graphite mono-chromated Cu-$K\alpha_1$ (1.5406 Å) and $K\alpha_2$ (1.54439 Å) radiations.

3.2.2. Synthesis

3.2.2.1. Synthesis of compound $[C_5H_{11}N]_6[V_{10}O_{28}]\cdot 4CH_3COOH\cdot 2H_2O$ (1)

2.0 g of sodium metavanadate (16.4 mmol) was dissolved in 50mL of water by gradual heating; to the resulting solution, 10 mL glacial acetic acid was added and pH was adjusted to 2 by drop wise addition of conc HCl. The above solution was filtered into a 100 mL beaker. In order to diffuse piperidine vapor into the resulting reaction mixture, the 100 mL of beaker containing reaction mixture was placed in 250 mL beaker containing piperidine and was covered with aluminum foil. After 10 days of exposure to the piperidine vapor, the reaction mixture was out taken from 250 ml beaker and exposed to atmosphere at room temperature. After three weeks, deep orange color crystals of compound **1** precipitated out from the reaction. Yield: 0.98 g (35 % based on sodium metavanadate). Anal. Calc. for $C_{38}H_{86}N_6O_{38}V_{10}$: C, 26.16; H, 4.97; N 4.82. Found: C, 26.0; H, 4.88; N, 4.81 %. IR (KBr, cm^{-1}): 3418(br), 2964(w),1707(sh), 1628(sh), 1568(s), 1410(s), 1263(s), 1089(m), 1022(s), 800(s), 659(w), 619(w), 555(w),434(w).

3.2.2.2. Synthesis of $[C_5H_{11}N]_6[V_{10}O_{28}]\cdot 4CH_3COOH\cdot 2H_2O$ (1) nanoparticles

The general synthetic procedure for the synthesis of nanoparticles of compound **1** is described as follows: a hexagonal macro crystal (shown at the centre of Figure 3.6) of compound $[C_5H_{11}N]_6[V_{10}O_{28}]\cdot 4CH_3COOH\cdot 2H_2O$ (**1**) is taken in a measured quantity of acetonitrile solvent in which the crystal of compound **1** is not soluble and is ultra-sonicated for a constant time in the ultra-sonication bath maintained at different temperatures. The resulting suspension is analyzed using various spectroscopic and electron microscopic techniques. Anal. Calc. for nanoparticles: C, 26.16; H, 4.97; N 4.82. Found: C, 26.28; H, 4.46; N, 4.86 %. IR (KBr, cm^{-1}): 3418(br), 2964(w),1709(sh), 1628(sh), 1581(s), 1410(s), 1263(s), 1087(m), 1018(s), 798(s), 657(w), 625(w), 557(w),437(w).

3.2.2.3. SEM-samples preparation

Compound **1** (0.3 mg/mL, 1.7×10^{-4} M) was placed in acetonitrile/ acetonitrile-water/dichloromethane solvent to obtain a suspension of compound **1**. One drop of this suspension was drop casted on a glass slide using micro-pipette and dried at room temperature.

3.2.2.4. TEM-samples preparation

As described above one drop of compound **1** suspension **(**0.3 mg/mL, 1.7×10^{-4} M), was drop casted on carbon coated copper grid.

3.2.3. Single crystal X-Ray diffraction

The data were collected at 298(2) K on a Bruker SMART APEX CCD area detector [λ(Mo-K_α) = 0.71073 Å], graphite monochromator, 2400 frames were recorded with an ω scan width of 0.3^o, each for 10 s, crystal-detector distance 60 mm, collimator 0.5 mm. The data were reduced by using SAINTPLUS and a multi-scan absorption correction using SADABS was performed. Structure solution and refinement were done using programs of SHELX-97. All non hydrogen atoms were refined anisotropically. Hydrogen atoms on the C atoms of the hexamine were introduced on calculated positions and were included in the refinement riding on their respective parent atoms. Hydrogen atoms of the crystal water could not be found in the crystal structures of compound **1** and **2**. The crystallographic information of compound **1** is listed in Table 3.1 (below).

3.3. Results and discussion

3.3.1. Synthesis of macro-size crystals of compound 1

Hexagonal-shape macro-crystals of compound $[C_5H_{11}N]_6[V_{10}O_{28}]\cdot 4CH_3COOH\cdot 2H_2O$ (**1**) were isolated by slow diffusion of piperidine in the form of vapor into the sodium meta-vanadate (pH 2) solution acidified with acetic acid at room temperature. The as synthesized crystals of compound **1** have been characterized by infrared spectral studies, elemental analysis, and unambiguously by a single-crystal X-ray diffraction technique.

3.3.2. Description of crystal structure of compound 1

The asymmetric unit in the crystal structure consists of half of the cluster unit, three piperdinium cations, two acetic acid molecules and one water molecule as shown in Figure 3.1, left (the other half of the cluster shown without atom labeling). Thus the molecular formula of compound **1** includes six piperdinium cations, one $[V_{10}O_{28}]^{6-}$ cluster unit, four acetic acid and two water molecules.

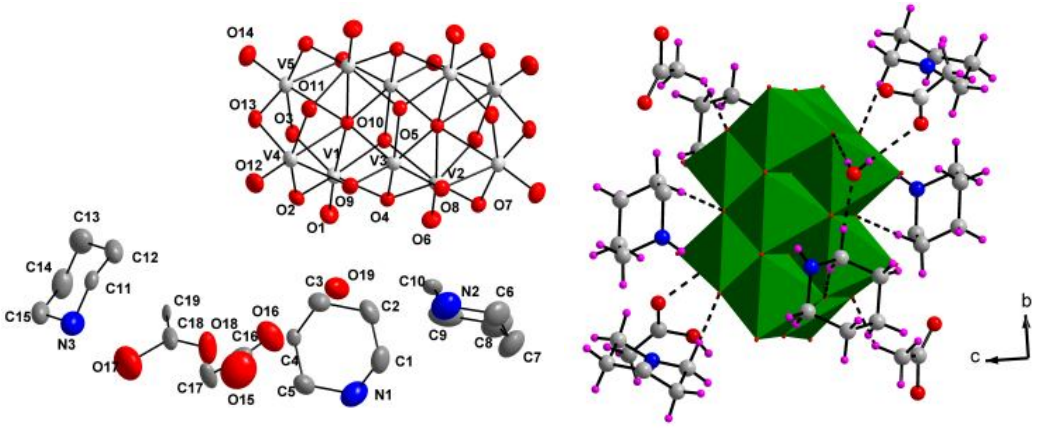

Figure 3.1. Left. Thermal ellipsoidal plot of the asymmetric unit in the crystal structure of compound **1**. Right. Hydrogen bonding situation around the $[V_{10}O_{28}]^{6-}$ cluster anion.

Since the vanadium cluster anion has surface oxygen atoms (terminal and bridging) that can act as hydrogen bond acceptors and piperidinium cation has C–H groups along with lattice water and acetic acid molecules, extensive hydrogen bonding interactions are expected to be observed in the relevant crystal. Figure 3.1(right)] demonstrates the hydrogen bonding situation involving the cluster anion, piperdinium cation, solvent water and acetic acid molecules; this leads to a ribbon type of supramolecular arrangement in the crystal structure of compound **1** as shown in Figure 3.2.

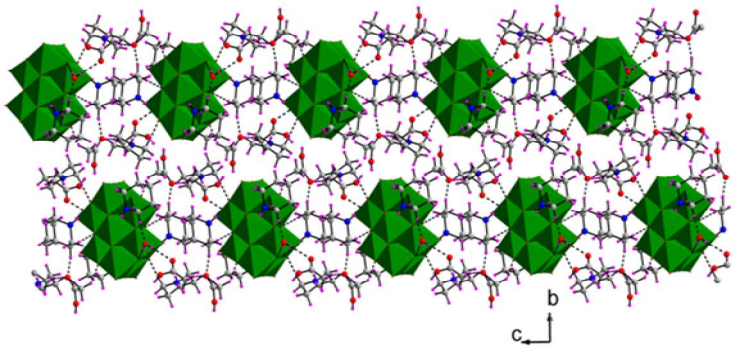

Figure 3.2. Ribbon-like supramolecular arrangement formed by hydrogen bonding interactions that involve all components in the crystal of compound **1**. The cluster anion is shown in polyhedral representation O···H separation of 2.5 Å was taken as a maximum limit.

Table 3.1. Crystal data and structure refinement for compound **1**.

	1
Formula	$C_{38}H_{86}N_6O_{38}V_{10}$
FW	1744.53
Temperature	298(2) K
Crystal system	Monoclinic
Space group	P2(1)/c
a/Å	11.6610(7)
b/Å	23.7205(14)
c/Å	12.0286(7)
β [°]	96.9790(10)^o
Volume	3302.5(3) Å^{-3}
Z	2
ρ_{cal}/ Mg m^{-3}	1.754 Mg/m^3
F(000)	1780
Crystal size	0.36 x 0.24 x 0.20 mm^3
Theta range for data collection	1.72 to 26.42^o
Reflections collected / unique	35176 / 6764
Data / restraints / parameters	6764 / 0 / 425
Goodness-of-fit on F^2	1.072
$R_1(F^2_0)$ [I > 2 σ(I)]	0.0626
wR_2 (F^2_0) [I > 2 σ(I)]	0.1522
$R_1(F^2_0)$ (all data)	0.0731
wR_2 (F^2_0) (all data)	0.1584
Largest diff. peak and hole [e.Å^{-3}]	1.096 and -0.888

Table 3.4. Hydrogen bonding parameters in the crystal structure of compound **1** [Å and °]

D-H···A	**d(D-H)**	**d(H···A)**	**d(D···A)**	**<(DHA)**
C(2)-H(2B)...O(1)#6	0.97	2.72	3.518(7)	140.0
C(2)-H(2A)...O(6)	0.97	2.65	3.593(7)	164.5
C(3)-H(3A)...O(16)	0.97	2.55	3.442(8)	153.0
C(4)-H(4A)...O(5)#6	0.97	1.82	2.793(5)	177.5
C(4)-H(4B)...O(18)	0.97	1.90	2.764(6)	146.7
C(5)-H(5A)...O(9)#5	0.97	2.82	3.553(7)	132.6
C(6)-H(6B)...O(12)#4	0.97	2.82	3.489(8)	127.1
C(6)-H(6A)...O(14)#1	0.97	2.82	3.765(9)	165.9
C(9)-H(9A)...O(6)	0.97	2.63	3.440(8)	141.3
C(10)-H(10B)...O(7)	0.97	1.97	2.908(6)	163.1
C(10)-H(10B)...O(8)	0.97	2.57	3.268(6)	128.8
C(10)-H(10A)...O(19)	0.97	1.87	2.823(8)	168.2
C(11)-H(11A)...O(2)#3	0.97	2.80	3.449(6)	124.6
C(11)-H(11A)...O(3)#3	0.97	1.96	2.923(6)	169.2
C(12)-H(12A)...O(7)#6	0.97	2.69	3.562(7)	149.2
C(12)-H(12B)...O(14)#3	0.97	2.83	3.596(7)	136.7
C(12)-H(12A)...O(13)#5	0.97	2.70	3.537(7)	145.4
C(14)-H(14B)...O(6)#2	0.97	2.89	3.498(8)	121.9
C(14)-H(14A)...O(13)#5	0.97	2.72	3.560(8)	144.7
C(14)-H(14A)...O(14)#5	0.97	2.83	3.568(8)	133.2
C(15)-H(15B)...O(1)#3	0.97	2.72	3.514(7)	139.7
C(17)-H(17A)...O(18)	0.96	1.63	2.568(6)	165.5
C(19)-H(19C)...O(12)#5	0.96	2.57	3.394(6)	144.6
C(19)-H(19C)...O(11)#5	0.96	1.82	2.615(5)	138.3

Symmetry transformations used to generate equivalent atoms

#1 -x+1,-y+1,-z; #2 -x+1,y-1/2,-z+3/2; #3 x,-y+1/2,z+1/2 ; #4 -x,-y+1,-z;

#5 x, y, z+1; #6 -x+1,-y+1,-z+1.

3.3.3. Synthesis of nanoparticles of compound 1

The general synthetic procedure for synthesis of nanoparticles of compound **1** is described as follows: a hexagonal macro crystal of $[C_5H_{11}N]_6[V_{10}O_{28}]\cdot 4CH_3COOH\cdot 2H_2O$ (**1**) is taken in a measured quantity of acetonitrile solvent in which the crystal (compound **1**) is not soluble, and the mixture is ultra-sonicated for a constant time in the ultra-sonication bath maintained at different temperatures. The resulting suspension is analyzed using various spectroscopic and electron microscopic techniques. Anal. Calc. for nanoparticles: C, 26.16; H, 4.97; N 4.82. Found: C, 26.28; H, 4.46; N, 4.86 %. IR (KBr, cm^{-1}): 3418(br), 2964(w),1709(sh), 1628(sh), 1581(s), 1410(s), 1263(s), 1087(m), 1018(s), 798(s), 657(w), 625(w), 557(w),437(w).

3.3.4. Infrared Spectroscopy

The Fourier-transform infrared (FTIR) studies (Figure 3.3) demonstrate that the nano-crystalline samples are identical to that of macro-sized crystals of $[C_5H_{11}N]_6[V_{10}O_{28}]\cdot 4CH_3COOH\cdot 2H_2O$ (**1**) indicating the conservation of {V-10} cluster in the nanoparticles.

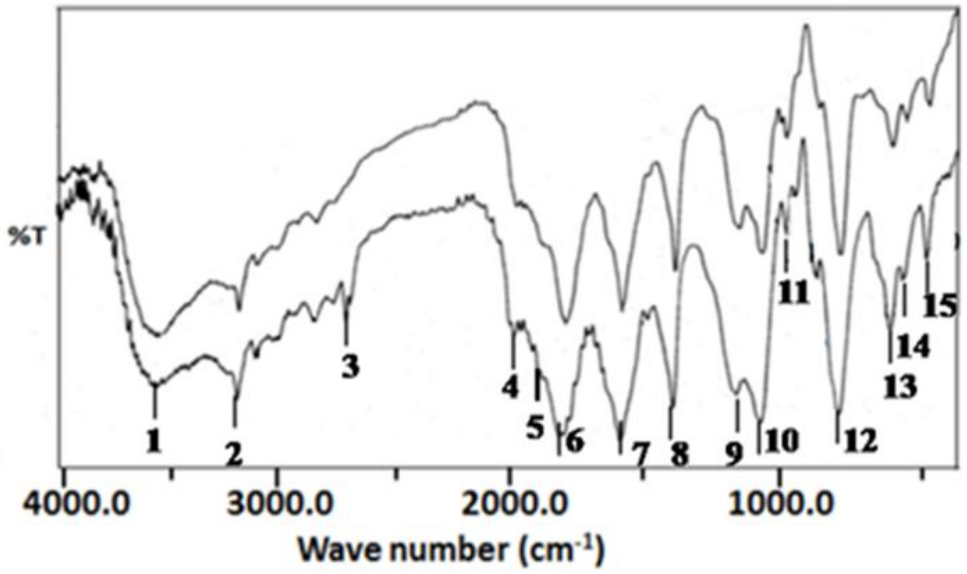

Figure 3.3. IR spectra of nano-crystals (top) and macro-crystals (bottom) of compound **1**. The units are in cm^{-1}. 1. 3418.17 (5.7); 2. 2964 (7.5); 3. 2534.69 (13.4); 4. 1701.16 (14.6); 5. 1628.07 (11.9). 6. 1568.27 (6.9); 7. 1410.09 (7.9); 8. 1263.49 (10.2); 9. 1098.88 (13.3); 10. 1022.36 (11.5). 11. 956.78 (19.2); 12. 800.53 (11.3); 13. 659.71 (18.5); 14. 619.21 (12.5); 15. 555.55 (21.4).

The infrared spectra of macro-crystals and nanoparticles show a strong band at 1022 cm^{-1} which is characteristic of the terminal V=O bond stretching.[20] In the Figure 3.3., the band appeared at 800 cm^{-1} is assigned to bridging V–O–V asymmetric vibrations, while band at around 550 cm^{-1} is assigned to symmetric V–O–V vibrations. The bands at 3418 and 1568 cm^{-1} have been assigned to N–H stretching and bending of organic piperidinium cations.

3.3.5. Powder XRD analysis

The observed PXRD patterns of nanoparticles along with macro-crystals and the simulated pattern (obtained from relevant single crystal data) are shown in Figure 3.4. The overall similarity of the observed PXRD pattern of the nano-crystalline samples with that, simulated from the single crystal data of as synthesized macro-crystals (compound **1**), indicates the phase identity.

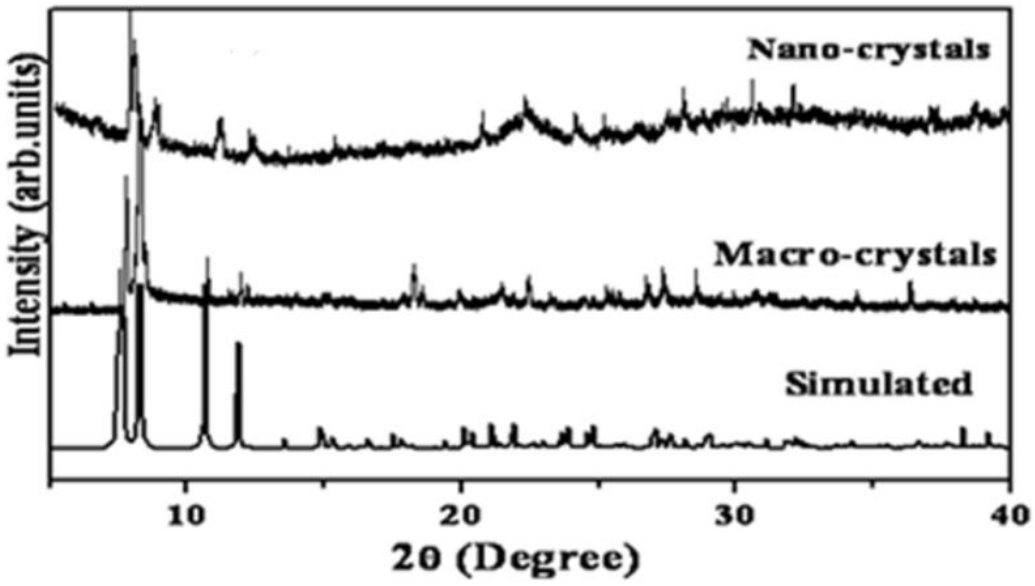

Figure 3.4. Top: powder X-ray diffraction pattern of nano-crystals; middle: powder X-ray diffraction pattern of macro-crystals; and bottom: simulated from single crystal data of compound **1**.

From Figure 3.4, it is observed that the PXRD pattern of nanoparticles is not one to one consistent with simulated PXRD pattern, especially at higher 2θ angles. This inconsistency can be attributed to the presence of some kind of strain in the sample, which is probably induced by sonication process.[21]

The selected area electron diffraction (SAED) pattern taken from a micro-flower (Figure 3.5, left and middle) and lattice planes were indexed to compound **1**; the measured *d* spacing values (SAED) are 7.450 Å, 3.305 Å and 2.450 Å, correspond well to the lattice spacing of (111), (043) and (371) planes of monoclinic macro-crystals of compound $[C_5H_{11}N]_6[V_{10}O_{28}]\cdot 4CH_3COOH\cdot 2H_2O$ (**1**). The energy dispersive x-ray spectroscopy (EDS) spectra given in Figure 3.5 (right) further confirms the presence of vanadium, carbon and nitrogen (other peaks are from glass substrate).

3.3.6. Morphological study

The macro-crystals of compound **1** are subjected to ultra-sonication at different temperatures in different solvents. The solvents used are water, acetonitrile, DCM, acetonitrile and water mixture (9:1). The polymer polyethyleneglycol also used to check the morphology of the particles. The morphological studies were done based on SEM and TEM images. In water the crystals are completely soluble, where as in acetonitrile and DCM they are dispersed.

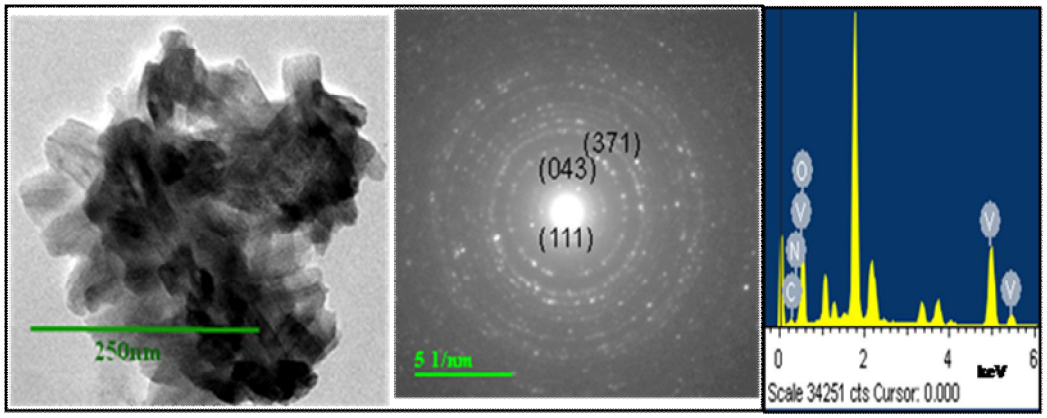

Figure 3.5. Left: TEM picture of a micro-flower; middle: selected area electron diffraction pattern of the micro-flower; right: energy dispersive spectrum of the micro-flowers.

In acetonitrile solvent the nanoparticles dispersed, are giving rise to various morphologies, such as, spherical nanoparticles, nano-rods, micro-flowers etc. The morphological variations are studied by using TEM and FESEM microscopy.

3.3.7. Reversible morphological transition observed in acetonitrile solvent starting from an as-synthesized macro-crystal as a function of sonication temperatures

The field emission SEM images of particles formed at room temperature ultra-sonication, are shown in Figure 3.6. The ultra-sonication at 50 ^{o}C leads to the formation of nano-rods with 35 nm to 300 nm thickness, 50 nm to 200 nm width and 200 nm to 5 μm length (Figure 3.6, 50 ^{o}C), whereas the sonication at 60 ^{o}C results in the formation of micro-flowers (Figure 3.6, 60 ^{o}C).

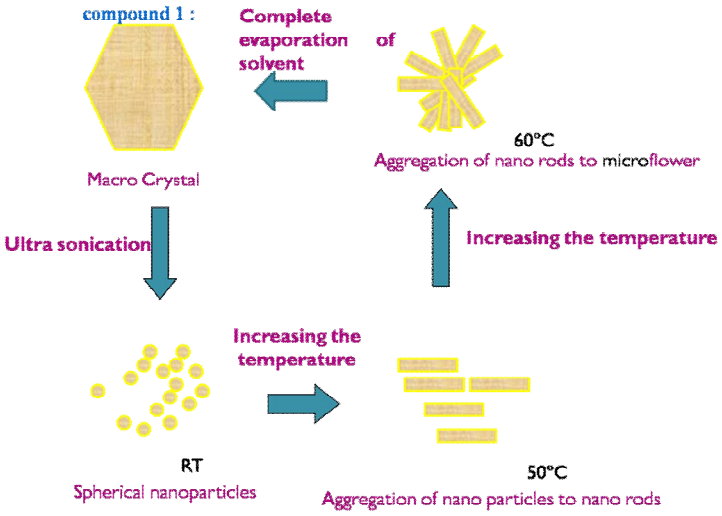

Scheme 3.1. The mechanism of reversible transition observed in the compound **1**.

The morphology of the structures, obtained from the substance, which was ultra-sonicated at 70 ^{o}C, suggests that a transition occurs by the fusion of the micro-flower aggregates (Figure 3.6, 70 ^{o}C); micrographs of the samples, obtained by further 10^{o}C rise in sonication temperature, shows further fusion into a prototype morphology of as synthesized macro-scale crystal as shown in Figure 3.6 (80 ^{o}C). Finally, the treatment of the suspension beyond 80 ^{o}C to dryness of the acetonitrile solvent leads to the hierarchical aggregation transforming back to the micro-crystal (Figure 3.6, top) of morphology, identical to the starting macro-crystal (centre of Figure 3.6) of compound **1**. Therefore, these morphological transformations illustrate the top-down and bottom up synthetic processes in a reversible cycle as presented in scheme 3.1.

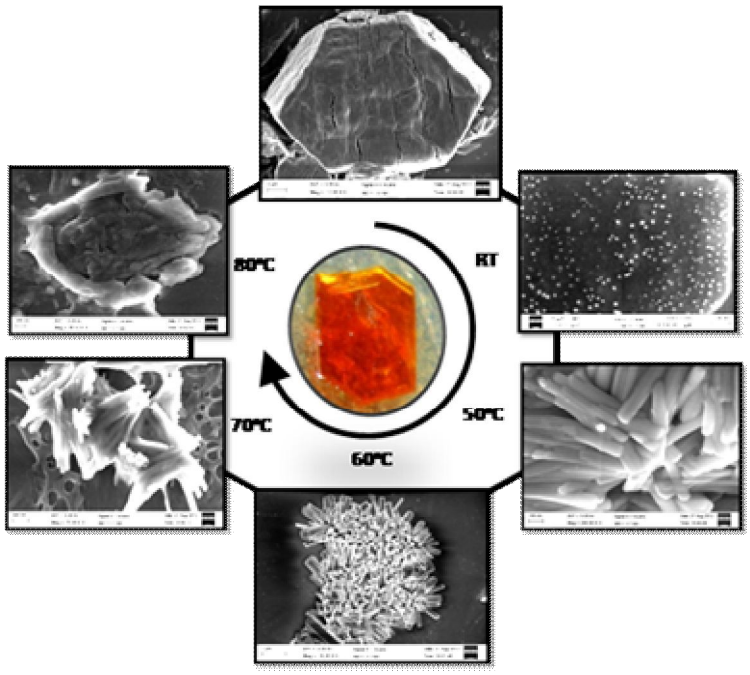

Figure 3.6. SEM images demonstrating reversible morphological transitions starting from an as-synthesized macro-crystal (at the centre) as a function of sonication temperatures.

This reversible morphological transition can be described as a result of breaking down of a macro-size as-synthesized crystal into nano-crystals (Figure 3.6) and wielding back to micro-sized crystal (Figure 3.6) as a function of sonications at different temperatures (external stimulus). Thus in the present study, the formation of these nano-structures from a macro-sized crystal needs an external stimulus.[22] The turning back of the nano-crystals to a micro-crystal form after drying the concerned acetonitrile solution at 80 ^{o}C can be argued as crystallization process to obtain a higher ordered form at higher temperature.

3.3.8. Solvent effects on the morphology

The solvent effects on the morphology of sono-synthesized particles have been studied. The deposition of compound **1** from solution of water/acetonitrile (1:9 v/v) at room temperature leads to the formation of rhombohedral shaped nanoparticles; at higher tem perature, the particles transform to flower like aggregates without formation of rod-shape nanoparticles (see following scheme 3.2). However, it did not result in the transformation of the aggregates as has been observed in the case

of pure acetonitrile solvent. Moreover, the flower-like morphology, obtained in the case of water / acetonitrile solvent, is different from those, derived from pure acetonitrile.

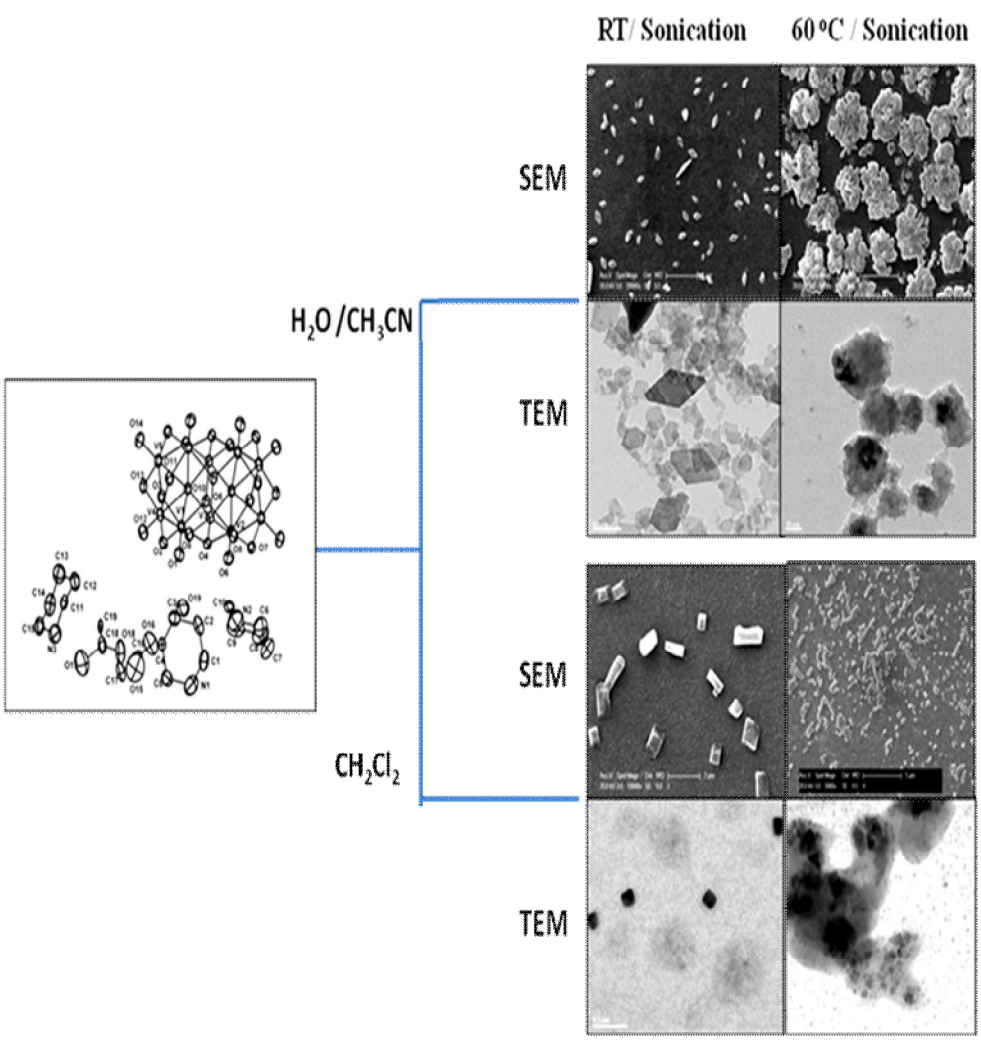

Scheme 3.2. Schematic representation of SEM and TEM images of compound **1**, sonicated in water / acetonitrile (1:9) and Dichloromethane.

The ultrasonication synthesis in dichloromethane solvent resulted in the formation of nano-cubes at room temperature; at higher temperatures (50 ^{o}C and above) the cubes tend to deform without any well defined morphology (see scheme 3.2).

3.4. Conclusion

In summary, we have demonstrated a simple synthetic strategy to obtain different nano-morphologies of $[C_5H_{11}N]_6[V_{10}O_{28}]\cdot 4CH_3COOH\cdot 2H_2O$ (**1**). The interesting aspects of this work are (i) ultra-sonication assisted top down synthesis of nanoparticles of compound **1**; (ii) different morphologies of nanoparticles can be obtained as function of solvent temperature; (iii) to our knowledge, this is the first report of reversible morphological transitions from a polyoxometalate compound.

3.5. References

1. Pope, M.T. Heteropoly and Isopoly Oxometalates, Springer, Berlin, **1983**.
2. Pope, M.T.; Muller, A. *Angew. Chem. Int. Ed. Engl.* **1991**, *30*, 34.
3. Livage, J. *Coord. Chem. Rev.* **1998**, *178*, 999.
4. Okuhara, T.; Mizuno, N.; Misono, M. *Adv. Catal.* **1996**, *41*, 113.
5. Hill, C. L.; -McCartha, C. M. P. *Coord. Chem. Rev.* **1995**, *143*, 407.
6. Noro, S.-i.; Tsunashima, R.; Kamiya, Y.; Uemura, K.; Kita, H.; Cronin, L.; Akutagawa, Nakamura, T. *Angew. Chem. Int. Ed. Engl.* **2009**, *48*, 8703.
7. Müller, A.; Penk, M.; Rohlfing, R.; Krickemeyer, E.; Döring, J.; *Angew. Chem. Int. Ed. Engl.* **1990**, *29*, 926.
8. Khenkin, A. M.; Weiner, L.; Wang, Y.; Neumann, R. *J. Am. Chem. Soc.* **2001**, *123*, 8531.
9. Haimov, A.; Neumann, R. *Chem. Commun.* **2002**, 876.
10. Maayan, G.; Ganchegui, B.; Leitner, W.; Neumann, R. *Chem. Commun.* **2006**, 2230.
11. Kozhevnikov, I. V. *Chem. Rev.* **1998**, *98*, 171.
12. Wu, P.; Xiao, Z.; Zhang, J.; Hao, J.; Chen, J.; Yin, P.; Wei, Y. *Chem. Commun.* **2011**, *47*, 5557.
13. Khan, M. I.; Aydemir, K.; Siddiqui, M. R. H.; Alwarthan, A. A.; Marshall, C. L. *Catalysis Lett.* **2011**, *141*, 538.
14. Gao, F.; Hua, R. *Catalysis Commun.* **2006**, *7*, 391.
15. Musumeci, C.; Rosnes, M. H.; Giannazzo, F.; Symes, M. D.; Cronin, L.; Pignataro, B. *ACS Nano* **2011**, *5*, 9992.

16. Liu, S.; Tang, Z. *Nano Today* **2010**, *5*, 267.
17. Clemente-Leon, M.; Coronado, E.; Gomez-Garcia, C. J.; Mingotaud, C.; Ravaine, S.; Romualdo-Torres, G.; Delhaes, P. *Chem. Eur. J.* **2005**, *11*, 3979.
18. Mai, L.; Han, C. *Mater. Lett.* **2008**, *62*, 1458.
19. Livage, J. *Materials* **2010**, *3*, 4175.
20. Krystyna, B.; Krystyna, K.; Przemysoaw, S.; *Transit. Metal Chem.* **2001**, *26*, 311.
21. Thompson, J. A.; Chapman, K. W.; Koros, W. J.; Jones, C. W.; Nair, S. *Micropor. Mesopor. Mater.* **2012**, *158*, 292.
22. Kuo, M. -C.; Chen, H. -F.; Shyue, J. -J.; Bassani, D. M.; Wong, K. -T. *Chem. Commun.* **2012**, *48*, 8051.

Decavanadate-based discrete compound and coordination polymer: synthesis, crystal structures, spectroscopy and nano-materials

4

Chapter 4 describes two decavanadate based compounds, $[HMTA]_2[Na(H_2O)_6]_2[H_2V_{10}O_{28}]\cdot 6H_2O$ (1) (HMTA = hexamethylene-tetramine) and $[Na_3(H_2O)_9]_{2n}[V_{10}O_{28}]_n$ (2), which have been synthesized in aqueous medium. Compound 1 (a discrete compound) is synthesized with organic and inorganic cations, wheeas compound 2 (a coordination polymer) has been isolated using only inorganic cations. An acidified aqueous solution of sodium metavanadate, on heating at 70 °C followed by addition of acetonitrile, results in the isolation of compound 2, the crystal structure of which showing it to be a two-dimensional coordination polymer, formed from the decavanadate cluster anion and the tri-sodium aqua-complex cation. Compounds 1 and 2 have been characterized by routine elemental analyses, FT-IR spectroscopy and unambiguously by single crystal X-ray crystallography. Among these two compounds, compound 2 exhibits an emission in the visible region at room temperature in its solid state (on excitation at 380 nm). Nano-crystals of compound 2 in the size range 50–70 nm were synthesized by ultrasonication of macro-crystals of compound 2 in acetonitrile solvent (0.5 mM). The nanoparticles were characterized by FT-IR and PXRD studies. The morphology of the nanoparticles of compound 2 were studied using FE-SEM, TEM and AFM techniques. As expected, these nanoparticles also display emission spectra at room temperature. The connectivity of the decavanadate oxygens with the metal cations plays an important role in compound 2 exhibiting emission spectra, because decavanadate cluster (as such) containing compounds generally do not show emission.

4.1. Introduction

Polyoxometalates (POMs) are extremely versatile building blocks for the construction of inorganic functional materials with a range of physical and chemical properties that are significant for their applications in the areas of materials science[1], magnetism[2], medicinal[3] and industrial chemistry.[4] Functionalized POMs give rise to vast diversity of materials, being used as building blocks for creating highly classy hierarchical systems with various interdependent functionalities.[5] The functionalization of the POM cluster anions to explore more selective applications[6] is an interesting aspect in recent POM chemistry. The functional POM frameworks have been achieved by using either pure organic linkers[7] or metal coordination complexes (with organic ligands) as linkers;[8] however, both these approaches are limited by the reduced stability of the concerned framework, because both linkers contain organic moieties that are not thermally stable. The assembly of a purely inorganic POM building unit offers high stability to the concerned network for the formation of new type of pure inorganic materials.[9] Thus, the planned synthesis of pure inorganic based materials, for example, the synthesis of polyanion-inorganic cation based polymeric compounds, is a big challenge in modern inorganic chemistry.[10] Programmable POM-based multi-functional nano-structures are reported on silica surfaces, that yield 0-D, 2-D and 3-D architectures, including nano-dots, discs, porous networks and layer-by-layer assemblies.[11] POMs are dynamically entered into the realm of the synthesis of metal nano-particles, and serve both as catalytic agents and stabilizers for the synthesis of Ag, Au, Pd and Pt nano-particles of reasonably good dispersity.[12] Silver and gold nano-particles containing POM-based organic–inorganic nano-composites find applications in the areas of sensing materials, catalysis and composite materials.[13] The large scale synthesis of POM-based spheres-, belts-, flake-, cube-, prism-, trigonal- and snowflake-like nanocrystals/nanoparticles were performed by a solution phase route using a wide range of surfactants.[14] Among the POMs, polyoxovanadates (POVs) are an important class of materials that have various applications in the fields of materials science, industrial chemistry and biology.[15] POV clusters have also been used as linkers for constructing vanadium framework containing materials, which can be called vanadium MOFs (VMOFs).[16] Among several POV cluster anions, the decavanadate cluster anion $[V_{10}O_{28}]^{6-}$ seems to be best known in the solid state phase.[17] Several discrete decavanadate cluster containing compounds have been isolated with alkali metals and transition metals as

macro-crystals.[18] Ramanan and co-workers have made a considerable contribution to fully oxidized vanadium based polyoxoanions in the presence of cage-like hexamethylenetetramine as a structure director.[19] Cronin and his group have described silver linked POM open frameworks for the directed fabrication of silver nano-materials.[20] The electrical properties of ammonium decavanadate single crystalline nano-rods have been reported by Mai and Han.[21] Pure inorganic polymeric complexes based on decavanadate complexes are relatively less explored. We have been exploring the self-assembly process of the decavanadate cluster, including its nano-morphological studies.[22]

The decavanadate cluster anion $[V_{10}O_{28}]^{6-}$ as the central core, two decavanadate based compounds $[HMTAH]_2[Na(H_2O)_6]_2[H_2V_{10}O_{28}]\cdot 6H_2O$ (**1**) (HMTA = hexamethylenetetramine) and $[Na_3(H_2O)_9]_{2n}[V_{10}O_{28}]_n$ (**2**) were discussed. A pure inorganic linker is chosen to extend the dimensionality of the decavanadate cluster in compound **2**. In the crystal structure of compound **2**, a tri-sodium-aqua cluster (supported on the decavanadate anion by a coordinate covalent bond) is observed. Overall, in this chapter the supramolecular assembly of the decavanadate cluster anion $[V_{10}O_{28}]^{6-}$ using an organic linker, hexamethylenetetramine (compound **1**), and the coordination assembly of the decavanadate cluster anion using an inorganic linker, the tri-sodium aqua cluster cation (compound **2**) were discussed. The nano-crystals of compound **2**, which are synthesized by ultra-sonication of the macro-crystals of compound **2** in acetonitrile solvent are discussed. The compound $[Na_3(H_2O)_9]_{2n}[V_{10}O_{28}]_n$ (**2**) is unique in the sense that it is an emissive inorganic coordination polymer based on a decavanadate cluster.

The compounds described in this chapter are

$[HMTAH]_2[Na(H_2O)_6]_2[H_2V_{10}O_{28}]\cdot 6H_2O$ (**1**),
$[Na_3(H_2O)_9]_{2n}[V_{10}O_{28}]_n$ (**2**).

4.2. Experimental details

4.2.1. Materials and physical methods

All the reactions were performed under ambient conditions. The starting materials, sodium metavanadate and HMTA were obtained from SISCO, acetonitrile from Sigma Aldrich and distilled water was used in all the experiments.

4.2.2. Characterization

Micro analytical (C, H, N) data were obtained with a FLASH EA 1112 Series CHNS analyzer. Infrared (IR) spectra were recorded on a KBr pellet with a JASCO FT/IR-5300 spectrometer in the region 400–4000 cm^{-1}. Electronic absorption spectra were obtained on a Cary 100 Bio UV–Vis spectrophotometer. Emission spectra were recorded on a spectrofluorimeter (FluoroLog-3, Horiba Jobin Yvon). Confocal fluorescence microscopic images of compound **2** nanoparticles were recorded on a Leica Laser Scanning confocal microscope (TCS SP2 AOBS), Germany. The morphology of the nanoparticles of compound (**2**) was obtained using a field emission-scanning electron microscope (FE-SEM) (Carl Zeiss, Ultra55). Transmission electron microscopic studies were carried out on a FEI Tecnai G2 S-Twin, FEI electron microscope operating at 200 kV and using a Gatan CCD camera. The vanadium content of the compound $[Na_3(H_2O)_9]_{2n}[V_{10}O_{28}]_n$ (**2**) was analyzed using a Varian 720-ES Inductively Coupled Plasma-Optical Emission Spectrometer (ICP-OES).

4.2.3. Synthesis

4.2.3.1. Synthesis of the compound [$HMTAH]_2[Na(H_2O)_6]_2[H_2V_{10}O_{28}]\cdot 6H_2O$ (1)

To the 100.0 mL aqueous solution of sodium metavanadate (2.0 g, 8.26 mmol) and hexamine (0.14 g, 1 mmol), acetic acid was added to maintain the pH value at 4.0. The resulting reaction mixture was stirred for 2 h and kept for crystallization. After 10 days, yellow needle shaped crystals of compound 1 appeared and were isolated by filtration. Yield: 40% based on V. IR (KBr, cm^{-1}): 3452(br), 2947(w), 2865(w), 1649(m), 1457(m),1369(m), 1238(s), 1013(s), 986(br), 953(sh), 805(m), 778(sh), 668(w), 509(w).

Anal. Calc. for. C12H64N8Na2O46V10 (1612.05): C, 8.94; H, 4.00; N, 6.95. Found: C, 8.91; H, 3.84; N, 6.91%.

4.2.3.2. Synthesis of the compound $[Na_3(H_2O)_9]_{2n}[V_{10}O_{28}]_n$ (2)

A 100.0 mL aqueous solution of sodium metavanadate (2.0 g, 8.26 mmol) was heated for 2 h at 70 °C. To this hot solution, acetic acid was added to maintain the pH value at 5.0; subsequently 60.0 mL acetonitrile was added to crystallize yellow color block-shaped crystals of **2**. Yield: 50% based on V. IR (KBr, cm^{-1}): 163 3463(br), 1621(s), 953(s), 849(s), 739(s), 602(w), 526(w), 449(w). Anal. Calc. for. $V_{10}Na_6O_{46}H_{36}$ (1419.42): V, 35.88; H, 2.55. Found: V, 35.02 (ICP-OES); H, 2.43%.

4.2.3.3. Synthesis of compound 2 nanoparticles

Nanoparticles of compound **2** were synthesized by the simple ultrasonication method. Hexagonal macro-crystals of compound **2** were taken in acetonitrile solvent and ultrasonicated for an hour under an ambient atmosphere. The solution drop was casted onto a glass plate and analyzed using various spectroscopic and microscopic techniques. IR (KBr, cm^{-1}): 3567(br), 1621(s), 986(sh), 947(s), 843(m), 723(w). Anal. Calc. for nanoparticles: H, 2.55. Found: H, 2.48%.

4.2.4. Crystal structure determination

Single crystal X-ray diffraction data were collected at 298(2) K on a Bruker SMART APEX CCD area detector system with Mo Ka radiation (k = 0.71073 Å) and with a graphite monochromator. 2400 frames were recorded with an x scan width of 0.3°, each for 10 s with a crystal detector distance of 60 mm and collimator distance of 0.5 mm. The data were reduced using SAINTPLUS[23] and a multi-scan absorption correction was performed using SADABS.[23] Structure solution and refinement were done using the programs of SHELX-97.[24] All non-hydrogen atoms were refined anisotropically. Hydrogen atoms on the C atoms of the hexamine were introduced in calculated positions and were included in the refinement, riding on their respective parent atoms. The Na atom in compound **1** suffers from a significant disorder problem which resolving was tried by applying the restraints ISOR or SIMU to the displacement parameters, but this was not successful. The hydrogen atoms of the water molecules were located in the crystal

structures of **1**and **2** through Fourier electron density maps. The crystallographic details and refinement parameters of compounds are listed in Table 4.1.

4.3. Results and discussion

4.3.1. Synthesis

The syntheses of polyoxovanadates have classically been performed in aqueous solutions (wet synthesis) or under hydrothermal conditions.[25] Compound **1** has been synthesized by the direct one pot reaction of sodium metavanadate aqueous solution together with hexamethylenetetramine (HMTA) at an ambient temperature. The pH of the concerned reaction mixture was adjusted to 4.0 by adding acetic acid. Addition of acetonitrile solvent to the hot acidified aqueous solution of sodium metavanadate at pH 5.0 results in the formation of compound **2**, which is a purely inorganic polymer with a trisodium-aqua complex as the cation. Notably, the decavanadate (POV) cluster anion exists in the di-protonated state in the compound $[HMTAH]_2[Na(H_2O)_6]_2[H_2V_{10}O_{28}]\cdot 6H_2O$ (**1**). It is well known that under an aqueous conditions, a number of vanadium species, for example $[H_6V_{10}O_{28}]$, $[H_5V_{10}O_{28}]^-$,$[H_4V_{10}O_{28}]^{2-}$, $[H_3V_{10}O_{28}]^{3-}$, $[H_2V_{10}O_{28}]^{4-}$, $[HV_{10}O_{28}]^{5-}$, $[V_{10}O_{28}]^{6-}$ etc. can exist in equilibrium, depending upon the pH of the concerned reaction mixture. [19]

4.3.2. Infrared spectroscopy

The infrared (IR) spectra exhibit characteristic features of the decavanadate cluster anion for all the compounds **1** and **2**. Compound **1** also shows the IR bands for hexamethylenetetramine. The IR spectra of the three compounds are shown in Figure 4.1. The V–O vibrations of the decavanadate anion are observed in the region 450–1000 cm^{-1}; the strong IR bands at around 950 cm^{-1} for all the three compounds (**1** and **2**) are attributed to stretching vibrations of the V–O terminal oxygen atom. The bands in the 750–600 cm^{-1} region are due to bridging V–O–V groups. The asymmetric vibrations of the V–O–V bridges are observed at 778 cm^{-1} (compound **1**), 739 cm^{-1} (compound **2**), while the symmetric bands are observed at 668 cm^{-1} (compound **1**) and 602 cm^{-1} (compound **2**).

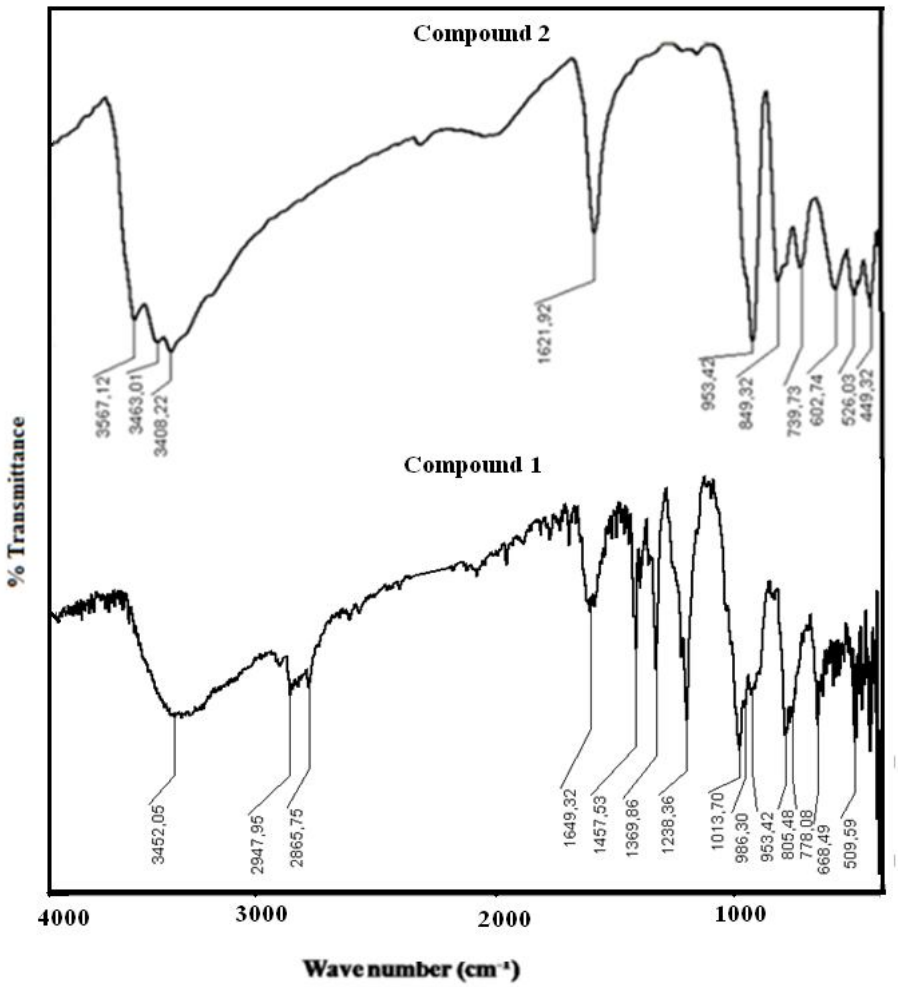

Figure 4.1. FT-IR spectra of macrocrystals of compounds **1** and **2**.

4.3.3. Thermal properties

Thermogravimetric analyses (TGA) were performed in the temperature range 30–1000 °C on polycrystalline samples in the air. The TG curve for the compound $[HMTAH]_2[Na(H_2O)_6]_2[H_2V_{10}O_{28}]\cdot 6H_2O$ (1) shows a first weight loss of 6.85% in the temperature range 94–153 °C. This weight loss corresponds to the loss of six water molecules (calculated mass loss for six water molecules is 6.7%). This includes six non-coordinated lattice water molecules. The second weight loss of 31.7% in the temperature range 120–219 °C might be due to the loss of two hexamine moieties and twelve sodium coordinated water molecules (calculated mass loss for two hexamine moieties is 17.53% and for twelve water molecules is 13.4%). The TG curve for the compound

$[Na_3(H_2O)_9]_{2n}[V_{10}O_{28}]_n$ (**2**) shows a weight loss of 22.34% in the temperature range 42–164 °C, which corresponds to the loss of 18 water molecules, coordinated to the tri-sodium cation (calculated 22.8% for 18 sodium coordinated water molecules). On further heating, the cluster disintegrates. The TG curves of the two com pounds **1** and **2** are graphically presented in Figure 4.2. The thermal behavior of the related compound $[Na_2(H_2O)_{10}][H_3V_{10}O_{28}[Na(H_2O)_2]\cdot 3H_2O$[19a], which on heating around 250 °C forms the cluster decomposition product $Na_xV_2O_5$, is quite comparable to that of compound **2** (present study). Similar thermal plots have been observed for the related decavanadate cluster containing compounds $(NH_4)_2[Ni(H_2O)_5(NH_3)]_2[V_{10}O_{28}]\cdot 4H_2O$ and $(NH_4)_2[Zn(H_2O)_6]_2V_{10}O_{28}\cdot 4H_2O$.[27,28] Thus it is always not true that the assembly of purely inorganic POM building units offers high stability to the concerned network.

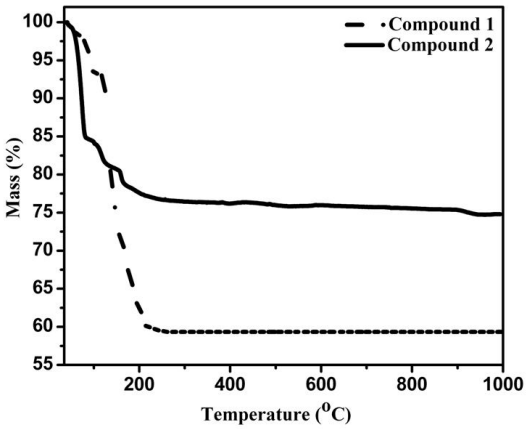

Figure 4.2. Thermogravimetric analysis for compounds **1**, **2** and **3**.

4.3.4. Description of the crystal structures

4.3.4.1. Compound $[HMTAH]_2[Na(H_2O)_6]_2[H_2V_{10}O_{28}]\cdot 6H_2O$ (1)

The asymmetric unit of compound **1** consists of half of the decavanadate cluster anion, one hexa-hydrated sodium coordination complex cation, one protonated HMTA cation and three lattice water molecules (Figure 4.3.). Thus the formulation of compound **1** is given as $[HMTAH]_2[Na(H_2O)_6]_2[H_2V_{10}O_{28}]\cdot 6H_2O$. The oxygen atoms of the decavanadate cluster are not coordinated to either the sodium cation or the HMTA cation directly, resulting in **1** being a discrete compound.

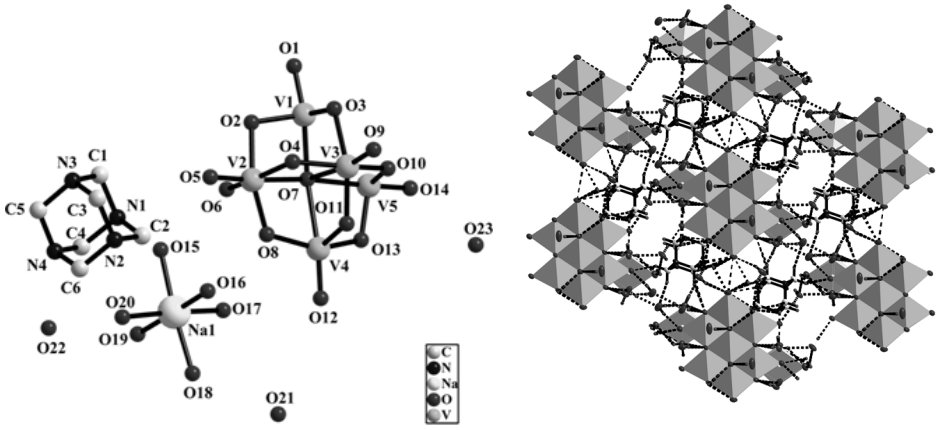

Figure 4.3. Ball and stick representation of the asymmetric unit in the crystal structure of compound **1** (hydrogen atoms are omitted for clarity); (b) 3-d network established due to the O–H ·····O interactions as well as C–H···O interactions in the compound **1**.

In the decavanadate polyanion, all the V–O oxygen bond lengths (V−O_t, V−O_b and V−O_c) are in the expected ranges according to reported literature (Table 4.2.). The sodium cation, coordinated to six water molecules, forms a octahedral coordination complex cation $[Na(H_2O)_6]^+$. The Na–O bond distances are in the expected range of 2.012–2.110 Å. Along with the sodium cation, the monoprotonated HMTA cation is present in the crystal structure. Two protons have been added to the decavanadate cluster anion to neutralize the overall charge (see the formula of compound **1**). The possibility of di-protonation to HMTA has been ruled out, because it is generally very difficult for the hexamethylenetetramine (HMTA) molecule to be di-protonated and is rarely known, especially at a pH value of 4.0 (it is the pH, at which compound **1** has been synthesized).

Table 4.2. Selected V–O distance range (Å) in compounds **1** and **2**

	$\{H_2V_{10}O_{28}\}^{4-}$ **1**	$\{V_{10}O_{28}\}^{6-}$ **2**
V–O(t)[a]	1.599(3)-1.610(3)	1.597(2)-1.610(1)
V–O(μ_2)[a]	1.690(5)-2.063(4)	1.683(3)-2.047(2)
V–O(μ_3)[a]	1.910(3)-2.015(4)	1.894(1)-2.014(2)
V–O(μ_6)[a]	2.087(3)-2.343(4)	2.110(2)-2.316(2)

[a] t, μ_2, μ_3 and μ_6 are terminal, doubly, triply and hexa bridged oxygen atoms respectively.

Table 4.3. Hydrogen bonding parameters in the crystal structure of compound **1** [Å and °]

D-H···A	**d(D-H)**	**d(H···A)**	**d(D···A)**	**<(DHA)**
O(15)-H(15A)...O(6)	0.80(3)	2.07(3)	2.871(3)	177(3)
O(16)-H(16A)...O(8)	0.76(4)	1.89(4)	2.643(3)	173(4)
O(16)-H(16B)...O(21)#5	0.79(3)	1.87(4)	2.644(3)	166(3)
O(17)-H(17B)...O(3)#2	0.76(4)	1.95(4)	2.713(3)	176(4)
O(17)-H(17A)...O(1)#1	0.73(4)	1.95(4)	2.679(3)	172(4)
O(18)-H(18A)...O(4)#2	0.78(4)	1.90(4)	2.673(3)	178(4)
O(19)-H(19B)...O(2)#2	0.71(3)	2.02(3)	2.717(3)	172(3)
O(19)-H(19A)...O(23)#3	0.77(4)	1.97(4)	2.711(3)	162(3)
O(20)-H(20A)...O(23)#3	0.69(4)	2.13(4)	2.760(3)	151(4)
O(21)-H(21B)...O(5)#7	0.85(4)	1.95(4)	2.783(3)	169(3)
O(21)-H(21A)...O(18)#6	0.82(4)	2.03(4)	2.830(3)	165(4)
O(22)-H(22B)...O(10)#7	0.81(4)	2.49(4)	3.237(3)	154(3)
O(22)-H(22B)...O(11)#7	0.81(4)	2.44(4)	3.098(3)	139(3)
O(22)-H(22B)...O(13)#7	0.81(4)	2.70(4)	3.283(3)	130(3)
O(22)-H(22A)...O(12)#8	0.76(5)	2.43(5)	3.160(3)	160(5)
O(23)-H(23B)...O(14)	0.80(4)	2.00(4)	2.798(3)	171(4)
C(1)-H(1A)...O(4)#8	0.96(3)	2.34(3)	3.220(3)	151(2)
C(2)-H(2A)...O(1)#2	0.97(3)	2.75(3)	3.681(3)	160(2)
C(4)-H(4A)...O(12)#7	0.96(3)	2.66(3)	3.275(3)	123(2)
C(4)-H(4A)...O(13)#7	0.96(3)	2.35(3)	3.244(3)	154(2)
C(5)-H(5B)...O(5)#9	0.96(3)	2.44(3)	3.156(3)	131(2)
C(5)-H(5A)...O(21)#10	0.94(3)	2.64(3)	3.316(3)	130(2)

Symmetry transformations used to generate equivalent atoms:

#1 -x,-y+1,-z+1 #2 x+1,y,z #3 x+1,y,z+1 #4 x,y+1,z #5 x,y+1,z+1
#6 -x+2,-y+1,-z+1 #7 -x+1,-y+1,-z+1 #8 x,y-1,z #9 -x+1,-y+1,-z+2 #10 -x+1,-y,-z+1

Due to presence of the sodium coordinated water molecules and lattice water molecules, extensive supramolecular interactions have been observed involving surface oxygen atoms of decavanadate anion (O−H···O_{dec}) as well as lattice molecules (O−H····O_{water}). The hexamethylenetetramine (HMTA) cation, having twelve protons, is also involved in

hydrogen bonding interactions (C−H···O) with the surface oxygen atoms of the decavanadate cluster anion and with the lattice water molecules. Each HMTA cation interacts with four adjacent decavanadate cluster anions. The combination of both O−H····O and C−H····O hydrogen bonding interactions results in the formation of a 3-D supramolecular network, as observed in the crystal structure of compound **1**. The relevant hydrogen bonding parameters are presented in Table 4.3.

4.3.4.2. Compound $[Na_3(H_2O)_9]_{2n}[V_{10}O_{28}]_n$ (2)

The asymmetric unit in the crystal structure of compound **2** consists of half of the decavanadate cluster anion that supports the tri-sodium aqua-complex cation. The 6− charge of decavanadate cluster anion $[V_{10}O_{28}]^{6-}$ is counter-balanced by two $[Na_3(H_2O)_9]^{3+}$ cations, and accordingly compound **2** can be formulated as $[Na_3(H_2O)_9]_{2n}[V_{10}O_{28}]_n$ (it is a coordination polymer). The full decavanadate cluster anion with two attached coordinated tri-sodium aqua-complex $[Na_3(H_2O)_9]^{3+}$ cations is shown in Figure 4.4(a). In the trisodium cluster, two sodium cations, namely Na3 and Na2, have an octahedral geometry, whereas the Na1 ion has a square pyramidal geometry. The Na3 octahedron is furnished by two bridging water molecules (O19 and O20), two monodentate coordinated water molecules (O22 and O23) and two terminal oxygen atoms (O9 and O12) from two different {V10} cluster anions. On the other hand, the coordination of the Na2 octahedron is completed by five bridging water molecules (O16, O17, O18, O19 and O20) and one monodentate coordinated water molecule (O21); notably no {V10} cluster oxygen atoms are coordinated to the Na2 cation, unlike the Na3 cation. The square pyramidal geometry around the Na1 cation can be described by three bridging water molecules (O16, O17 and O18), one monodentate coordinated water molecule (O15) and one l3-oxygen atom (O3) of the {V10} cluster anion.

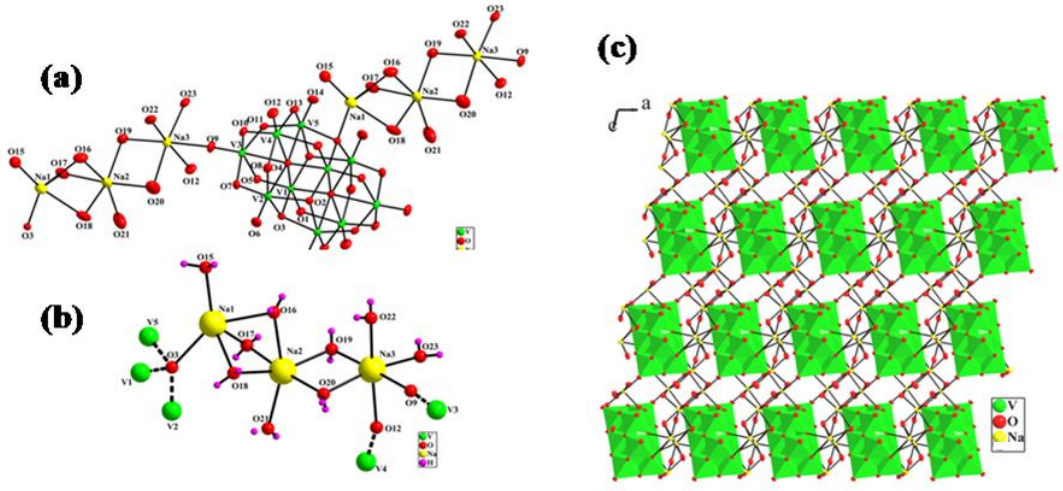

Figure 4.4. (a) Ball and Stick representation of compound **2** (hydrogen atoms are omitted for clarity) (b) The trisodium cation coordinated with the decavanadate anion (c) 2-D network established in the coordination polymer of compound **2**, along *ac* plane.

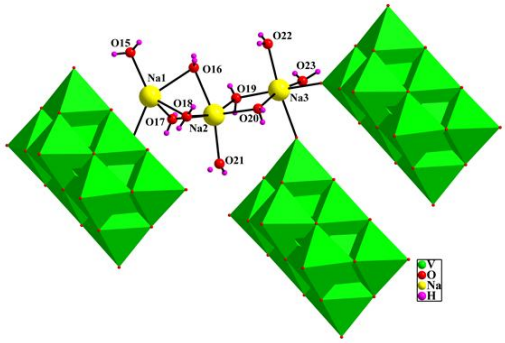

Figure 4.5. The tri-sodium aqua cation coordinated with the three surrounding decavanadate anions in compound **2**.

In total, two water molecules (O19 and O20) bridge between the Na3 and Na2 cations, and three water molecules (O16, O17 and O18) bridge between the Na2 and Na1 cations to form a tri-sodium-aqua-cluster $[Na_3(H_2\ O)_9]^{3+}$, as shown in Figure 2(b). The terminal sodium cations Na1 and Na3 are connected to the oxygen atoms of the {V10} cluster anions to extend the dimensionality into the layer-like structure, as shown in Figure 2(c). Interestingly, the mode of connectivity of the terminal sodium cations (Na1 and Na3) with surrounding different decavanadate clusters is different from each other: the Na3 cation is connected to two different V=O type terminal oxygen atoms (O9 and O12) from two different decavanadate cluster anions, whereas the Na1 cation is connected to the μ_3-O

type oxygen atom (O3) of the decavanadate cluster. This interesting connectivity from the μ_3-O type oxygen atom of the {V10} cluster to a sodium cation is very rare in decavanadate chemistry; this mode of connectivity probably causes the deviation of the geometry of Na1 polyhedron from a normal octahedral geometry to an unusual square pyramidal geometry around sodium. The coordination of the terminal Na1 with the {V10} cluster through the μ_3-type oxygen atom (O3) precludes water molecules from entering into its (Na1) coordination sphere, thereby it forms relatively longer bonds with the μ_2-type bridging water oxygen atoms. Overall, in the crystal structure, each tri-sodium aqua-cluster connects to three {V10} cluster anions (Figure 4.4(b) and also Figure 4.5) and extends its dimensionality along a layer to form a 2D coordination polymer, as shown in Figure 4.4(c).

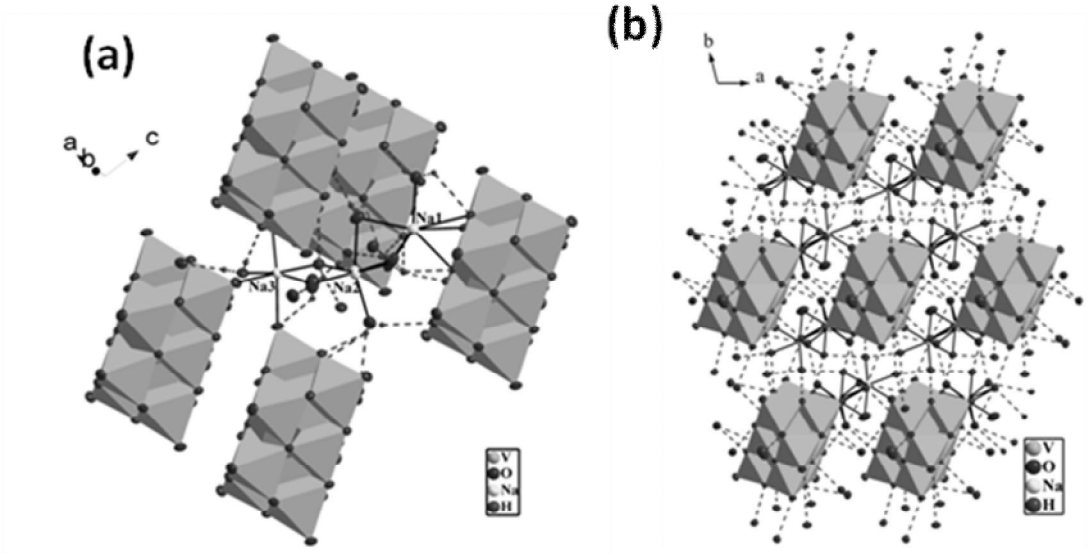

Fig. 4.6. (a) The O−H···O interactions between the water molecules of tri-sodium aqua cation with its surrounding five decavanadate anions in compound **2**. (b) The O−H···O hydrogen bonding interactions between the anion and cation showing extension from 2D coordination polymer/sheet to a 3D-supramolecular network in compound **2**.

The water hydrogen atoms of the tri-sodium aqua-complex cation show extensive hydrogen bonding interactions (O−H···O) with the surrounding five decavanadate cluster anions. These O−H···O interactions between the anion and cation extends the 2D coordination polymer/sheet into a 3D-supramolecular network (Figure 4.6). The relevant hydrogen bonding parameters are presented in Table 4.4. The bond lengths and bond angles are presented in Table 4.5.

Table 4.1. Crystal data and structure refinement for compounds **1** and **2**.

	1	**2**
Molecular formula	$C_{12}H_{64}N_8Na_2O_{46}V_{10}$	$H_{36}Na_6O_{46}V_{10}$
Formula weight	1612.08	1419.63
Temperature	298K	298K
Wavelength	0.71073 Å	0.71073 Å
Crystal system	Triclinic	Triclinic
Space group	*P-1*	*P-1*
a/Å	9.6133(15)	8.5430(11)
b/Å	11.9795(19)	10.8231(14)
c/Å	12.611(2)	11.6268(15)
α [°]	100.204(2)	105.485(2)
β [°]	105.023(2)	99.414(2)
γ [°]	113.619(2)	101.233(2)
Volume[^{3}]	1218.7(3)	989.4(2)
Z	1	1
ρ_{cal}/ Mg m^{-3}	2.194	2.383
Goodness-of-fit on F^2	1.050	1.104
$R_1(F^2_0)$ [I > 2 σ(I)]	0.0324	0.0251
wR_2 (F^2_0) [I > 2 σ(I)]	0.0863	0.0716
$R_1(F^2_0)$ (all data)	0.381	0.0265
wR_2 (F^2_0) (all data)	0.0897	0.0727
Largest diff. peak and hole [e.Å^{-3}]	0.724/-0.621	0.324/-0.460

Table 4.4. Hydrogen bonding parameters in the crystal structure of compound **2** [Å and °]

D-H···A	d(D-H)	d(H···A)	d(D···A)	<(DHA)
O(15)-H(15A)...O(11)#10	0.85(3)	2.06(3)	2.890(2)	167(3)
O(15)-H(15B)...O(12)#1	0.80(3)	2.26(3)	3.049(2)	170(3)
O(16)-H(16B)...O(2)#10	0.77(3)	2.18(3)	2.939(3)	168(3)
O(16)-H(16A)...O(14)#9	0.73(3)	2.20(3)	2.927(3)	178(3)
O(17)-H(17A)...O(6)	0.75(4)	2.40(4)	3.126(3)	164(4)
O(17)-H(17B)...O(15)#7	0.73(3)	2.18(3)	2.898(3)	171(3)
O(17)-H(17A)...O(14)#1	0.75(4)	2.64(4)	3.088(2)	120(3)
O(18)-H(18A)...O(5)	0.79(4)	2.05(4)	2.781(2)	155(4)
O(18)-H(18B)...O(8)#4	0.84(4)	2.20(4)	2.965(2)	152(4)
O(19)-H(10B)...O(13)#9	0.71(3)	2.23(3)	2.927(2)	167(3)
O(19)-H(10A)...O(23)#8	0.90(3)	1.91(3)	2.798(3)	170(3)
O(20)-H(20B)...O(12)#6	0.73(3)	2.69(4)	3.191(4)	128(4)
O(20)-H(20A)...O(21)#2	0.64(5)	2.45(5)	3.079(4)	166(6)
O(21)-H(21B)...O(7)	0.58(5)	2.32(5)	2.890(3)	165(7)
O(21)-H(21A)...O(7)#6	0.80(4)	2.57(4)	3.260(3)	145(4)
O(22)-H(22B)...O(6)#6	0.71(3)	2.17(3)	2.827(3)	156(3)
O(22)-H(22A)...O(11)#5	0.69(4)	2.11(4)	2.775(2)	164(4)
O(23)-H(23A)...O(10)#5	0.64(3)	2.10(3)	2.735(2)	170(4)
O(23)-H(23B)...O(22)#5	0.87(3)	2.02(3)	2.888(3)	175(3)

Symmetry transformations used to generate equivalent atoms:

#1 -x+1,-y+1,-z+1 #2 -x+2,-y+1,-z #3 x-1,y,z #4 x+1,y,z #5 -x+1,-y,-z

#6 -x+1,-y+1,-z #7 -x+2,-y+2,-z+1 #8 x,y+1,z #9 x+1,y+1,z #10 -x+2,-y+1,-z+1

4.3.5. Comparison of the crystal structures

The compound $[HMTAH]_2[Na(H_2O)_6]_2[H_2V_{10}O_{28}]\cdot 6H_2O$ (**1**) is a doubly protonated discrete decavanadate cluster anion with a sodium hexahydrate coordination complex and protonated HMTA as the cations. The synthesis of compound **1** is a very simple and well known method to isolate the decavanadate cluster with protonated organic cations. In the relevant crystal structure (compound **1**), the singly protonated HMTA cation neither coordinates to the sodium octahedral hexa-aqua complex nor coordinates to the decavanadate cluster anion; this is because the N atoms of the organic ligand

hexamethylenetetramine (HMTA) are generally reluctant to be involved in any metal ion coordination. The compound $[Na_3(H_2O)_9]_{2n}[V_{10}O_{28}]_n$ (**2**) is a purely inorganic coordination polymer with an interesting tri-sodium aqua-complex cation, which is supported by the decavanadate cluster anion. The further coordination of these $[Na_3(H_2O)_9]^{3+}$ cations, supported on the $[V_{10}O_{28}]^{6-}$ cluster anion, to other surrounding $[V_{10}O_{28}]^{6-}$ cluster anions result in the formation of a two-dimensional (2D) extended structure (coordination polymer) in the crystal structure of compound **2**.

Interestingly, in the crystal structure, the tri-sodium cluster cation connects to the decavandate cluster anion involving terminal oxygen atoms as well as μ_3-type bridging oxygen atom. The connectivity through this μ_3-type bridging oxygen atom is very rare in POV chemistry. Each tri-sodium aqua-complex cation connects with three surrounding decavanadate cluster anions (Figure 4.5) in a cation to anion ratio of 1:3, resulting in a 2D sheet. These 2D sheets are further extended into a 3D supramolecular network due to extensive hydrogen bonding interactions between the water molecules of the tri-sodium aqua complex cations and surface oxy gen atoms of the decavanadate anion. The connectivity of the disodium aqua cations to the decavanadate cluster anions are vastly reported in the literature; however, to our knowledge, the coordination connectivity of a tri-sodium aqua cluster cation to the decavanadate cluster anion is not much explored.

This the cage-like organic cation HMTA (protonated hexamethylenetetramine) forms a zero-dimensional (0D) structure in case of compound **1**, the tri-sodium aqua cluster forms a 2D structure in case of compound **2**.

4.3.6. UV –Visible and Flourescence Spectroscopy

The electronic absorption spectra of solid macro-crystals of compounds **1** and **2** were measured at room temperature (Figure 4.10(a)). The UV–Vis spectra of compounds **1** and **2** are very similar due to the presence of same decavanadate cluster anion in both compounds. The electronic spectra of these compounds reveal peaks at around 220 nm and a shoulder at 280 nm (compound **1**) and 380 nm (compound **2**), which have been assigned to O→V charge transfer transitions.

Interestingly, compound **2** exhibits emission in the solid state as well as in its nano-particle suspension state in acetonitrile. The macro-crystals of compound **2**, upon excitation at 380 nm, show an emission peak at around 460 nm, as shown in Figure 4.10(b). On the other hand, compound **1** does not exhibit any emission (on excited at a wavelength of 290 nm), even though compound **1** contains the same POV cluster anion as contained by compound **2**. The most striking difference in coordination chemistry between compound **2** and compound **1** is the coordination of the triply-bridged oxygen atom of the decavanadate cluster anion to a sodium atom of tri-sodium aqua-complex cation $[Na_3(H_2O)_9]^{3+}$ in the crystal of compound **2**, which is absent in compound 1. This special coordination of a triply-bridged oxygen atom of the decavanadate cluster anion to a sodium cation (in compound **2**) can be correlated with a charge transfer from the 'p' orbital of the oxygen atom to the 'd' orbital of vanadium. Thus upon excitation at 380 nm, compound **2** exhibits an emission at around 460 nm which can be attributed to the O→V charge transfer transition.[26]

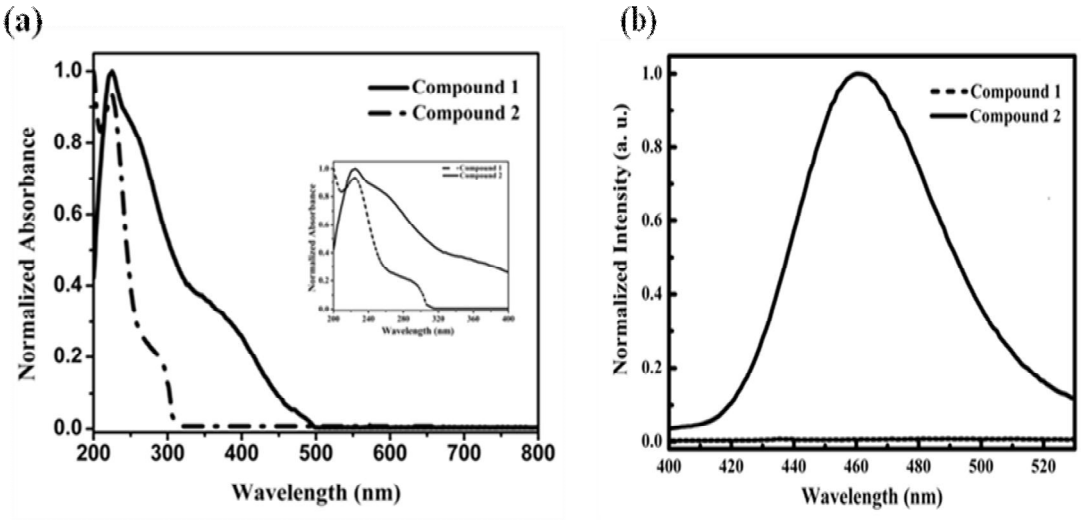

Figure 4.10. (a) Diffuse reflectance (solid state electronic absorption) spectra of compounds **1** and **2**; (b) The emission spectra of the macro-crystals of compounds **1** and **2**.

Nanoparticles have large surface area: can this surface area be contributed in photo-luminescence emission or enhanced non-radiative transition for compound $[Na_3(H_2O)_9]_{2n}[V_{10}O_{28}]_n$ (**2**). In view of this, we have prepared and characterized nano-crystals of compound **2** and performed their photo-emission studies, that are described in following section.

4.3.7.1. Synthesis, characterization and photo-physical studies of nano-crystals of compound $[Na_3(H_2O)_9]_{2n}[V_{10}O_{28}]_n$ (2)

The macro-crystals of compound **2** were subjected to ultrasonication in acetonitrile solvent. During the ultrasonication in acetonitrile solvent, the macro-crystals are dispersed into smaller sized nanoparticles. The nanoparticles are synthesized at two concentrations, 1 mM (14.2 mg in 10 mL of solvent) and 0.5 mM (7.1 mg in 10 mL of solvent) by ultrasonication for 1hr. The FT-IR spectra of the nanoparticles exhibits the decavanadate-type characteristic features in the range 450–1000 cm^{-1}. V–O terminal oxygen vibrations are found at 947 cm^{-1}.

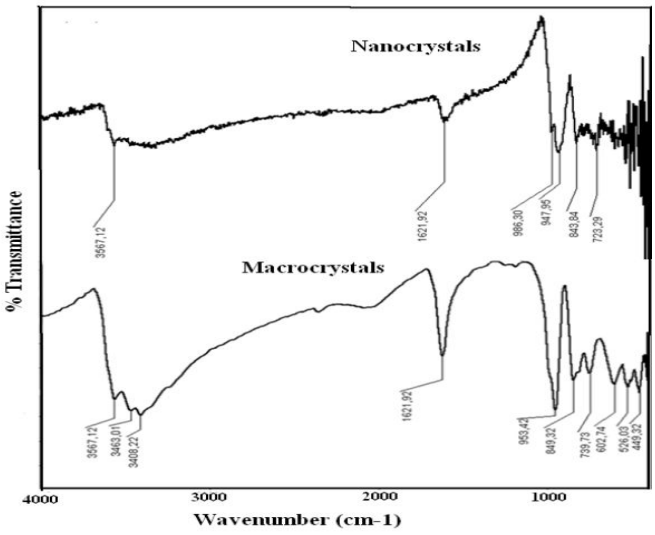

Figure 4.11. FT-IR spectra of nanocrystals and macrocrystals of compound **2.**

The asymmetric vibrations of V–O–V bridges are observed at 723 cm^{-1}, while the symmetric bands are located at around 590 cm^{-1}. The FT-IR spectra of the nanoparticles and macro-crystals are shown in Figure 4.11. The observed powder x-ray diffraction pattern of the nanocrystals were matched with the theoretical powder pattern, simulated from single crystal data of the corresponding macro-crystal data (Figure 4.12.).

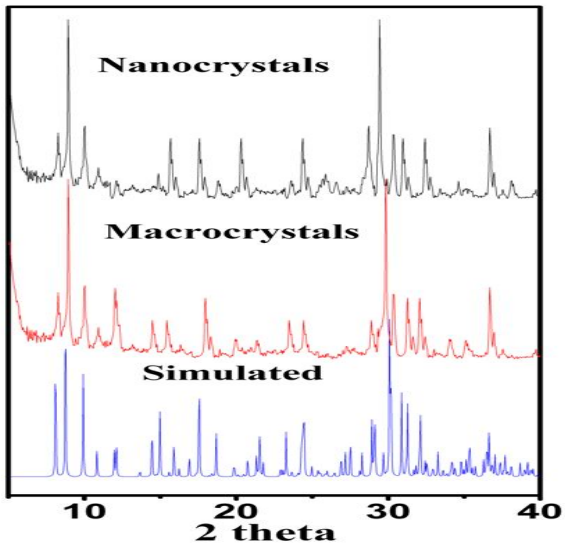

Figure 4.12. Powder X-ray diffraction pattern of nanocrystals, macrocrystals and simulated from single crystal data of compound **2.**

The chemical composition of compound **2** nanoparticles was confirmed by EDS equipped with FE-SEM, which shows that the obtained nanoparticles have the same elemental composition as the bulk macro-crystals (Figure 4.15.).

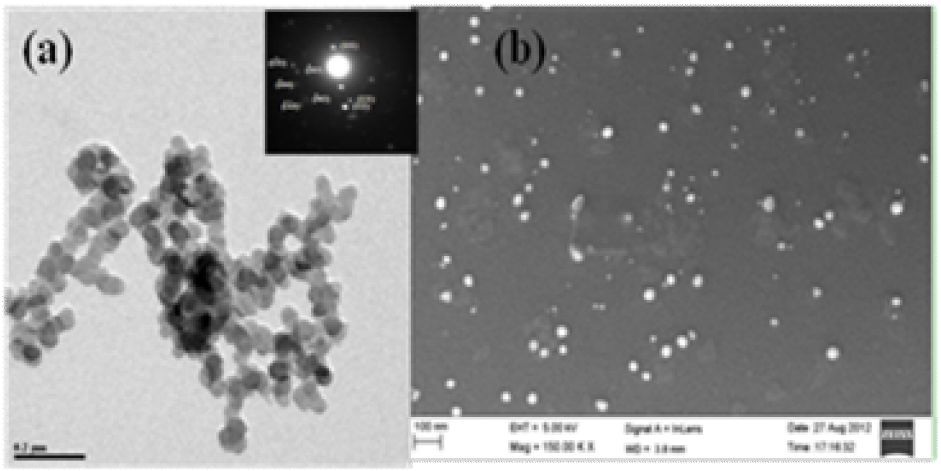

Figure 4.13. (a) TEM (scale bar = 0.2 µm) image of nanoparticles of compound **2** (0.5 mM) [Index: SAED pattern]; **(b)** FE-SEM (scale bar = 100 nm) image of nanoparticles of compound **2**(0.5 mM).

The morphology of these nanoparticles was studied using the TEM, FE-SEM and AFM techniques. The sizes of the nanopaticles (synthesized from 1 mM concentration) span the range 100 to 500 nm, with no particular morphology (Figure 4.14). For the nanoparticles

synthesized from 0.5 mM concentration, the TEM and FE-SEM images show a uniform size distribution (about 70-50 nm range) which are well dispersed in the solution with nearly spherical morphology.

The selected area electron diffraction (SAED) pattern of the nanoparticles (Figure 4.13(a) inset) shows that the nanoparticles are crystalline in nature. From the SAED pattern, the measured d-spacing values of 5.89, 3.31, 3.08, 2.96, 2.78, 2.74, 2.69 and 2.29 correspond to the hkl planes (101), (121), (-203), (222), (-104), (2-32), (-302) and (-1-43) respectively. These lattice planes belong to triclinic macro-crystals of compound **2**, as far as single crystal X-ray data are concerned.

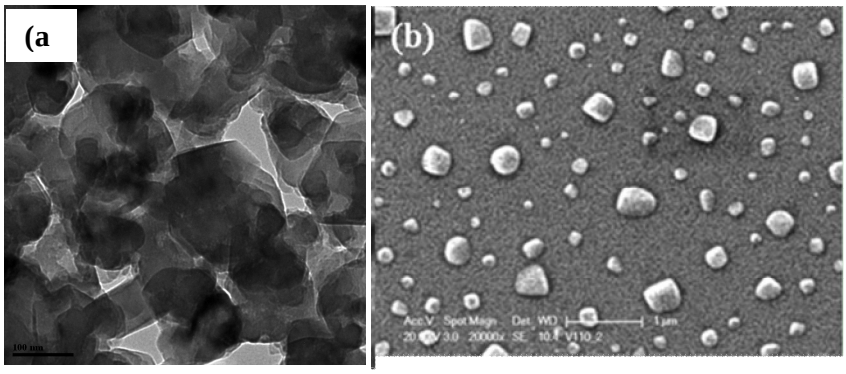

Figure 4.14. (a) TEM (scale bar = 0.1 μm); **(b)** SEM (scale bar = 1 μm) images of nanoparticles of compound **2** (1 mM).

The morphology of these nanoparticles was studied using the TEM, FE-SEM and AFM techniques. The sizes of the nanopaticles (synthesized from 1 mM concentration) span the range 100 to 500 nm, with no particular morphology (Figure 4.14). For the nanoparticles synthesized from 0.5 mM concentration, the TEM and FE-SEM images show a uniform size distribution (about 70-50 nm range) which are well dispersed in the solution with nearly spherical morphology.

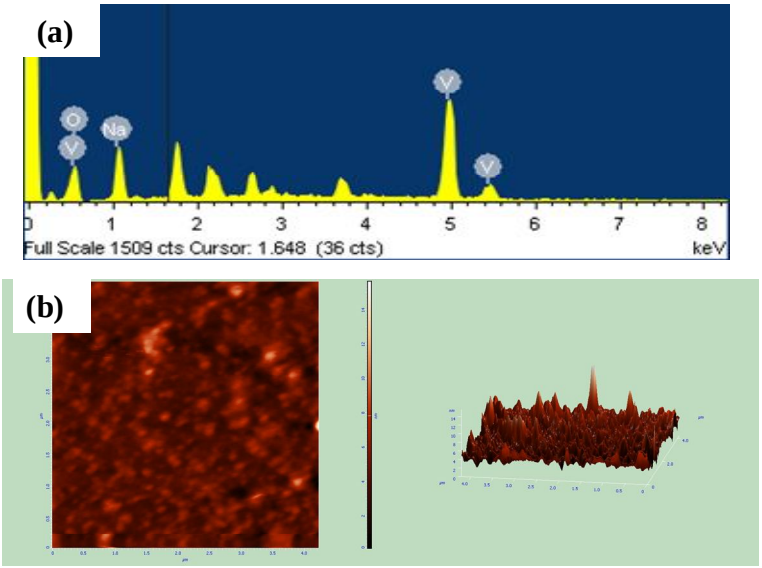

Figure 4.15. (a) EDS image nanoparticles of compound **2**(0.5 mM) **(b)** 2D and 3D views of AFM topography images of nanoparticles of compound **2** (0.5 mM).

Examination of the AFM images, (Figure 4.15.) reveals that the size of the nanoparticles are consistent with the TEM and FE-SEM studies.

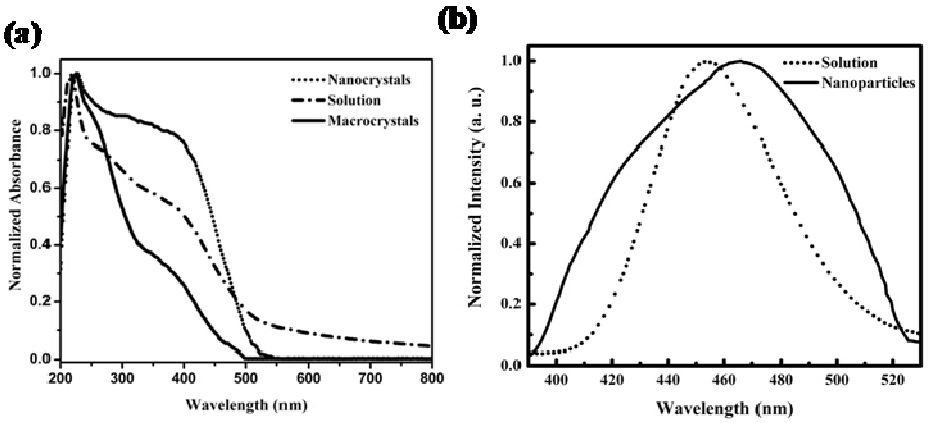

Figure 4.16. (a) UV-visible spectra of nanoparticles, solution ($5x10^{-4}$ M) and macro-crystals of compounds **2**; **(b)** The fluorescent spectrum of the nanoparticles and solution ($5x10^{-4}$ M) of compound **2**.

The nanoparticles, formed by drop-casting the solution on a quartz plate, on excited at wavelength 380 nm, show an emission band at around 460 nm, as displayed in the Figure 4.16, like that shown by the corresponding macro-crystals. Thus, the re-sizing of the particles from macro-size to nano-size does not have any influence on the emission features of compound **2**. The laser confocal fluorescence microscopy images of

nanoparticles of compound **2** (Figure 4.17) also display a blue emission maximum peak at 460 nm (on excitation with a 380 nm Ar^+ laser), which is consistent with the conventional emission spectroscopic data.

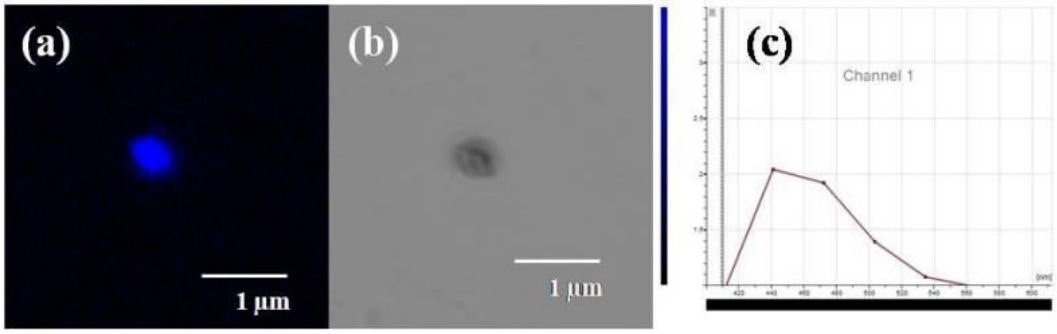

Figure 4.17. Laser confocal microscopy images of nanoparticles of compound **2**; (a) After excitation at 380 nm; (b) Before excitation; and (c) The fluorescence spectrum recorded by excitation at 380 nm.

4.4. Conclusion

In summary, we have synthesized and characterized two decavanadate based compounds, where compound **1** is a discrete cluster containing compound with the protonated organic ligand HMTA and sodium hexahydrate as cations and compound **2** is an organic free inorganic coordination polymer, which contains the decavanadate cluster anion supported tri-sodium-aqua-cluster cation. The connectivity of terminal and triply bridging oxygen atoms of the decavanadate cluster anion with the trisodium aqua cations (in the case of compound **2**), extends the dimensionality to a 2-D sheet-like structure. We have successfully synthesized and characterized nanoparticles of compound **2** by ultrasonication of the relevant macro-crystals. It is worth mentioning that compound **2** displays emission at room temperature in both the macro-crystal and nanoparticle states, which is a rare example for a decavanadate cluster system.

4.5. References

1. (a) Long, D. -L.; Abbas, H.; Kögerler, P.; Cronin, L. *Angew. Chem. Int. Ed.* **2005**, *44*, 3415;
   (b) Streb, C.; Long, D. -L.; Cronin, L. *Chem. Commun.* **2007**, 471;
   (c) Zeng, H.; Newkome, G. R.; Hill, C. L. *Angew. Chem.* **2000**, *112*, 1841.
2. (a) Müller, A.; Kögerler, P.; Dress, A. W .M. *Coord. Chem. Rev.* **2001**, *222*, 193;
   (b) Yamase, T.; Fukaya, K.; Nojiri, H.; Ohshima, Y. *Inorg. Chem.* **2006**, *45*, 7698;
   (c) Arumuganathan, T.; Rao, A. S.; Kumar, T. V.; Das, S. K. *J. Chem. Sci.* **2008**, *120*, 95.
3. Tiago, T.; Martel, P.; Guitiérrez-Merino, C.; Aureliano, M. *Biochim. Biophys. Acta* **2007**, *1774*, 474.
4. Zeng, H.; Newkome, G. R.; Hill, C. L. *Angew. Chem., Int. Ed.* **2000**, *39*, 1771.
5. Long, D. -L.; Tsunashima, R.; Cronin, L. *Angew. Chem., Int. Ed*. **2010**, *49*, 1736.
6. Arumuganathan, T.; Rao, A. S.; Das, S. K. *Cryst. Growth Des.* **2010**, *10*, 4272.
7. (a) Tripuramallu, B. K.; Das, S. K. *Cryst. Growth Des.* **2013**, *13*, 2426;
   (b) Ishii, Y.; Takenaka, Y.; Konishi, K. *Angew. Chem.* **2004**, *116*, 2756;
   (c) Streb, C.; Long, D. -L.; Cronin, L. *Cryst. Eng. Commun.* **2006**, *8*, 629.
8. (a) Wang, X. -L.; Qin, C.; Wang, E. -B.; Su, Z. -M.; Li, Y. G.; Xu, L. *Angew. Chem.* **2006**, *118*, 7571;
   (b) Dolbecq, A.; Mellot-Draznieks, C.; Mialane, P.; Marrot, J.; Férey, G; Sécheresse, F. *Eur. J. Inorg. Chem.* **2005**, 3009.
9. Streb, C.; Ritchie, C.; Long, D. -L.; Kögerler, P.; Cronin, L. *Angew. Chem., Int. Ed*. **2007**, *46*, 7579.
10. Venegas-Yazigi, D.; Hermosilla-Ibáñez, P.; Costamagna, J.; Spodine, E.; Vega, A.; Paredes-Garcia, V.; Fur, E. L. *Macromol. Symp*. **2011**, *304*, 80.
11. Musumeci, C.; Luzio, A.; Pradeep, C. P.; Miras, H.N.; Rosnes, M. H.; Song, Y. -F.; Long, D. -L.; Cronin, L.; Pignataro, B. *J. Phys. Chem.* **2011**, *C115*, 4446.
12. Troupis, A.; Triantis, T.; Hiskia, A.; Papaconstantinou, E. *Eur. J. Inorg. Chem.* **2008**, 5579.
13. Kishore, P. S.; Viswanathan, B.; Varadarajan, T. K. *Nanoscale Res. Lett.* **2008**, *3*, 14.
14. (a) Wang, X. -H.; Kang, Z. -H.; Wang, E. -B. *Chin. J. Inorg. Chem.* **2006**, *22*, 2186;

(b) Shen, Y.; Peng, J.; Pang, H.; Zhang, P.; Chen, D.; Chen, C.; Zhang, H.; Meng, C.; Su, Z. *Chem. Eur. J.* **2011**, *17*, 3657.

15. (a) Pope, M. T.; Müller, A. *Angew. Chem., Int. Ed.* **1991**, *30*, 34;
(b) Pope, M. T. *Heteropoly and Isopoly Oxometalates*, Springer-Verlag, Berlin,**1983**;
(c) Pope, M. T.; Müller A. (*Eds.*), *Polyoxometalates: From Platonic Solids to Anti-Retroviral Activity*, Kluwer Academic, The Netherlands, **1994**.
16. Kanoo, P.; Ghosh, A. C.; Maji, T. K. *Inorg. Chem.* **2011**, *50*, 5145.
17. Bukietynska, K.; Krot, K.; Starynowicz, P. *Transition Met. Chem.* **2001**, *26*, 311.
18. (a) Lee, U.; Jung, Y. -H.; Joo, H. -C. *Acta Cystallogr.* **2003**, *E59*, i72;
(b) Lee, U. *Acta Cystallogr.* **2006**, *E62*, i176;
(c) Khan, M. I.; Tabussum, S.; Zheng, C. *J. Clust. Sci.* **2001**, *12*, 583;
(d) Mestiri, I.; Ayed, B.; Haddad, A. *J. Clust. Sci.* **2013**, *24*, 85;
(e) Lü, Y.; Feng, Y. *Chin. J. Chem.* **2010**, *28*, 2404;
(f) Krasil'nikov, V. N.; Shtin, A. P.; Perelyaeva, L. A.; Baklanova, I. V.; Tyutyunnik, A. P.; Zubkov, V. G. *Russ. J. Inorg. Chem.* **2010**, *55*, 162;
(g) Guilherme, L. R.; Massabni, A. C.; Dametto, A. C.; Corrêa, R. d. S.; Araujo, A. S. d. *J. Chem. Crystallogr.* **2010**, *40*, 897;
(h) Nilsson, J.; Nordlander, E.; Behrens, U.; Rehder, D. *Acta Cryst.* **2010**, *E66*, i30;
(i) Pei, J.; Yu, B.; Song, H.-b.; Yan, X.q.; Zhang, Y.; Geng, X.; Wang, Y.; Yan, J.; Sun, B. *J. Mol. Struct.* **2005**, *779*, 43.
19. (a) Duraisamy, T.; Ramanan, A.; Vittal, J.J. *Cryst. Eng.* **2000**, *3*, 237;
(b) Duraisamy, T.; Ojha, N.; Ramanan, A.; Vittal, J.J. *Chem. Mater.* **1999**, *11*, 2339.
20. McGlone, T.; Streb, C.; Busquets-Fité, M.; Yan, J.; Gabb, D.; Long, D. -L.; Cronin, L. *Cryst. Growth Des.* **2011**, *11*, 2471.
21. Mai, L.; Han, C. *Mater. Lett.* **2008**, *62*, 1458.
22. Yerra, S.; Supriya, S.; Das, S. K. *Inorg. Chem. Commun.* **2013**, *35*, 54.
23. Bruker, SADABS, SMART, SAINT and SHELXTL, *Bruker AXS Inc.*, Madison, Wisconsin, USA, **2000**.
24. Sheldrick, G.M. SHELX-97, *Program for Crystal Structure Solution and Analysis*, University of Gottingen, Gottingen, Germany, **1997**.
25. Long, D. -L.; Burkhholder, E.; Cronin, L. *Chem. Soc. Rev.* 2007, *36*, 105.

26. Sun, R. Q.; Zhang, H. H.; Wu, X. Y.; Huang, C. C.; Chen, Y. P. *Spectrosc. Spect. Anal.* **2006**, *26*, 282.

27. Putrevu, N. R.; Doedens, R. J.; Khan, M. I. *Inorg. Chem. Commun.* **2013**, *38*, 5.

28. Udomvech, A.; Kongrat, P.; Pakawatchai, C.; Phetmung, H. *Inorg. Chem. Commun.* **2012**, *17*, 132..

Organic free decavanadate based materials: inorganic linkers to obtain extended structures

5

This chapter describes the syntheses and crystal structures of three decavanadate based extended structures containing compounds $[\{Na_3(H_2O)_8(\mu_2\text{-}H_2O)_6Ag_2\}HV_{10}O_{28}]_n\cdot 6nH_2O$ ***(1),*** $[Co(H_2O)_6]_n[\{Na_2(H_2O)_6(\mu_2\text{-}H_2O)_4Co(H_2O)_2\}V_{10}O_{28}]_n\cdot 4nH_2O$ ***(2) and*** $[Zn(H_2O)_6]_n[\{Na_2(H_2O)_6(\mu_2\text{-}H_2O)_4Zn(H_2O)_2\}V_{10}O_{28}]_n\cdot 4nH_2O$ ***(3). Compounds 1, 2 and 3 crystallize in triclinic space group P-1. Compound 1 is a three-dimensional inorganic solid, whereas compounds 2 and 3 are isomorphous one-dimensional inorganic polymers. In the crystal structure of compound 1, the silver (I) cation is coordinated to the terminal oxygen as well as bridging oxygen atoms of decavanadate anion and it is also connected to bridging oxygen atom of trimeric sodium aqua cluster cation. In the crystals of compound 2, one hexa-hydrated cobalt cation is present as a counter cation and one "di-sodium cobalt aqua-complex" cation is supported on the*** $[V_{10}O_{28}]^{6-}$ ***cluster anion by coordinate covalent bond. Compound 3 is isostructural with compound 2, with*** Zn^{2+} ***present (in compound 3) in the place of*** Co^{2+} ***(in compound 2). The crystal structures of compounds 1, 2 and 3 are further analyzed by O–H···O hydrogen bonding interactions. Compounds 1, 2 and 3 are characterized by routine elemental analyses, FT-IR spectroscopy and unambiguously by single crystal X-ray crystallography.***

5.1. Introduction

The modern chemical research on polyoxometalate-based inorganic materials has attracted synthetic chemists because of their prospective applications in various research areas, such as catalysis,[1-3] conductive materials,[4] medicinal chemistry,[5-6] and materials science.[7] Polyoxometalates[8-10] cover a wide range of metal-oxide based compounds that are versatile as far as size and topology of the concerned polyoxometalate (POM) cluster are concerned. The important step in the assembly of well-designed POM clusters in obtaining metal-oxide based frameworks has so far been achieved by using transition metal coordination complex (with organic ligands) fragments as linkers or by using pure organic linkers. Both these approaches, however, are limited by the reduced framework stability intrinsic to metal–organic framework materials, because organic fragments of metal-organic frameworks are not thermally stable. In contrast, pure inorganic POM-based frameworks offer higher thermal stability. Thus, designing and synthesizing new materials,[11] formed from POM cluster anion and pure inorganic cationic entity (organic free) are of considerable interests in modern inorganic chemistry as far as metal-oxide based inorganic materials are concerned.

Among polyoxometalates (POMs), the polyoxovanadates (POVs) are important in many areas, for example, biological sciences,[12-15] industrial chemistry,[16] material chemistry,[17-18] electrochemistry[19] and magnetochemistry[20]. The decavanadate cluster anion, $[V_{10}O_{28}]^{6-}$ is one of the important building block among POVs in constructing inorganic-organic hybrid materials.[21-22] Decavanadate-based pure inorganic compounds are also reported[23-26] including $[Ni(H_2O)_6]_2[Na(H_2O)_3]_2[V_{10}O_{28}]\cdot 4H_2O$,[27] $Na_4Ni(V_{10}O_{28})\cdot 23H_2O$[28] and $CuNa_4V_{10}O_{28}\cdot 23H_2O$[29]. We have been working on POM / POV based organic free polymeric inorganic materials,[11,30-32] which were reported in literature are interesting because of the assembly of POM building units by purely inorganic linkers offers high stability to the concerned network of the resulting inorganic materials. Inorganic linkers are generally metal-aqua coordination complexes, that are generally formed in situ during synthesis. Metal ions, that act as linkers, include generally Na^+, K^+, Ln^{3+} (lanthanides), transition metal cations etc. The literature on silver ion as a linker to link POV cluster anions into extended structures is hardly known.[33-35] In these extended structures, the silver ion linker is stabilized with organic ligands (mostly organic solvent molecules). Pure inorganic silver ion linker, that connects POV cluster anions into a material, is not yet

known. In this chapter, the synthesis and crystal structure of a decavanadate based material $[\{Na_3(H_2O)_8(\mu_2\text{-}H_2O)_6Ag_2\}HV_{10}O_{28}]_n \cdot 6nH_2O$ (**1**), in which the decavanadate cluster anions (building blocks) are linked by sodium-aqua-silver-aqua cluster cation resulting in an extended three-dimensional structure, have been described. In this chapter, two more decavanadate based compounds decavanadate based compounds $[Co(H_2O)_6]_n[\{Na_2(H_2O)_6(\mu_2\text{-}H_2O)_4Co(H_2O)_2\}V_{10}O_{28}]_n \cdot 4nH_2O$ (**2**) and $[Zn(H_2O)_6]_n[\{Na_2(H_2O)_6(\mu_2\text{-}H_2O)_4Zn(H_2O)_2\}V_{10}O_{28}]_n \cdot 4nH_2O$ (**3**) have been described for comparison reason, though the nickel analogue of these two compounds (compounds **2** and **3**) has already been reported earlier.[27]

The compounds described in this chapter are

$[\{Na_3(H_2O)_8(\mu_2\text{-}H_2O)_6Ag_2\}HV_{10}O_{28}]_n \cdot 6nH_2O$ (**1**)
$[Co(H_2O)_6]_n[\{Na_2(H_2O)_6(\mu_2\text{-}H_2O)_4Co(H_2O)_2\}V_{10}O_{28}]_n \cdot 4nH_2O$ (**2**)
$[Zn(H_2O)_6]_n[\{Na_2(H_2O)_6(\mu_2\text{-}H_2O)_4Zn(H_2O)_2\}V_{10}O_{28}]_n \cdot 4nH_2O$ (**3**)

5.2. Experimental details

5.2.1. Materials and general consideration

The starting materials, sodium metavanadate, sodium tungstate dihydrate, cobalt chloride and zinc chloride were obtained from SISCO, acetonitrile was from Sigma Aldrich; distilled water was used throughout the experiment. Micro analytical data (only for hydrogen in the present work) were obtained with a FLASH EA 1112 Series CHNS Analyzer. Infrared (IR) spectra were recorded on a JASCO FT/IR-5300 spectrometer with KBr pellets of corresponding compounds in the region of 400–4000 cm^{-1}. Powder X-ray diffraction patterns were recorded on a Bruker D8-Advance diffractometer using graphite monochromated Cu Kα1 (1.5406 Å) and Kα2 (1.54439 Å) radiations. Thermogravimetric analyses were carried out on a STA 409 PC analyzer and corresponding masses were analyzed by QMS 403 C mass analyzer, under the flow of N_2 gas with a heating rate of 5 $^{\circ}C\ min^{-1}$, in the temperature range of 30-1000 $^{\circ}C$.

5.2.2. Synthesis

The title compounds have been synthesized by simple one-pot reactions at room temperature as described below.

5.2.2.1. Synthesis of compound $[\{Na_3(H_2O)_8(\mu_2\text{-}H_2O)_6Ag_2\}HV_{10}O_{28}]_n \cdot 6nH_2O$ (1)

100.0 mL aqueous solution of sodium metavanadate (2.0 g, 8.26 mmol) was heated for 6 hrs at 70 °C. To this hot solution, acetic acid was added to maintain the pH 5.0; subsequently 25.0 mL of aqueous solution of silver oxide (0.5 g, 2.15 mmol) and 60.0 mL acetonitrile were added to crystallize reddish-yellow color block-shaped crystals of compound **1**. The crystals of compound **1** have been isolated by filtration. Yield: 45% based on vanadium. IR (KBr, cm^{-1}): 3473(br), 1616(s), 1145(w), 99(sh), 958(s), 849(m), 739(m), 597(m), 520(w). Anal. Calcd. For. $Ag_2H_{41}Na_3O_{48}V_{10}$ (1603): H, 2.58. Found: H, 2.71.

5.2.2.2. Synthesis of compound $[Co(H_2O)_6]_n[\{Na_2(H_2O)_6(\mu_2\text{-}H_2O)_4Co(H_2O)_2\}V_{10}O_{28}]_n \cdot 4nH_2O$ (2)

100.0 mL aqueous solution of sodium metavanadate (2.0 g, 8.26 mmol) was heated for 6 hrs at 70 °C. To this warm solution, acetic acid was added to maintain the pH 5.0; subsequently 25.0 mL of an aqueous solution of $CoCl_2.6H_2O$ (0.5 g, 2.10 mmol) and 60.0 mL acetonitrile were added to crystallize yellow color block-shaped crystals of **2**. The crystals of compound **2** have been isolated by filtration. Yield: 50% based on vanadium. IR (KBr, cm^{-1}): 3547 (br), 1616 (s), 991(sh), 953(s), 843(s), 805(w), 745(m), 591(w), 526(w). Anal. Calcd. For. $Co_2H_{44}Na_2O_{50}V_{10}$ (1517): H, 2.92. Found: H, 2.86.

5.2.2.3. Synthesis of compound $[Zn(H_2O)_6]_n[\{Na_2(H_2O)_6(\mu_2\text{-}H_2O)_4Zn(H_2O)_2\}V_{10}O_{28}]_n \cdot 4nH_2O$ (3)

This synthesis is same as the procedure described for compound **2** except the addition of anhydrous $ZnCl_2$ (0.5 g, 3.66 mmol) in place of $CoCl_2.6H_2O$ (which was used for the synthesis of compound 2). The crystals compound **3** were isolated by filtration. Yield:50% based on vanadium. IR (KBr, cm^{-1}): 3424 (br), 1632 (s), 991(sh), 964(s), 843(s), 810(w), 750(m), 597(w), 531(w). Anal. Calcd. For. $Zn_2H_{44}Na_2O_{50}V_{10}$ (1530) : H, 2.90. Found: H, 2.83.

5.2.3. X-ray crystallography

The data were collected at 298(2) K on a Bruker SMART APEX CCD area detector system [λ(Mo-K_α) = 0.71073 Å] with graphite monochromator; 2400 frames were recorded with an ω scan width of 0.3^o, each for 10 second exposure. Crystal-detector distance was 60 mm with collimator diameter of 0.5 mm. The data were reduced by using SAINTPLUS[36] and a multi-scan absorption correction was performed using SADABS.[37] Structure solution and refinement were done using programs of SHELXS-97 and SHELXL-97 respectively.[38-39] All non hydrogen atoms were refined anisotropically. Hydrogen atoms of the lattice water molecules as well as coordinated water molecules could not be found in the crystal structures of the title compounds. The crystallographic information of compounds **1**, **2** and **3** is described in Table 5.4.

5.3. Results and discussion

5.3.1. Synthesis

The synthetic method for these compounds is simple one pot wet fashion reaction. Compound $[\{Na_3(H_2O)_8(\mu_2\text{-}H_2O)_6Ag_2\}HV_{10}O_{28}]_n\cdot 6nH_2O$ (**1**) is synthesized by adding the acetonitrile and aqueous silver oxide to the hot acidified aqueous solution of sodium metavanadate at pH 5.0, which is a purely inorganic polymer, where the di-silver tri-sodium aqua complex $\{Na_3(H_2O)_8(\mu_2\text{-}H_2O)_6Ag_2\}^{5+}$ act as the cation. When, in the same synthesis, a first row transition metal salt, namely, cobalt chloride is added instead of silver oxide, compound $[Co(H_2O)_6]_n[\{Na_2(H_2O)_6(\mu_2\text{-}H_2O)_4Co(H_2O)_2\}V_{10}O_{28}]_n\cdot 4nH_2O$ (**2**) is formed, whereby the mono-cobalt di-sodium aqua-complex $\{Na_2(H_2O)_6(\mu_2\text{-}H_2O)_4Co(H_2O)_2\}^{4+}$ and $[Co(H_2O)_6]^{2+}$ act as the cations to counter valance the negative charge of the decavanadate anion. Zinc analogue (compound **3**) of compound **2** has been isolated by adding zinc chloride instead of cobalt chloride. Decavanadate exists in mono-porotonated form in compound **1** and in compounds **2** and **3**, the decavanadate cluster is not protonated, even though all the compounds **1**−**3** have been isolated at the same pH 5.0. In this synthesis, silver ion plays an unique role in the sense that a different type silver-sodium aqua cluster cation $\{Na_3(H_2O)_8(\mu_2\text{-}H_2O)_6Ag_2\}^{5+}$ is formed (in the case of compound **1**) in contrast to a common mixed metal cation $\{Na_2(H_2O)_6(\mu_2\text{-}H_2O)_4M(H_2O)_2\}^{4+}$ (M = Co^{2+}, Zn^{2+}, Ni^{2+}) observed in the case compounds **2** and **3** and for nickel analogue [34]. We believe that soft nature of silver ion makes this difference, as

evidenced by the fact that silver ion is penta-coordinated with oxygen donors (compound **1**) and cobalt and zinc ions are hexa-coordinated with oxygen donors in compounds **2** and **3** respectively.

5.3.2. Infrared spectroscopy

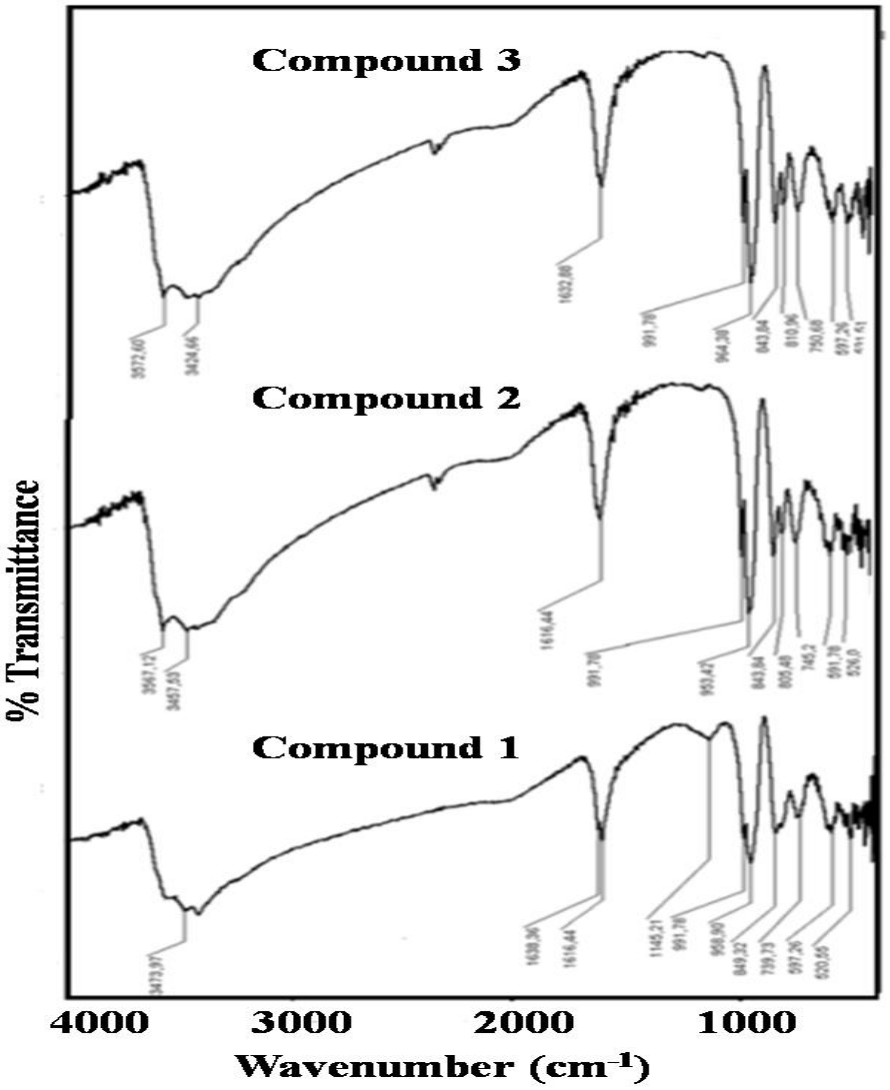

Figure 5.1. FT-IR spectra of compounds **1**, **2** and **3**.

The vibrational spectra of the three compounds are shown in Figure 5.1. The IR spectra exhibit characteristic features of the decavanadate anion in all the three compounds as in all these compounds, decavanadate anion is common. The decavanadate V–O vibrations are found in the region 980–950 cm^{-1}. Thus the strong IR bands at 958 cm^{-1} (compound

1), at 953 cm^{-1} (compound **2)** and at 964 cm^{-1} (compound **3)** are attributed to asymmetric and symmetric stretching vibrations of respective V=O terminal oxygen atom. The bands in the 750–600 cm^{-1} region are due to bridging V–O–V groups. The asymmetric vibrations of V–O–V bridges are observed at 739 cm^{-1} (compound **1),** at 745 cm^{-1} (compound **2**) and at 750 cm^{-1} (compound **3**).

5.3.3. Powder XRD analysis

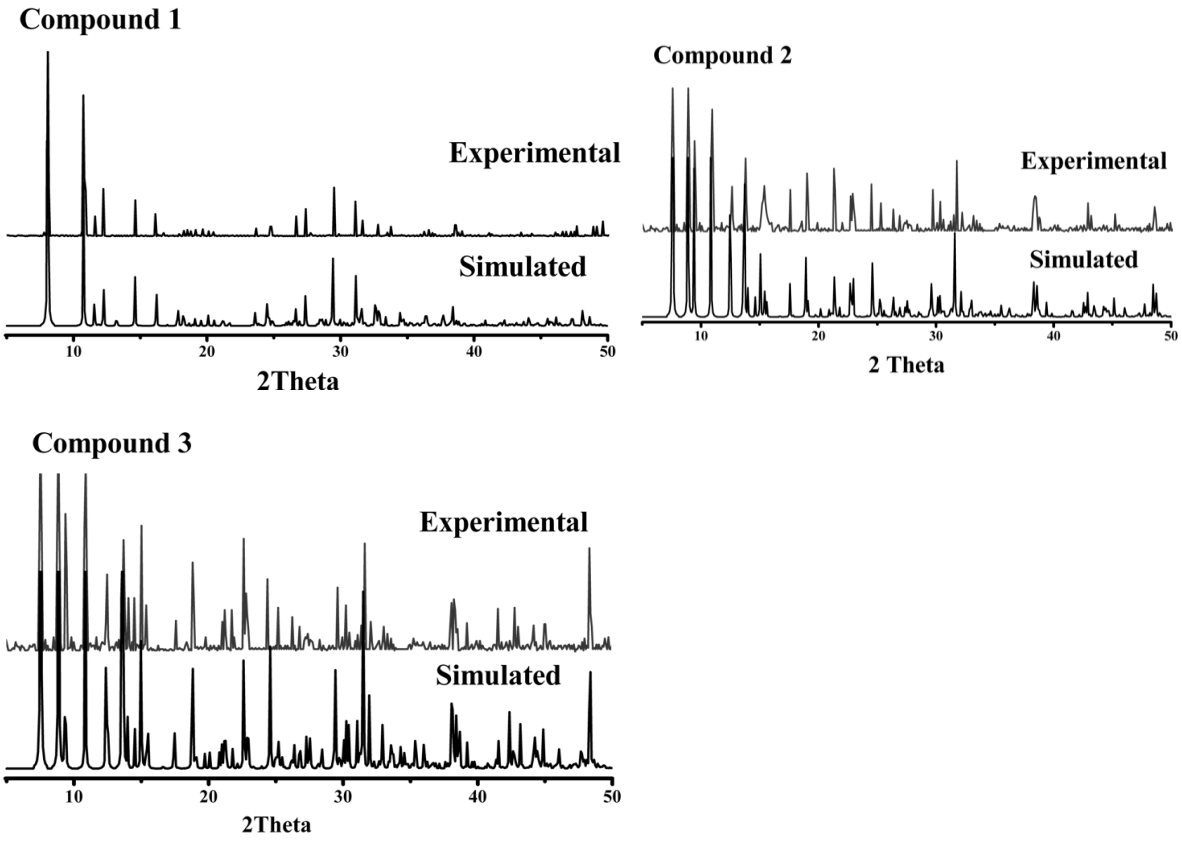

Figure 5.2. PXRD pattern of compounds **1**, **2** and **3**.

The X-ray powder diffraction data for the grinded crystals of the compounds **1**−**3** have been recorded for the confirmation of phase purity (Figure 5.2)**.** As experimental / observed PXRD patterns for compounds **1**, **2** and **3** are in good agreement with the PXRD patterns, simulated from their corresponding single crystal X-ray data, it confirms the phase purity of the bulk compounds.

5.3.4. Thermal Properties

TGA studies were carried out under flow of N_2 for crystalline compounds **1**–**3** in the temperature range of 30–1000 °C. The TG curve for compound [{$Na_3(H_2O)_8(\mu_2$-$H_2O)_6Ag_2$}$HV_{10}O_{28}$]·$6H_2O$ (**1**) shows the first weight loss of 6.71 % in the temperature range 73–135 °C, which corresponds to loss of six lattice water molecules (calculated mass loss of six water molecules is 6.73 %); the second weight loss of 15.55 % in the temperature range of 136-314 °C corresponds to loss of fourteen coordinated water molecules (calculated mass loss of fourteen water molecules coordinated to tri-sodium cation and silver cations is 15.72 %). Further weight loss is due to decomposition of decavanadate anion.

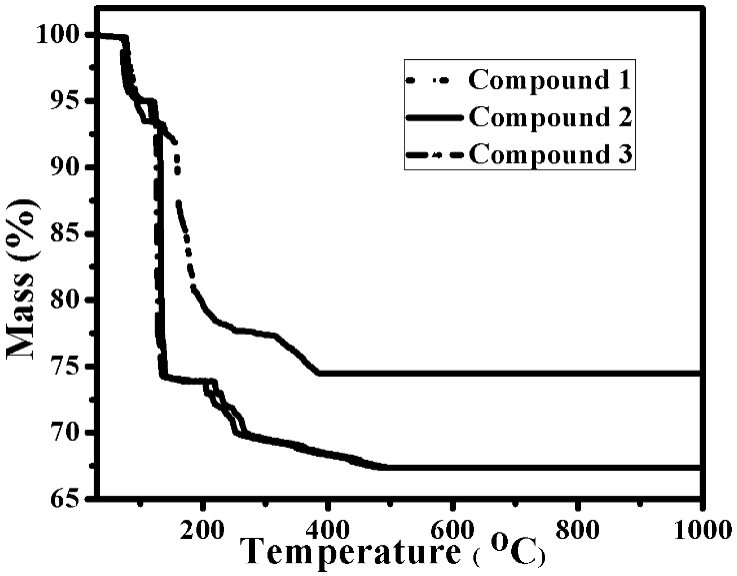

Figure 5.3. TG graphs of compounds **1**, **2** and **3**.

Compounds $[Co(H_2O)_6]_n${$[Na_2(H_2O)_6(\mu$-$H_2O)_4Co(H_2O)_2]V_{10}O_{28}\}_n \cdot 4nH_2O$ (**2**) and $[Zn(H_2O)_6]_n\{[Na_2(H_2O)_6(\mu_2$-$H_2O)_4Zn(H_2O)_2]V_{10}O_{28}\}_n \cdot 4nH_2O$ (**3**) are isomorphous and hence show identical TG/mass curves. Each compound contains four water molecules (four lattice water molecules), which are evolved in the temperature range of 70–125 °C with a loss of 4.65 % for **2**, and 4.71 % for **3** (calculated weight loss for four water molecules: 4.73 % for **2** and 4.73 for **3**). The second weight loss corresponds to 18 water molecules (calculated mass loss of twelve water molecules coordinated to di-sodium cobalt cation and six water molecules coordinated hexa-aqua cobalt cation), which are evolved in the temperature range of 110-220 °C with a loss of 20.96 % for **2** and 21.03 %

for **3** (calculated weight loss for eighteen water molecules: 21.31 % for **2** and 21.16 % for **3**) and further weight losses are due to the structural decomposition of decavanadate anion. Thermogravimetric curves of the compounds **1**-**3** are shown in Figure 5.3.

5.3.5. Description of the crystal structures

5.3.5.1. Crystal structure of $[Na_3(H_2O)_8(\mu_2\text{-}H_2O)_6Ag_2HV_{10}O_{28}]_n \cdot 6nH_2O$ (1)

The asymmetric unit in the crystal structure of compound **1** consists of half of the decavanadate cluster anion, one Ag^+ ion, two Na^+ ions (one in general position and the other one in special position), four terminal waters (coordinated), three μ_2-bridging water molecules and three lattice water molecules as shown in Figure 5.4.(a).

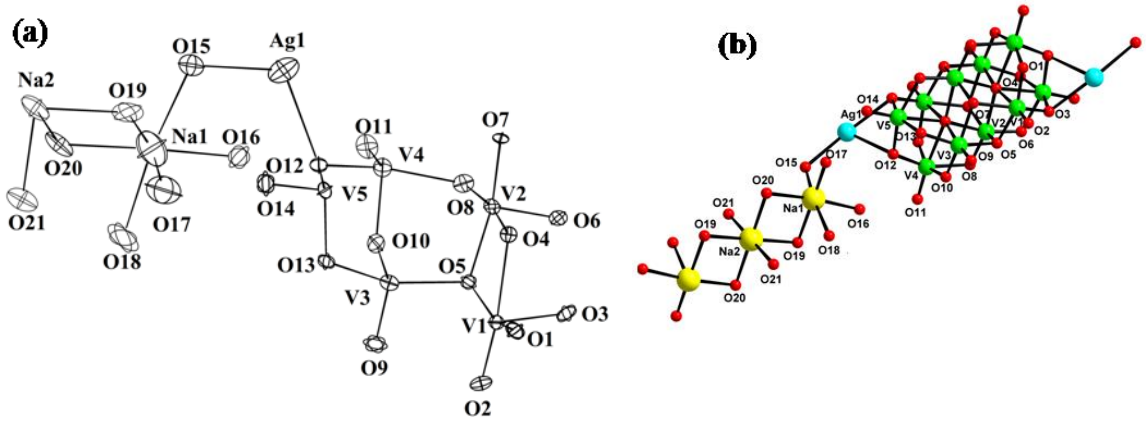

Figure 5.4. Thermal ellipsoidal plot of the asymmetric unit of compound **1** with 50% probability (excluding lattice water molecules) and (b) molecular structure of compound **1**.

Accordingly, compound **1** is formulated as $[\{Na_3(H_2O)_8(\mu_2\text{-}H_2O)_6Ag_2\}HV_{10}O_{28}]\cdot 6H_2O$, considering the number of cations present and charge of decavanadate. The molecular structure of compound **1** is shown in Figure 5.4.(b). The crystal structure of compound **1** consists of monoprotonated decavanadate cluster anion $[HV_{10}O_{28}]^{5-}$, stabilized with a mixed metal cation $\{Na_3(H_2O)_8(\mu_2\text{-}H_2O)_6Ag_2\}^{5+}$ and six lattice water molecules. The cation $\{Na_3(H_2O)_8(\mu_2\text{-}H_2O)_6Ag_2\}^{5+}$ is formed by the dimeric silver(I) cation $[Ag_2(\mu_2\text{-}H_2O)_2]^{2+}$ (in which the μ_2-bridging waters, namely two crystallographic related O15 water molecules, do not bridge between the silver atoms in the dimer but bridge this dimer to two sodium ions from two different sodium trimer from both sides of the silver dimer) and

trimeric sodium(I) cation $[Na_3(H_2O)_8(\mu_2\text{-}H_2O)_4]^{3+}$. Thus these two cations are connected with a bridging water molecule (O15) to form the resulting mixed metal pentameric cation (Figure 5.5).

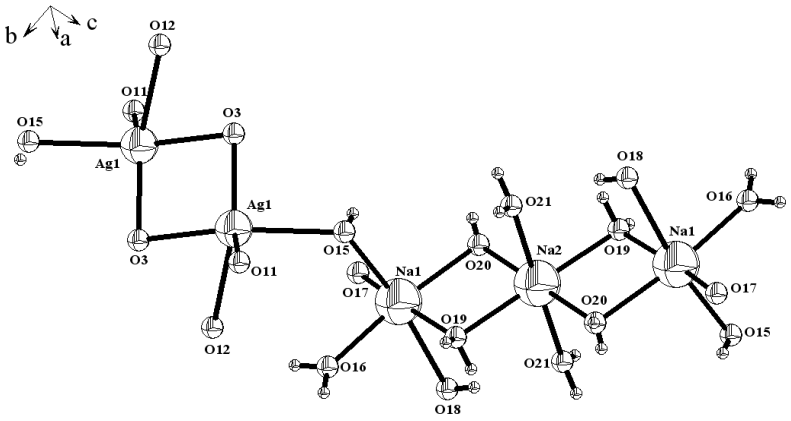

Figure 5.5. A view of the linkage of silver dimer with tri-sodium-aqua cation in the crystal structure of compound **1** (hydrogen atoms are omitted for clarity).

In the crystal structure, the decavanadate anion has a framework, similar to that reported by Evans in 1966.[40] Interestingly, the silver dimer, observed in the crystal structure, is unique in the sense that this silver dimer is exclusively formed from two crystallographically related μ_2-O atoms (namely O3 in the crystal structure) from two different decavanadate cluster anions. Thus in the silver dimer, these bridging oxgens are μ_4-type, each bridging two silver atoms in the dimer and two vanadium atoms of the decavanadate cluster anion as shown in Figures 5.6 and 5.7.

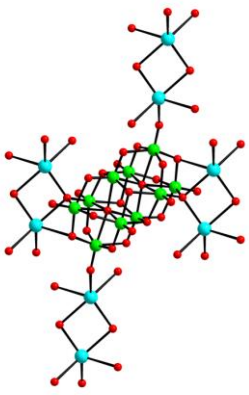

Figure 5.6. Linking of silver dimers around a decavanadate cluster anion in compound **1**.

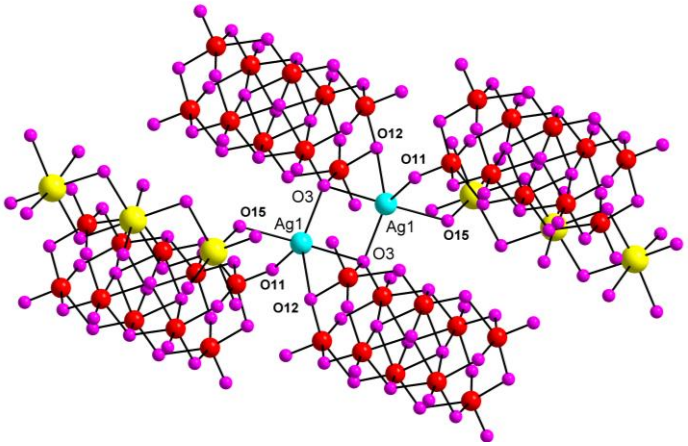

Figure 5.7. Coordination of a silver dimer to its surrounding decavanadate cluster anions and tri-sodium-aqua cluster cations.

In the crystal structure, each monoprotonated decavanadate cluster anion $[HV_{10}O_{28}]$ is linked with its surrounding four dimeric silver $\{Ag_2(\mu_4\text{-}O)_2\}^{2+}$ cations: two dimers through its doubly bridged oxygen atoms (O3 and O12) and two dimers through terminal oxygen atoms (O11) as shown in Figure 5.6. Each silver dimer is additionally stabilized by its terminal linkage to a μ_2-bridging oxygen (O12), terminal oxygen (O11) of decavanadate cluster anion and to a water molecule (O15) of the tri-sodium-aqua cluster (Figure 5.7).

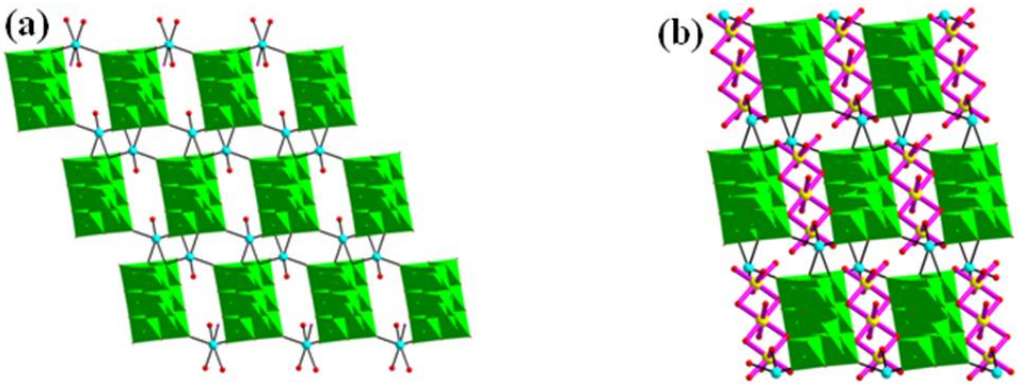

Figure 5.8. (a) 2-Dimensional layered structure established by the decavanadate cluster anion and silver dimer in the compound **1** along *ab* plane; (b) 3-dimensional network established in the polymer of compound **1** due to interlinking of 2D sheet with the trimeric sodium cation along *b*-axis.

Table 5.1. Selected bond lengths [Å] and angles [°] for compound **1**

V(1)-O(1)	1.607(6)	V(3)-O(9)	1.606(6)	V(1)-O(7)#3	2.019(6)
V(1)-O(2)	1.829(6)	V(3)-O(10)	1.811(6)	V(2)-O(4)#3	2.118(6)
V(1)-O(3)	1.831(6)	V(3)-O(13)	1.845(6)	V(3)-O(4)#3	2.225(5)
V(1)-O(4)	2.250(5)	V(4)-O(8)	2.056(6)	V(4)-O(1)#3	1.852(6)
V(1)-O(5)	1.992(6)	V(4)-O(10)	1.886(6)	V(3)-O(7)#3	1.999(5)
V(2)-O(4)	2.141(5)	V(4)-O(11)	1.601(6)	O(4)-V(5)#3	2.315(6)
V(2)-O(5)	1.949(5)	V(4)-O(12)	1.829(6)	V(5)-O(6)#3	2.039(6)
V(2)-O(6)	1.688(6)	V(5)-O(12)	1.844(5)	V(4)-O(4)#3	2.303(5)
V(2)-O(7)	1.913(5)	V(5)-O(13)	1.827(6)	V(5)-O(3)#3	1.921(6)
V(2)-O(8)	1.688(6)	V(5)-O(14)	1.581(7)	V(5)-O(4)#3	2.315(6)
V(3)-O(5)	1.982(6)	O(6)-V(5)#3	2.039(6)	O(3)-Ag(1)#3	2.556(6)
Ag(1)-O(3)#3	2.556(6)	Ag(1)-O(15)	2.528(7)	Ag(1)-O(3)#2	2.409(5)
O(11)-Ag(1)#1	2.365(6)	O(3)-Ag(1)#4	2.409(5)	Na(1)-O(15)	2.471(9)
Na(1)-O(16)	2.357(10)	Na(1)-O(17)	2.025(16)	Na(1)-O(18)	2.629(13)
Na(1)-O(19)	2.263(11)	Na(2)-O(20)#5	2.345(8)	Na(1)-O(20)	2.407(11)
Na(2)-O(20)	2.345(8)	Na(2)-O(21)	2.417(7)	Na(2)-O(19)#5	2.372(9)
O(1)-V(1)-O(2)	102.4(3)	O(2)-V(1)-O(3)	104.4(3)	O(2)-V(1)-(7)#3	98.5(3)
O(1)-V(1)-O(3)	95.1(3)	O(2)-V(1)-O(4)	173.6(3)	O(5)-V(1)-O(4)	76.5(2)
O(1)-V(1)-O(7)#3	89.7(2)	O(3)-V(1)-O(5)	90.6(2)	O(7)#3-V(1)-O(4)	75.6(2)
O(5)-V(2)-O(4)#3	80.4(2)	O(4)#3-V(2)-O(4)	78.7(2)	O(9)-V(3)-O(10)	103.8(3)
O(5)-V(2)-O(4)	80.1(2)	O(8)-V(2)-O(4)#3	87.5(3)	O(9)-V(3)-O(13)	102.1(3)
O(6)-V(2)-O(4)#3	165.4(2)	O(8)-V(2)-O(7)	98.4(3)	O(9)-V(3)-O(5)	100.0(3)
O(6)-V(2)-O(4)	86.8(2)	O(8)-V(2)-O(5)	97.4(3)	O(9)-V(3)-O(7)#3	99.7(3)
O(6)-V(2)-O(5)	96.3(3)	O(8)-V(2)-O(4)	166.2(3)	O(9)-V(3)-O(4)#3	175.3(3)
O(6)-V(2)-O(7)	97.5(3)	O(5)-V(3)-O(7)#3	76.3(2)	O(10)-V(3)-O(7)#3	155.2(2)
O(13)-V(5)-O(12)	93.3(3)	O(14)-V(5)-O(3)#3	100.6(3)	O(14)-V(5)-O(4)#3	174.2(3)
O(14)-V(5)-O(6)#3	99.7(3)	O(14)-V(5)-O(12)	104.3(3)	O(14)-V(5)-O(13)	103.2(3)
O(15)-Na(1)-O(18)	171.2(4)	O(16)-Na(1)-O(20)	174.0(4)	O(17)-Na(1)-O(18)	92.0(5)
O(16)-Na(1)-O(18)	88.7(4)	O(17)-Na(1)-O(19)	170.7(5)	O(17)-Na(1)-O(20)	83.7(5)
O(17)-Na(1)-O(16)	99.9(5)	O(19)-Na(1)-O(16)	85.2(4)	O(19)-Na(1)-O(20)	90.6(4)
O(19)-Na(1)-O(18)	80.3(3)	O(19)#5-Na(2)-O(21)	90.5(3)	O(20)-Na(2)-O(20)#5	180.0(4)
O(20)-Na(2)-O(19)#5	90.5(3)	O(20)-Na(2)-O(21)	88.5(3)	O(20)#5-Na(2)-O(21)	91.5(3)
O(20)-Na(1)-O(18)	86.3(4)	O(20)-Na(2)-O(21)#5	91.5(3)	O(21)-Na(2)-O(21)#5	179.9(1)
O(3)#2-Ag(1)-O(15)	93.1(2)	O(15)-Ag(1)-O(3)#3	151.4(2)	O(11)#1-Ag(1)-O(15)	82.4(2)

Symmetry transformations used to generate equivalent atoms:

#1 -x+1,-y+2,-z+1 #2 x,y-1,z #3 -x,-y+3,-z+1 #4 x,y+1,z #5 -x+1,-y+1,-z+2

The repetitive linking of this $\{Ag_2(\mu_4\text{-}O)_2\}^{2+}$ dimer, in which each silver shows a distorted square pyramidal geometry, with its surrounding decavanadate cluster anions results in the formation of a two-dimensional network (Figure 5.8(a)). These two-dimensional layers are further perpendicularly / laterally connected by $[Na_3(H_2O)_8(\mu_2\text{-}H_2O)_4]^{3+}$ cluster cations resulting in the construction of a three-dimensional (3D)

framework (Figure 5.8(b)). The formation of 3D network can logically be described by the fact that the Ag—O15 water bond is perpendicular to the 2D layer, formed by the silver dimers and decavanadate anions. All the sodium ions in the tri-sodium aqua-complex cation are in octahedral geometry. In the tri-sodium aqua-cluster cation, the Na2 is central sodium ion, which connects two terminal sodium ions (Na1). The four equatorial positions of Na2 octahedra are furnished by four bridging water molecules (two crystallographically related O19 and two crystallographically related O20) and axial positions are coordinated by two crystallographically related O21 water molecules. It is interesting to note that the tri-sodium aqua-cation acting as a secondary linker (a pure inorganic cation) extends the dimensionality of the silver–decavanadate 2D sheet (Figure 5.8(a)) to 3-D network (Figure 5.8(b)). The selected bond lengths and bond angles of compounds **1** are presented in Table 5.1.

5.3.5.2. Description of Crystal Structures of $[Co(H_2O)_6]_n\{[Na_2(H_2O)_6(\mu_2\text{-}H_2O)_4Co(H_2O)_2]V_{10}O_{28}\}_n\cdot 4nH_2O$ (2) and $[Zn(H_2O)_6]_n\{[Na_2(H_2O)_6(\mu_2\text{-}H_2O)_4Zn(H_2O)_2]V_{10}O_{28}\}_n\cdot 4nH_2O$ (3)

Compounds **2** and **3** are isomorphous. Therefore one of these two crystal structures will be discussed in details. The crystal structure of compound **2** consists of a decavanadate cluster anion, that supports the di-sodium cobalt aqua-complex cation by coordinate covalent bond, a hexahydrated cobalt cation and four lattice water molecules. The thermal ellipsoidal plot of the molecular structure of compound **2** is shown in Figure 5.9.

The six negative charges of decavanadate cluster anion counter-balanced by one $[Na_2(H_2O)_6(\mu\text{-}H_2O)_4Co(H_2O)_2]^{4+}$ cation and a hexa coordinated cobalt aqua complex $[Co(H_2O)_6]^{2+}$ cation. In the tri-nuclear di-sodium cobalt aqua complex cation, the central Co(II) ion, having an octahedral geometry, is bridged by two crystallographically related O18 water molecules and two crystallographically related O20 water molecules to two adjacent crystallographically related sodium ions. The axial positions of central cobalt ion are coordinated by two crystallographically related O19 water molecules as shown in Figure 5.10(a).

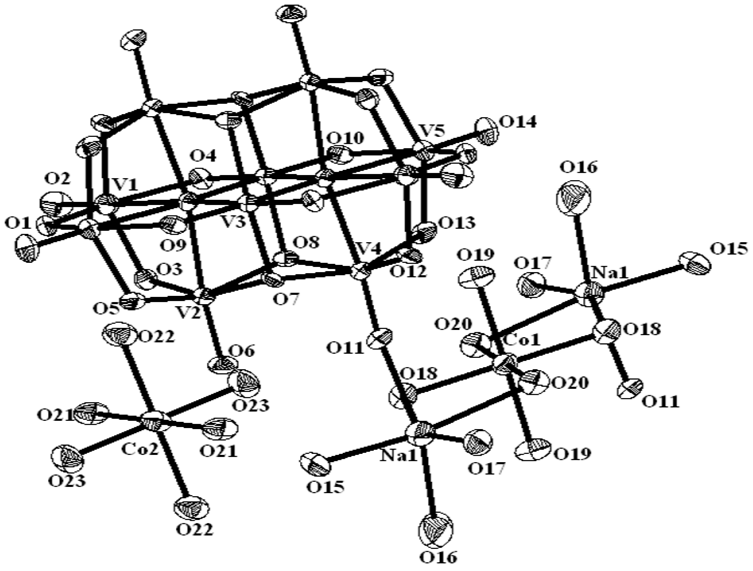

Figure 5.9. Thermal view of the compound **2** with 50 % probability (hydrogen atoms and solvent water molecules are omitted for clarity).

In the crystal structure, the decavanadate moiety is coordinated to di-sodium cobalt aqua-complex cation via O11 terminal oxygen atom of decavanadate cluster anion, thereby extending into a 1D chain as shown in Figure 5.10(b). In the di-sodium cobalt aqua-complex, two sodium atoms namely Na1 (crystallogriphically equivalent) are octahedral geometry and cobalt atom namely Co1 is also in octahedral geometry. The other discrete hydrated cobalt cation is coordinated with six water molecules (O21, O22, O23 and their crystallographically related halves) with an octahedral environment. Due to presence of the coordinated water molecules and lattice water molecules, an extensive supramolecular hydrogen bonding interactions have been observed involving surface oxygen atoms of decavanadate anion (O−H···O_{dec}) as well as lattice molecules (O−H···O_{water}) in the crystal structures of both the compounds **2** and **3**, leading to a 3D supramolecular network (Figure 5.11). The selected bond lengths and bond angles of compounds **2** and **3** are presented in Tables 5.2 and 5.3 respectively.

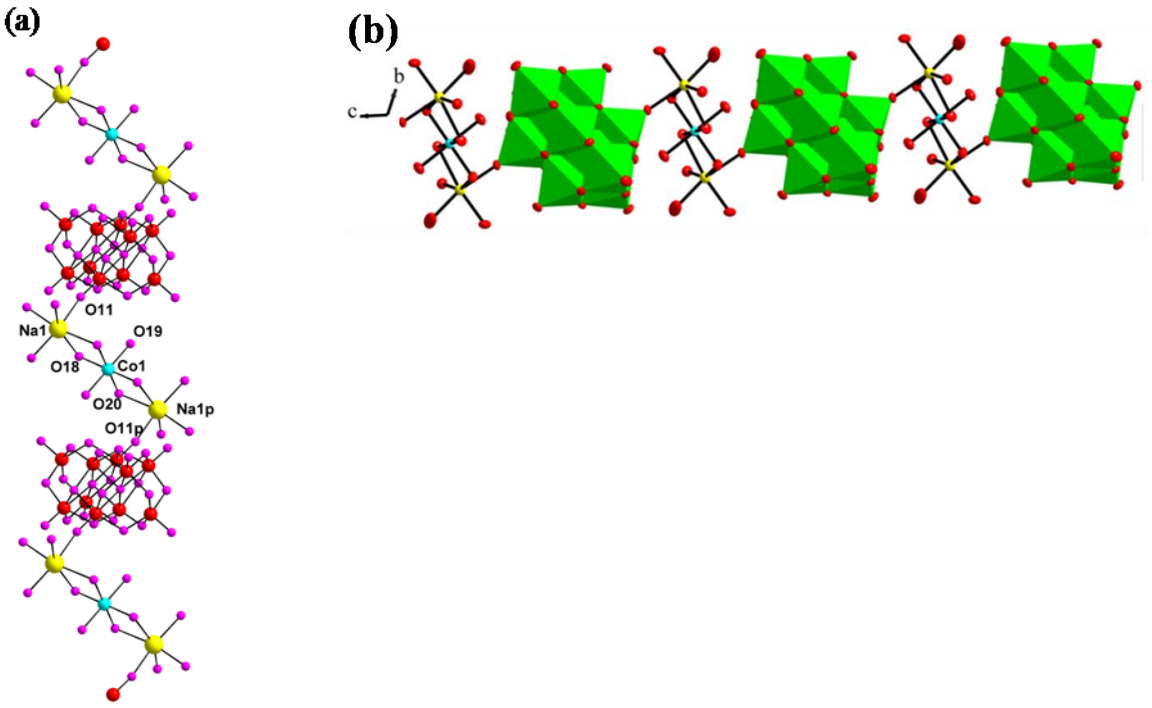

Figure 5.10. (a) Chain like arrangement, formed by decavanadate cluster anion and di-sodium cobalt-aqua cluster cation. Na1 and Na1p are crystallographically related atoms; similarly O11 and O11p are crystallographically related atoms. p, 2-x, 1-y, 1-z; (b) 1-D chain established by coordination of di-sodium-cobalt aqua cation with the decavanadate anion in compound **2** along *a*-axis.

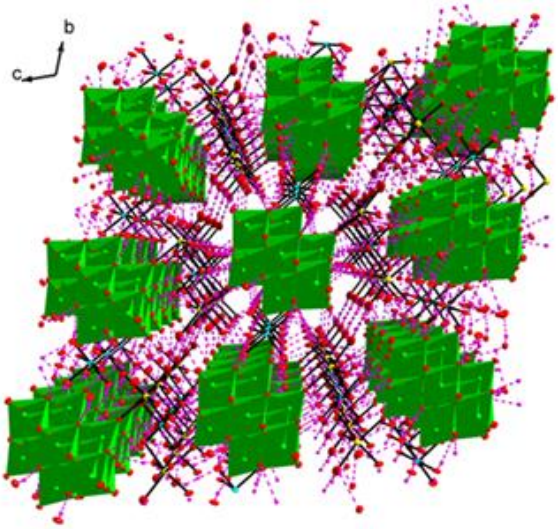

Figure 5.11. 3-D network established in the compound **3** due to O–H···O hydrogen bonding interactions involving coordinated and lattice water molecules, along *a*-axis.

Table 5.2. Selected bond lengths [Å] and angles [°] for compound **2**

V(1)-O(1)	1.816(7)	V(3)-O(9)	1.676(7)	V(5)-O(9)	2.038(7)
V(1)-O(2)	1.591(7)	V(3)-O(7)#1	1.927(6)	V(5)-O(10)	2.319(6)
V(1)-O(3)	1.857(6)	V(3)-O(10)#1	2.113(7)	V(5)-O(13)	1.842(6)
V(1)-O(4)	2.037(6)	V(3)-O(10)	2.116(6)	V(5)-O(14)	1.598(7)
V(1)-O(10)#1	2.297(6)	V(3)-O(8)	1.897(6)	Na(1)- O(11)	2.380(7)
V(1)-O(12)#1	1.886(6)	V(4)-O(7)	1.972(6)	Na(1)-O(16)	2.303(10)
V(2)-O(3)	1.814(7)	V(4)-O(8)	1.983(6)	Na(1)-O(15)	2.336(9)
V(2)-O(5)	1.795(7)	V(4)-O(10)	2.223(6)	Na(1)-O(17)	2.380(8)
V(2)-O(6)	1.598(6)	V(4)-O(11)	1.591(6)	Na(1)-O(18)	2.535(8)
V(2)-O(7)	1.979(6)	V(4)-O(12)	1.788(6)	Na(1)-O(20)#3	2.559(8)
V(2)-O(8)	1.985(6)	V(4)-O(13)	1.844(7)	Co(1)-O(18)#3	2.097(7)
V(2)-O(10)#1	2.199(6)	V(5)-O(1)#1	1.829(7)	Co(1)-O(18)	2.097(7)
V(3)-O(4)	1.670(6)	V(5)-O(5)#1	1.879(6)	Co(1)-O(20)	2.137(6)
Co(1)-O(20)#3	2.137(6)	Co(1)-O(19)	2.072(6)	Co(1)-O(19)#3	2.072(6)
Co(2)-O(21)	2.063(7)	Co(2)-O(21)#2	2.063(7)	Co(2)-O(22)	2.129(7)
Co(2)-O(22)#2	2.129(7)	Co(2)-O(23)	2.063(8)	Co(2)-O(23)#2	2.063(8)
O(1)-V(1)-O(2)	103.3(4)	O(1)-V(1)-O(3)	91.7(3)	O(1)-V(1)-O(4)	156.4(3)
O(2)-V(1)-O(3)	101.7(3)	O(2)-V(1)-O(4)	100.2(3)	O(3)-V(1)-O(4)	84.2(3)
O(3)-V(2)-O(7)	156.6(3)	O(3)-V(2)-O(8)	90.9(3)	O(5)-V(2)-O(3)	95.4(3)
O(5)-V(2)-O(7)	89.9(3)	O(5)-V(2)-O(8)	155.2(2)	O(6)-V(2)-O(3)	102.3(3)
O(6)-V(2)-O(5)	102.7(3)	O(6)-V(2)-O(7)	98.8(3)	O(6)-V(2)-O(8)	99.3(3)
O(7)-V(2)-O(8)	75.6(3)	O(4)-V(3)-O(7)#1	96.5(3)	O(4)-V(3)-O(8)	99.0(3)
O(8)-V(3)-O(10)	79.8(2)	O(9)-V(3)-O(7)#1	96.2(3)	O(9)-V(3)-O(8)	98.6(3)
O(9)-V(3)-O(10)	87.2(3)	O(9)-V(3)-O(10)#1	165.3(3)	O(10)#1-V(3)-O(10)	78.1(3)
O(7)-V(4)-O(8)	75.8(3)	O(7)-V(4)-O(10)	76.5(2)	O(8)-V(4)-O(10)	75.4(2)
O(11)-V(4)-O(7)	101.0(3)	O(11)-V(4)-O(8)	99.5(3)	O(11)-V(4)-O(10)	174.7(3)
O(13)-V(4)-O(7)	154.6(3)	O(13)-V(4)-O(8)	88.8(3)	O(13)-V(4)-O(10)	80.2(2)
O(1)#1-V(5)-O(13)	92.5(3)	O(5)#1-V(5)-O(9)	81.9(3)	O(9)-V(5)-O(10)	74.1(2)
O(13)-V(5)-O(9)	84.3(3)	O(13)-V(5)-O(10)	77.7(2)	O(14)-V(5)-O(1)#1	104.4(3)
O(14)-V(5)-O(9)	100.1(3)	O(14)-V(5)-O(10)	174.2(3)	O(14)-V(5)-O(13)	102.3(3)
O(11)-Na(1)-O(18)	87.8(3)	O(15)-Na(1)-O(11)	81.5(3)	O(15)-Na(1)-O(17)	87.7(3)
O(15)-Na(1)-O(18)	114.1(3)	O(16)-Na(1)-O(11)	168.6(4)	O(16)-Na(1)-O(15)	88.4(4)
O(16)-Na(1)-O(17)	98.5(4)	O(16)-Na(1)-O(18)	91.7(4)	O(17)-Na(1)-O(11)	86.3(3)
O(17)-Na(1)-O(18)	156.2(3)	O(18)-Co(1)-O(20)	93.7(3)	O(19)-Co(1)-O(18)	91.4(3)
O(19)-Co(1)-O(20)	89.7(3)	O(21)#2-Co(2)-O(21)	180.0	O(21)-Co(2)-O(22)	87.3(3)
O(21)-Co(2)-O(23)	85.7(3)	O(21)#2-Co(2)-O(23)	94.3(3)	O(23)-Co(2)-O(22)	90.4(3)

Symmetry transformations used to generate equivalent atoms:

#1 -x+1,-y+1,-z #2 -x,-y,-z

Table 5.3. Selected bond lengths [Å] and angles [°] for compound **3**

V(1)-O(1)	1.592(2)	V(1)-O(2)	1.820(2)	V(1)-O(3)	1.882(2)
V(1)-O(4)	2.049(2)	V(1)-O(5)	2.324(2)	V(1)-O(12)#3	1.859(2)
V(2)-O(3)	1.808(2)	V(2)-O(5)	2.220(2)	V(2)-O(6)	1.814(2)
V(2)-O(7)	1.607(2)	V(2)-O(8)#3	1.991(2)	V(2)-O(10)	1.991(2)
V(3)-O(4)	1.681(2)	V(3)-O(5)#3	2.111(2)	V(3)-O(5)	2.120(2)
V(3)-O(8)	1.906(2)	V(3)-O(9)	1.675(2)	V(3)-O(10)	1.939(2)
V(4)-O(5)#3	2.238(2)	V(4)-O(8)#3	2.015(2)	V(4)-O(10)	1.977(2)
V(4)-O(11)	1.603(2)	V(4)-O(12)	1.842(2)	V(4)-O(13)	1.803(2)
V(5)-O(2)#3	1.821(2)	V(5)-O(5)#3	2.309(2)	V(5)-O(6)#3	1.869(2)
V(5)-O(9)	2.043(2)	V(5)-O(13)	1.891(2)	V(5)-O(14)	1.596(2)
Na(1)-O(11)	2.392(3)	Na(1)-O(15)	2.336(4)	Na(1)-O(16)	2.371(3)
Na(1)-O(17)	2.313(4)	Na(1)-O(18)	2.539(3)	Na(1)-O(20)#1	2.557(3)
Zn(1)-O(18)	2.098(3)	Zn(1)-O(18)#1	2.098(3)	Zn(1)-O(19)	2.062(2)
Zn(1)-O(19)#1	2.062(2)	Zn(1)-O(20)	2.141(2)	Zn(1)-O(20)#1	2.141(2)
Zn(2)-O(21)	2.129(3)	Zn(2)-O(21)#2	2.129(3)	Zn(2)-O(22)	2.053(3)
Zn(2)-O(22)#2	2.053(3)	Zn(2)-O(23)	2.084(3)	Zn(2)-O(23)#2	2.084(3)
O(1)-V(1)-O(2)	103.97(12)	O(1)-V(1)-O(3)	102.54(12)	O(1)-V(1)-O(4)	100.14(11)
O(1)-V(1)-O(5)	174.24(11)	O(1)-V(1)-O(12)#3	102.37(12)	O(2)-V(1)-O(3)	90.73(10)
O(3)-V(2)-O(10)	90.11(9)	O(6)-V(2)-O(5)	81.23(9)	O(6)-V(2)-O(8)#3	90.39(10)
O(6)-V(2)-O(10)	156.28(10)	O(7)-V(2)-O(3)	102.80(11)	O(7)-V(2)-O(5)	174.00(10)
O(10)-V(4)-O(8)#3	75.90(8)	O(11)-V(4)-O(5)#3	174.69(10)	O(11)-V(4)-O(8)#3	99.70(11)
O(12)-V(4)-O(5)#3	80.32(9)	O(12)-V(4)-O(8)#3	88.82(9)	O(12)-V(4)-O(10)	154.54(9)
O(13)-V(4)-O(5)#3	81.39(9)	O(13)-V(4)-O(8)#3	155.47(9)	O(13)-V(4)-O(10)	91.37(9)
O(13)-V(4)-O(12)	94.74(10)	O(2)#3-V(5)-O(13)	91.52(10)	O(2)#3-V(5)-O(6)#3	91.74(10)
O(2)#3-V(5)-O(9)	155.91(10)	O(6)#3-V(5)-O(13)	154.54(10)	O(6)#3-V(5)-O(5)#3	77.74(8)
O(11)-Na(1)-O(18)	87.62(10)	O(15)-Na(1)-O(16)	87.87(12)	O(11)-Na(1)-O(20)#1	88.61(10)
O(15)-Na(1)-O(11)	80.88(12)	O(16)-Na(1)-O(11)	86.46(10)	O(15)-Na(1)-O(20)#1	168.48(13)
O(15)-Na(1)-O(18)	114.45(12)	O(17)-Na(1)-O(15)	88.92(19)	O(17)-Na(1)-O(20)#1	102.00(17)
O(17)-Na(1)-O(11)	168.18(14)	O(17)-Na(1)-O(18)	91.2(3)	O(16)-Na(1)-O(20)#1	86.78(10)
O(17)-Na(1)-O(16)	99.2(2)	O(16)-Na(1)-O(18)	155.65(12)	O(18)-Zn(1)-O(18)#1	180.00(14)
O(19)-Zn(1)-O(18)	91.98(11)	O(18)-Zn(1)-O(20)	93.54(10)	O(18)-Zn(1)-O(20)#1	86.46(10)
O(21)#2-Zn(2)-O(21)	180.0(10)	O(22)-Zn(2)-O(21)	87.06(11)	O(22)-Zn(2)-O(21)#2	92.94(11)
O(22)#2-Zn(2)-O(22)	180.0	O(22)-Zn(2)-O(23)	84.54(11)	O(22)-Zn(2)-O(23)#2	95.46(11)
O(23)#2-Zn(2)-O(21)	90.91(12)	O(23)-Zn(2)-O(21)	89.09(12)	O(23)#2-Zn(2)-O(23)	180.00(17)

Symmetry transformations used to generate equivalent atoms:

#1 -x+1,-y+2,-z+1 #2 x,y-1,z #3 -x,-y+3,-z+1 #4 x,y+1,z #5 -x+1,-y+1,-z+2

Table 5.4. Crystallographic data for compounds $[\{Na_3(H_2O)_8(\mu_2\text{-}H_2O)_6Ag_2\}\text{-}HV_{10}O_{28}]_n\cdot 6nH_2O$ (**1**), $[Co(H_2O)_6]_n[\{Na_2(H_2O)_6(\mu_2\text{-}H_2O)_4Co(H_2O)_2\}V_{10}O_{28}]_n\cdot 4nH_2O$ (**2**) and $[Zn(H_2O)_6]_n[\{Na_2(H_2O)_6(\mu_2\text{-}H_2O)_4Zn(H_2O)_2\}V_{10}O_{28}]_n\cdot 4nH_2O$ (**3**).

	Compound 1	**Compound 2**	**Compound 3**
Molecular formula	$Ag_2H_{41}Na_3O_{48}V_{10}$	$Co_2H_{44}Na_2O_{50}V_{10}$	$Zn_2H_{44}Na_2O_{50}V_{10}$
Formula weight	1603	1517	1530
Temperature	298K	298K	298K
Wavelength	0.71073 Å	0.71073 Å	0.71073 Å
Crystal system	Triclinic	Triclinic	Triclinic
Space group	P-1	P-1	P-1
a [Å]	8.8270(6)	8.3427(16)	8.3477(7)
b [Å]	10.3400(8)	10.7951(16)	10.8486(12)
c [Å]	11.1153(8)	12.491(2)	12.5864(11)
α[deg]	89.006(6)	109.842(14)	109.934(9)
β [deg]	79.878(6)	93.151(14)	93.329(7)
Γ[deg]	71.080(6)	100.017(14)	100.051(8)
Volume[$Å^3$]	943.90(12)	1034.1(3)	1046.55(17)
Z	1	1	1
Calculated density[Mg m^{-3}]	2.821	2.437	2.428
F[000]	782	750	756
Crystal size [mm]	0.26 x 0.18 x 0.18	0.26 x 0.20 x 0.18	0.28x 0.18 x 0.16
θ range for data collection [deg]	2.82 to 24.71	2.89 to 29.08	2.86 to 24.71
Reflections collected/unique	5701 / 3212	5865/3925	6579/3557
R (int)	0.0411	0.0768	0.0259
Data/restraints/parameters	3212/ 15 / 330	3925/0/292	3557/33/380
Goodness-of-fit on F^2	1.042	1.033	1.089
R_1/wR_2 [I > 2σ(I)]	0.0585/0.1475	0.0762/0.1843	0.0317/0.0792
R_1/wR_2 (all data)	0.0865/ 0.1669	0.1228/0.2617	0.0374/0.0826
Largest diff. Peak/hole [$e^-Å^3$]	1.908/ -1.921	1.041/-1.480	0.463/-0.813

5.3.6. Comparison of the crystal structures:

The compound **1**, is polyanion-polycation inorganic polymer with monoprotonated decavanadate cluster anion and pentameric silver (I) and sodium (I) aqua- complex cation. The synthesis of the compounds **1-3** is a very simple one pot reaction. It is very interesting to note that on changing the metal linker cation from Ag^{1+} to Co^{2+} / Zn^{2+} transition metal ion in the same synthesis, the dimensionality of the extended structures is changed. Although the decavanadate based clusters with the transition metal cations and with other organic cations are very well known, the polymeric compounds with the pure inorganic polycation are not well-explored. The copper containing decavanadate cluster containing polymeric compound was characterized with 3D framework[29] and nickel containing decavanadate based polymeric structure was characterized with 2D framework[28] in literature. We also found 3D structure in silver containing system (compound **1**). The basic difference between the crystal structures compound **1** and isomorphous compounds **2** / **3** is in the case of compound **1**, the primary linker is silver dimer forming a 2D sheet-like arrangement and sodium trimeric-aqua complex cation is the secondary linker, that connect the 2D layers laterally resulting in the formation of 3D network. However, in the case of compound **2** / **3**, the only linker di-sodium cobalt aqua complex / di-sodium zinc aqua-complex cation links the decavanadate anion from opposite sides and form a one-dimensional chain-like structure.

5.4. Conclusion

In this chapter, three decavanadate based polyanion-polycation polymers of transition metal and sodium cations have been described. In compound **1**, the decavanadate anion is coordinated with surrounding dimeric silver cations through coordinate covalent bonds (using both terminal and bridging oxygen atoms of the decavanadate cluster) and its repetition result in the formation of a 2D sheet. These 2D sheets are intern connected laterally by trimeric sodium-aqua cation, thereby extending the dimensionality to the 3D framework. In the case of compound **2 / 3**, di-sodium cobalt aqua-complex cation / di-sodium zinc aqua-complex cation acts as the linker, linking decavanadate anions into 1D chains. To the best of our knowledge, compound **1** is a unique example, in which a silver oxo-dimer $\{Ag_2(\mu_4\text{-}O)_2\}^{2+}$ is formed exclusively from oxygen atoms of decavanadate cluster anions.

5.5 References

1. Okuhara, T.; Mizuno, N.; Misono, M. *Adv. Catal.* **1996**, *41*, 113.
2. Hill, C. L.; Kim, G. –S.; Prosser-McCartha, C. M.; Judd, D. *Mol. Eng.* **1993**, *3*, 263.
3. Hill, C. L.; Prosser-McCartha, C. M. *Coord. Chem. Rev.* **1995**, *143*, 407.
4. Coronado, E.; Giménez-Saiz, C.; Gómez-Garcia, C. J. *Coord. Chem. Rev.* **2005**, *249*, 1776.
5. Rhule, J. T.; Hill, C. L.; Judd, D. A.; Schinazi, R. F. *Chem. Rev.* **1998**, *98,* 327.
6. Yamase, T. *Mol. Eng.* **1993**, *3*, 241.
7. Pope, M. T.; Yamase, T. *Polyoxometalate Chemistry for Nanocomposite Design*, *ed.* Kluwer, Dordrecht, **2002**.
8. Pope, M. T.; Müller, A. *Angew. Chem. Int. Ed.***1991**, *30*, 34.
9. Rao, A .S.; Arumuganathan, T.; Shivaiah, V.; Das, S. K. *J. Chem. Sci.* **2011**, *123*, 229.
10. Arumuganathan, T.; Rao, A. S.; Das, S. K. *Cryst. Growth Des.* **2010**, *10*, 4272.
11. Manikumari, S.; Shivaiah, V.; Das, S. K. *Inorg. Chem.* **2002**, *41*, 6953.
12. Soares, S.S.; Aureliano, M.; Joaquim, N.; Coucelo, J. M. *J. Inorg. Biochem.* **2003**, *94*, 285.
13. Krstić, D.; Colović, M.; Bosnjaković-Pavlović, N.; Bire, A. S. –D.; Vasić, V. *Gen. Physiol. Biophys.* **2009**, *28*, 302.
14. Soares, S. S.; Henao, F.; Aureliano, M.; Gutiérrez-Merino, C. *Chem. Res. Toxicol.* **2008**, *21*,607.
15. Fritsch, M.; Aluker, M.; Murdoch, F. E. *Biochem.* **1999**, *38*, 6987.
16. Ding, Y.; Zhao, W.; Song, W.; Zhang, Z.; Ma, B. *Green Chem.* **2011**, *13*, 1486.
17. Breen, J. M.; Schmitt, W. *Angew. Chem. Int. Ed.* **2008**, *47*, 6904.
18. Zhang, L.; Schmitt, W. *J. Am. Chem. Soc.* **2011**, *133* , 11240.
19. Ni, E.; Uematsu, S.; Quan, Z.; Sonoyama, N. *J Nanopart Res* **2013**, *15*, 1732.
20. Barbour, A.; Luttrell, R. D.; Choi, J.; Musfeldt, J. L.; Zipse, D.; Dalal, N. S.; Boukhvalov, D. W.; Dobrovitski, V. V.; Katsnelson, M. I.; Lichtenstein, A. I.; Harmon, B. N.; Kögerler, P. *Phys. Rev.* **2006**, *B 74*, 014411 (1).
21. Kasuga, N. C.; Umeda, M.; Kidokoro, H.; Ueda, K.; Hattori, K.; Yamaguchi, K.; *Cryst. Growth Des.* **2009**, *9*, 1494.

22. Xu, W.; Jiang, F.; Zhou, Y.; Xiong, K.; Chen, L.; Yang, M.; Feng, R.; Hong, M. *Dalton Trans.***2012**, *41*, 7737.
23. Mestiri, I.; Ayed, B.; Haddad, A. *J. Clust. Sci.* **2013**, *24*, 85.
24. Duraisamy, T.; Ramanan, A.; Vittal, J. J. *Cryst. Eng.* **2000**, *3*, 237.
25. Khan, M. I.; Tabussum, S.; Zheng, C.; *J. Clust. Sci.* **2001**, *12*, 583.
26. Miras, H. N.; Raptis, R. G.; Lalioti, N.; Sigalas, M. P.; Baran, P.; Kabanos, T. A. *Chem. Eur. J.* **2005**, *11*, 2295.
27. Higami, T.; Hashimoto, M.; Okeya, S. *Acta Cryst.* **2002**, *C58*, i144.
28. Sun, Z. –G.; Long, L. −S.; Ren, Y. –P.; Huang, R. –B.; Zheng, L. -S.; Ng, S. W. *Acta Cryst.* **2002**, *E58*, i34.
29. Lida, A.; Ozeki, T. *Acta Cryst.* **2003**, *C59*, i41.
30. Shivaiah, V.; Reddy, P. V. N.; Cronin, L.; Das, S. K. *J. Chem. Soc., Dalton Trans.* **2002**, 3781.
31. Shivaiah, V.; Das, S. K. *J. Chem. Sci.* **2005**, *117*, 227.
32. Arumuganathan, T.; Das, S. K. *Inorg. Chem.* **2009**, *48*, 496.
33. G. –T. Pan, M. –H. Lai, R. –C. Juang, T. –W. Chung, T. C.-K. Yang, Ind. Eng. Chem. Res. 50 (2011) 2807−2814.
34. Y. Qi, E. Wang, J. Li, Y. Li, J. Solid State Chem. 182 (2009) 2640–2645.
35. C. Streb, R. Tsunashima, D. A. MacLaren, T. M. Glone, T. Akutagawa, T. Nakamura, A. Scandurra, B. Pignataro, N. Gadegaard, L. Cronin, Angew. Chem. Int. Ed. 48 (2009) 6490–6493.
36. SAINT: Software for the CCD Detector System; Bruker Analytical X-ray Systems, Inc.: Madison, WI, 1998.
37. SADABS: Program for Absorption Correction; Sheldrick, G. M. University of Gottingen: Gottingen, Germany, 1997.
38. SHELXS-97: Program for Structure Solution; Sheldrick, G. M. University of Gottingen: Gottingen, Germany, 1997.
39. SHELXL-97: Program for Crystal Structure Analysis; Sheldrick, G. M. University of Gottingen: Gottingen, Germany, 1997.
40. H. T. Evans Jr., Inorg. Chem. 5 (1966) 967-977.

Summary and future scope

6

This chapter demonstrates the future scope of this thesis work. In second chapter of the thesis, we have described the synthesis of mixed addenda Lindqvist cluster containing compounds. According to literature studies, the mixed addenda cluster associated compounds can be used as good catalysts. The crystal structures and properties of decavanadate-based compounds with organic cations have been demonstrated in the chapter 3. This chapter is also described by nano-crystals, that have been characterized by microscopic techniques. Chapter 4 depicts the isolation and supramolecular property of pure inorganic polymeric materials based on decavanadate anion by changing the counter cations, for example, hexamethylenetetramine, tri-sodium aqua-complex cation. The final working chapter 5, describes the isolation of 3-dimensional to 1-dimensional decavanadate based cluster containing compounds, where the decavanadate is functionalized with metal cations.

Synthesis of some more mixed addenda cluster anions (with appropriate cations) and various polymeric decavanadate cluster containing materials including their catalytic applications are our future dream. We wish to extend our work concerning the nano-crystals of decavanadate cluster containing compounds to obtain silver and gold nanoparticles supported decavanadate clusters, which can be used in catalysis and medicine. The nano-sized POM anions can also be stabilized and isolated with various surfactants to synthesize the nanopartices of POMs (below 10 nm size). The relevant efforts have already been undertaken in our laboratory.

List of Publications

1. Decavanadate-based discrete compound and coordination polymers: Synthesis, crystal structures, spectroscopy and nano-materials
Sridevi Yerra, Bharat Kumar Tripuramallu, Samar K. Das, *Polyhedron,* **2014**, *81*, 147-153.

2. Synthesis and structural characterization of Lindqvist type mixed-metal cluster anion $[V_2W_4O_{19}]^{4-}$ in discrete and coordination polymer compounds
Sridevi Yerra, Srinivasa Rao Amanchi, Samar K. Das, *J. Mol. struct.*, **2014**, *1062*, 53-60.

3. Reversible morphological transition between nano-rods to micro-flowers through micro-hexagonal crystals in a sonochemical synthesis based on a polyoxovanadate compound
Sridevi Yerra, Sabbani Supriya, Samar K. Das, *Inorg. Chem. Comm.*, **2013**, *35*, 54-57.

4. Organic free decavanadate based materials: inorganic linkers to obtain extended structures
Sridevi Yerra, Samar K. Das (Submitted for publication).

Poster and Oral Presentations

1. **Y. Sridevi**, S. Supriya and Samar K. Das*, Sonochemical synthesis of nano-size decavanadate anionic clusters: Characterization and their morphological studies.

   (i) Poster presentation at "**MODERN TRENDS IN INORGANIC CHEMISTRY [MTIC-XV]**" which was held in Department of Chemistry, *IIT*, Roorkee, India on December, **2014**.

   (ii) Poster presentation and oral presentation at "**Chemfest-2013** (***In-house***)" which was held in School of Chemistry, *University of Hyderabad*, Hyderabad, India on February, **2013**.

2. **Y. Sridevi** and Samar K. Das*, Synthesis of Tungsten Based Polyoxometalate Clusters and their Mixed Addenda Systems: Characterization And Catalytic Properties.

   Poster presentation at "**Chemfest-2012** (***In-house***)" which was held in School of Chemistry, *University of Hyderabad*, Hyderabad, India on February, **2012**.

3. **Y. Sridevi** and Samar K. Das*, Macro- and Nano-sized Crystals of a Polyoxovanadate Cluster anion with and without Organic Cations: Synthesis and Characterization.

   Poster presentation at "**Chemfest-2010** (***In-house***)" which was held in School of Chemistry, *University of Hyderabad*, Hyderabad, India on January, **2010**.